TRANSIENT CHARACTERISTICS OF HUMIDITY SENSORS AND THEIR APPLICATION TO ENERGY WHEELS

A Thesis Submitted to the College of

Graduate Studies and Research

in Partial Fulfillment of the Requirements

for the Degree of

Master of Science

in the Department of Mechanical Engineering

University of Saskatchewan

Saskatoon, Canada

By

YIHENG WANG

PERMISSION TO USE

In presenting this thesis in partial fulfilment of the requirements for a Postgraduate degree from the University of Saskatchewan, I agree that the Libraries of the University may make it freely available for inspection. I further agree that permission for copying of this thesis in any manner, in whole or in part, for scholarly purpose may be granted by the professor and professors who supervised my thesis work or, in their absence, by the Head of Department in which my thesis work was done. It is understood that any copying, publication, or use of this thesis or parts thereof for financial gain shall not be allowed without my written permission. It is also understood that due recognition shall be given to me and to the University of Saskatchewan in any scholarly use which may be made of any material in my thesis.

Requests for permission to copy or to make other use of material in this thesis in whole or part should be addressed to:

Head of Department of Mechanical Engineering
University of Saskatchewan
Saskatoon, Saskatchewan (S7N 5A9)

ABSTRACT

Rotary air-to-air energy exchangers (also called energy wheels) transfer both heat and moisture between supply and exhaust airstreams in buildings. In this thesis, it is hypothesized that the transient step response characteristics of an energy wheel are uniquely related to the steady-state cyclic response of the wheel. The primary objective of this research is to study the transient response of a humidity/temperature sensor and measure energy wheel performance with a new test procedure that uses only transient response characteristics.

In this thesis, the transient characteristics of a humidity/temperature sensor and an energy wheel to a step change in relative humidity and temperature are investigated through two types of measurements. One test uses a small airflow, at controlled temperature and humidity conditions, passing through a small section of a porous wheel while measuring the outlet conditions after the inlet conditions are suddenly changed. For a step input, it is shown that the outlet humidity/temperature sensor data correlate with an exponential function with two time constants. Since the transient response characteristics of the humidity/temperature sensor must be known to predict the response of the wheel alone, a second test is required that is similar to the first test except that the wheel is removed. This test is used to obtain the transient response of the sensor alone. Data from these tests show that both the sensor and the sensor plus wheel have two sets of two time constants. An analysis is presented to determine the transient response of the wheel alone using the correlated properties of the sensor alone and the sensor with a wheel upstream.

The challenge undertaken in this research was the development of a more flexible, lower cost test facility than that presented in ASHRAE Standard 84-1991(Method of Testing Air-to-Air Heat Exchangers). In future work, this new laboratory experimental test facility should be adapted to test most types of energy wheels. The configuration allows a wide range of mass flow rates, inlet supply air temperatures and relative humidities.

Uncertainty analysis is used for each transient test for the sensors and air-to-air energy wheels to specify the sensor and wheel plus sensor characteristics. This uncertainty analysis shows that accurate sensor calibration under equilibrium conditions and the start time for the humidity sensor step change is crucial to achieve low uncertainties in the transient behaviour of sensor and energy wheels. Knowing the uncertainty in the characteristics of the sensors and the wheel plus sensors the uncertainty in the transient response of the wheel alone is predicted.

The first time constant of the humidity sensor is found to be about 3 seconds, while the second time constant is found to be about 100 seconds. It is found that the predicted response of the wheel alone gives time constants that are about 6 seconds and 140 seconds. Other researchers can use this information presented in this thesis to estimate the effectiveness of an energy wheel.

ACKNOWLEDGEMENTS

A sincere thank-you to my supervisors, Professor Robert W. Besant and Professor Carey J. Simonson. Without your expertise and encouragement, my Master's program would have not ended on a happy note as it did. Thank you for everything. Thanks to Dr. Wei Shang, my research group leader, for your time and truly interesting discussion, research related and not. Thanks also to Dr. Hong Chen for your helpful and innovative suggestion in my research work and my life. Big thanks to the staff of Thermal Sciences Lab, Mr. Dave Deutscher, Mr. Darren Braun and Mr. Chris James, for your help with the experimental studies.

Thanks are also extended to Rugang Chen, Yan Wang, Xiaodong (Rachel) Nie and Haisheng Fan in the same research group for your support, encouragement and interesting discussion during this time.

Special thanks to my families: Mom, Grandmother, Uncles and Aunts for your love and encouragement in many ways with words and actions.

Financial assistance is acknowledged and appreciated from: the National Sciences and Engineering Research Council of Canada (NSERC) and Venmar CES Inc. for providing financial assistance on this research work.

DEDICATION

To my mother, Jiali Wang, my grandmother, Peiqiu Wu,
and my late grandfather, Jingxian Wang.

TABLE OF CONTENTS

PERMISSION TO USE……i

ABSTRACT.....ii

ACKNOWLEDGEMENTS……iv

TABLE OF CONTENTS……....vi

LIST OF TABLES……....viii

LIST OF FIGURES…….…….xiv

NOMENCLATURE……....xviii

1. INTRODUCTION.....1

1.1. Background 1

1.2. Research Concept..... 3

1.3. Literature Review..... 4

1.3.1. Measurement of Transient Humidity Changes..... 4

1.3.2. Measurement of Transient Temperature Changes 6

1.4. Research Objectives 7

1.5. Procedure or Methodology and Scope of Research 7

2. TEST FACILITY AND INSTRUMENTATION.....9

2.1. Design and Description of the Test Facility..... 9

2.2. Instrumentation and Steady-state Calibration 13

2.2.1. Humidity Measurement..... 13

2.2.2. Temperature Measurement..... 14

2.3. Data Acquisition..... 15

3. TRANSIENT SENSOR RESPONSE AND DATA ANALYSIS.....16

3.1. Transient Response of the Humidity/Temperature Transmitter..... 17

3.1.1. Humidity Change Only ($\Delta RH \neq 0$, $\Delta T = 0$) 18

3.1.2. Humidity and Temperature Change ($\Delta RH \neq 0$, $\Delta T \neq 0$) 20

3.1.3. Temperature Change Only ($\Delta RH = 0$ and $\Delta T \neq 0$) 21

3.1.4. Conditions with Constant Humidity Ratio ($\Delta W = 0$)..... 22

3.2. Transient Data Correlation 23
3.2.1. Transient Relative Humidity Data Correlation 24
3.2.2. Transient Temperature Data Correlation 37
3.2.3. Comparison of Transient Temperature Measurement 44
3.3. Uncertainty Analysis 48
4. TESTS ON ENERGY WHEELS 54
4.1. Measured Outlet Relative Humidity Response of Energy Wheels 58
4.2. Measured Outlet Temperature Response of Energy Wheels 63
4.2.1. Humidity/Temperature Transmitter Temperature Data 64
4.2.2. Thermocouple Temperature Data 69
4.3. Analysis of Energy Wheel Data 71
4.4. Uncertainty Analysis 86
4.4.1. Uncertainty of Energy Wheel plus Sensor Response 86
4.4.2. Uncertainty of Energy Wheel Response 88
5. RESEARCH SUMMARY AND CONCLUSIONS 90
5.1. Research Summary 90
5.2. Conclusions 91
5.3. Future Work 92
REFERENCES 93
APPENDIX A: DESIGN DRAWINGS 95
APPENDIX B: HEAT CONDUCTION INSIDE THE ENERGY WHEEL 97
APPENDIX C: CALCULATION OF WHEEL RESPONSE 99
C.1. Adsorption Case 99
C.2. Desorption Case 100
C.3. Verification of The Energy Wheel Response Equation 101
C.3.1. Adsorption Case 102
C.3.2. Desorption Case 103

LIST OF TABLES

Table 2.1. Operating conditions for the sensor or energy wheel testing. 11

Table 2.2. Steady state RH calibration for two outlet transmitters. 14

Table 2.3. Steady-state temperature calibration for two outlet transmitters. 15

Table 3.1. Adsorption coefficients (x_1, x_2) and time constants (t_1, t_2) in equation (3.1) that describe the transient humidity response of the humidity/temperature transmitter with $\Delta RH \neq 0$, $\Delta T = 0$, $V_{air} = 1.6$m/s during three trials at different wet side humidity conditions. .. 26

Table 3.2. Desorption coefficients (x_1, x_2) and time constants (t_1, t_2) in equation (3.2) that describe the transient humidity response of the humidity/temperature transmitter with $\Delta RH \neq 0$, $\Delta T = 0$, $V_{air} = 1.6$m/s during three trials at different wet side humidity conditions. .. 27

Table 3.3. Adsorption coefficients (x_1, x_2) and time constants (t_1, t_2) in equation (3.1) that describe the transient humidity response of the humidity/temperature transmitter with $\Delta RH \neq 0$, $\Delta T = 0$, $V_{air} = 1.6$m/s during three time intervals with one wet side humidity condition. 29

Table 3.4. Desorption coefficients (x_1, x_2) and time constants (t_1, t_2) in equation (3.2) that describe the transient humidity response of the humidity/temperature transmitter with $\Delta RH \neq 0$, $\Delta T = 0$, $V_{air} = 1.6$m/s during three time intervals with one wet side humidity condition. 29

Table 3.5. Adsorption coefficients (x_1, x_2) and time constants (t_1, t_2) in equation (3.1) that describe the transient humidity response of the humidity/temperature transmitter with $\Delta RH \neq 0$, $\Delta T = 0$, $V_{air} = 0.8$m/s during three trials at different wet side humidity conditions. .. 30

Table 3.6. Desorption coefficients (x_1, x_2) and time constants (t_1, t_2) in equation (3.2) that describe the transient humidity response of the humidity/ temperature transmitter with $\Delta RH \neq 0$, $\Delta T = 0$, $V_{air} = 0.8$m/s during three trials at different wet side humidity conditions. .. 30

Table 3.7. Adsorption coefficients (x_1, x_2) and time constants (t_1, t_2) in equation (3.1) that describe the transient humidity response of the humidity/ temperature transmitter with $\Delta RH \neq 0$, $\Delta T = 0$, $V_{air} = 0.4$m/s during three trials at different wet side humidity conditions. .. 31

Table 3.8. Desorption coefficients (x_1, x_2) and time constants (t_1, t_2) in equation (3.2) that describe the transient humidity response of the humidity/ temperature transmitter with $\Delta RH \neq 0$, $\Delta T = 0$, $V_{air} = 0.4$m/s during three trials at different wet side humidity conditions. .. 31

Table 3.9. Adsorption coefficients (x_1, x_2) and time constants (t_1, t_2) in equation (3.1) describing the transient humidity response of the humidity/temperature transmitter with $\Delta RH \neq 0$, $\Delta T \neq 0$ and $V_{air} = 1.6$m/s. 33

Table 3.10. Desorption coefficients (x_1, x_2) and time constants (t_1, t_2) in equation (3.2) describing the transient humidity response of the humidity/temperature transmitter with $\Delta RH \neq 0$, $\Delta T \neq 0$ and $V_{air} = 1.6$m/s. 33

Table 3.11. Adsorption coefficients (x_1, x_2) and time constants (t_1, t_2) in equation (3.1) describing the transient humidity response of the humidity/temperature transmitter with $\Delta RH \neq 0$, $\Delta T \neq 0$ and $\Delta W=0$, V_{air}=1.6m/s during three trials at different wet side humidity. 34

Table 3.12. Desorption coefficients (x_1, x_2) and time constants (t_1, t_2) in equation (3.2) describing the transient humidity response of the humidity/temperature transmitter with $\Delta RH \neq 0$, $\Delta T \neq 0$ and $\Delta W=0$, V_{air}=1.6m/s during three trials at different wet side humidity. 34

Table 3.13. Average coefficients describing the transient humidity response of the humidity/temperature transmitter. 36

Table 3.14. Increasing coefficients (y_1, y_2) and time constants (t_1, t_2) in equation (3.11) that present the transient temperature response of the humidity/temperature transmitter with $\Delta RH \neq 0$, $\Delta T \neq 0$, V_{air}=1.6m/s. 39

Table 3.15. Decreasing coefficients (y_1, y_2) and time constants (t_1, t_2) in equation (3.12) that present the transient temperature response of the humidity/temperature transmitter with $\Delta RH \neq 0$, $\Delta T \neq 0$, V_{air}=1.6m/s. 39

Table 3.16. Increasing coefficients (y_1, y_2) and time constants (t_1, t_2) in equation (3.11) that present the transient temperature response of the humidity/temperature transmitter with $\Delta RH=0$, $\Delta T \neq 0$, V_{air}=1.6m/s. 40

Table 3.17. Decreasing coefficients (y_1, y_2) and time constants (t_1, t_2) in equation (3.12) that present the transient temperature response of the humidity/temperature transmitter with $\Delta RH=0$, $\Delta T \neq 0$, V_{air}=1.6m/s. 40

Table 3.18. Increasing coefficients (y_1, y_2) and time constants (t_1, t_2) in equation (3.11) that present the transient temperature response of the humidity/temperature transmitter with $\Delta RH \neq 0$, $\Delta T \neq 0$, $\Delta W=0$, V_{air}=1.6m/s. 40

Table 3.19. Decreasing coefficients (y_1, y_2) and time constants (t_1, t_2) in equation (3.12) that present the transient temperature response of the humidity/temperature transmitter with $\Delta RH \neq 0$, $\Delta T \neq 0$, $\Delta W=0$, V_{air}=1.6m/s. 41

Table 3.20. Average coefficients describing transient temperature response of the temperature sensor in the humidity/temperature transmitter. 42

Table 3.21. Transient characteristics of the humidity/temperature transmitter under various operating conditions. 43

Table 3.22. Increasing coefficients (y_1, y_2) and time constants (t_1, t_2) in equation (3.11) that represent the transient temperature response of the thermocouple with $\Delta RH \neq 0$, $\Delta T \neq 0$, V_{air}=1.6m/s. 46

Table 3.23. Decreasing coefficients (y_1, y_2) and time constants (t_1, t_2) in equation (3.12) that represent the transient temperature response of the thermocouple with $\Delta RH \neq 0$, $\Delta T \neq 0$, V_{air}=1.6m/s. 46

Table 3.24. Increasing coefficients (y_1, y_2) and time constants (t_1, t_2) in equation (3.11) that represent the transient temperature response of the thermocouple with $\Delta RH=0$, $\Delta T\neq 0$, V_{air}=1.6m/s. 46

Table 3.25. Decreasing coefficients (y_1, y_2) and time constants (t_1, t_2) in equation (3.12) that represent the transient temperature response of the thermocouple with $\Delta RH=0$, $\Delta T\neq 0$, V_{air}=1.6m/s. 47

Table 3.26. Increasing coefficients (y_1, y_2) and time constants (t_1, t_2) in equation (3.11) that represent the transient temperature response of the thermocouple with $\Delta RH\neq 0$, $\Delta T\neq 0$, $\Delta W=0$, V_{air}=1.6m/s. 47

Table 3.27. Decreasing coefficients (y_1, y_2) and time constants (t_1, t_2) in equation (3.12) that represent the transient temperature response of the thermocouple with $\Delta RH\neq 0$, $\Delta T\neq 0$, $\Delta W=0$, V_{air}=1.6m/s. 47

Table 3.28. Average coefficients describing the transient temperature response of the thermocouple. 48

Table 3.29. Uncertainty of each coefficient describing the transient humidity response of the humidity/temperature transmitter. 51

Table 3.30. Uncertainty of each coefficient describing the transient temperature response of the humidity/temperature transmitter and the thermocouple. 52

Table 4.1. Adsorption coefficients (X_1, X_2) and time constants (T_1, T_2) in equation (4.1) describing the transient humidity response of a 100mm thick molecular sieve wheel plus the humidity/temperature transmitter ($\Delta RH\neq 0$, $\Delta T=0$, and V_{air}=1.6m/s). 60

Table 4.2. Desorption coefficients (X_1, X_2) and time constants (T_1, T_2) in equation (4.2) describing the transient humidity response of a 100mm thick molecular sieve wheel plus the humidity/temperature transmitter ($\Delta RH\neq 0$, $\Delta T=0$, and V_{air}=1.6m/s). 61

Table 4.3. Adsorption coefficients (X_1, X_2) and time constants (T_1, T_2) in equation (4.1) describing the transient humidity response of a 100mm thick silica gel wheel plus the humidity/temperature transmitter ($\Delta RH\neq 0$, $\Delta T=0$, and V_{air}=1.6m/s). 61

Table 4.4. Desorption coefficients (X_1, X_2) and time constants (T_1, T_2) in equation (4.2) describing the transient humidity response of a 100mm thick silica gel wheel plus the humidity/temperature transmitter ($\Delta RH\neq 0$, $\Delta T=0$, and V_{air}=1.6m/s). 61

Table 4.5. Adsorption coefficients (X_1, X_2) and time constants (T_1, T_2) in equation (4.1) describing the transient humidity response of a 100mm thick silica gel wheel plus humidity/temperature transmitter in different time intervals ($\Delta RH\neq 0$, $\Delta T=0$ and V_{air}=1.6m/s). 62

Table 4.6. Desorption coefficients (X_1, X_2) and time constants (T_1, T_2) in equation (4.2) describing the transient humidity response of a 100mm thick silica gel wheel plus humidity/temperature transmitter in different time intervals ($\Delta RH\neq 0$, $\Delta T=0$ and V_{air}=1.6m/s). 62

Table 4.7. Coefficients (X_1, X_2) and time constants (T_1, T_2) in equations (4.1) and (4.2) describing the transient humidity response of a 100mm thick molecular sieve wheel plus the humidity/temperature transmitter ($\Delta RH \neq 0$, $\Delta T \neq 0$ and V_{air}=1.6m/s,). 63

Table 4.8. Coefficients (X_1, X_2) and time constants (T_1, T_2) in equations (4.1) and (4.2) describing the transient humidity response of a 100mm thick silica gel wheel plus the humidity/temperature transmitter ($\Delta RH \neq 0$, $\Delta T \neq 0$ and V_{air}=1.6m/s). 63

Table 4.9. Coefficients (Y_1, Y_2) and time constants (T_1, T_2) in equations (4.4) and (4.5) describing the transient temperature response of a 100mm thick molecular sieve wheel plus the humidity/temperature transmitter ($\Delta RH \neq 0$, $\Delta T \neq 0$ and V_{air}=1.6m/s,). 66

Table 4.10. Coefficients (Y_1, Y_2) and time constants (T_1, T_2) in equations (4.4) and (4.5) describing the transient temperature response of a 100mm thick silica gel wheel plus the humidity/temperature transmitter ($\Delta RH \neq 0$, $\Delta T \neq 0$ and V_{air}=1.6m/s). 66

Table 4.11. Average coefficients describing the transient humidity response of a molecular sieve and a silica gel energy wheel plus humidity/temperature transmitter. 67

Table 4.12. Average coefficients describing the transient temperature response of a molecular sieve and a silica gel energy wheel plus humidity/temperature transmitter. 67

Table 4.13. Transient characteristics of the energy wheel plus the humidity/temperature transmitter 68

Table 4.14. Coefficients (Y_1, Y_2) and time constants (T_1, T_2) in equations (4.4) and (4.5) describing the transient temperature response of a 100mm thick molecular sieve wheel plus a thermocouple with $\Delta RH \neq 0$, $\Delta T \neq 0$ and V_{air}=1.6m/s. 70

Table 4.15. Coefficients (Y_1, Y_2) and time constants (T_1, T_2) in equations (4.4) and (4.5) describing the transient temperature response of a 100mm thick silica gel wheel plus a thermocouple with $\Delta RH \neq 0$, $\Delta T \neq 0$ and V_{air}=1.6m/s. 70

Table 4.16. Average coefficients describing the transient temperature response of the energy wheel plus the thermocouple. 70

Table 4.17. Adsorption coefficients (α_1, α_2) and time constants (τ_1, τ_2) in equations (4.19) describing the transient humidity response of a 100mm thick molecular sieve wheel ($\Delta RH \neq 0$, $\Delta T = 0$, V_{air}=1.6m/s). 75

Table 4.18. Desorption coefficients (α_1, α_2) and time constants (τ_1, τ_2) in equations (4.20) describing the transient humidity response of a 100mm thick molecular sieve wheel ($\Delta RH \neq 0$, $\Delta T = 0$, V_{air}=1.6m/s). 75

Table 4.19. Adsorption coefficients (α_1, α_2) and time constants (τ_1, τ_2) in equation (4.19) describing the transient humidity response of a 100mm thickness silica gel wheel ($\Delta RH \neq 0$, $\Delta T = 0$ and V_{air}=1.6m/s). 76

Table 4.20. Desorption coefficients (α_1, α_2) and time constants (τ_1, τ_2) in equation (4.20) describing the transient humidity response of a 100mm thickness silica gel wheel ($\Delta RH \neq 0$, $\Delta T=0$ and $V_{air}=1.6m/s$). 76

Table 4.21. Adsorption coefficients (α_1, α_2) and time constants (τ_1 and τ_2) in equation (4.19) describing the transient humidity response of a silica gel wheel in different time intervals ($\Delta RH \neq 0$, $\Delta T=0$, $V_{air}=1.6m/s$). 77

Table 4.22. Desorption coefficients (α_1, α_2) and time constants (τ_1 and τ_2) in equation (4.20) describing the transient humidity response of a silica gel wheel in different time intervals ($\Delta RH \neq 0$, $\Delta T=0$, $V_{air}=1.6m/s$). 77

Table 4.23. Coefficients (α_1, α_2) and time constants (τ_1, τ_2) in equations (4.19) and (4.20) describing transient humidity response of a 100mm thick molecular sieve wheel ($\Delta RH \neq 0$, $\Delta T \neq 0$ and $V_{air}=1.6m/s,$). 79

Table 4.24. Coefficients (α_1, α_2) and time constants (τ_1, τ_2) in equations (4.19) and (4.20) describing transient humidity response of a 100mm thickness silica gel wheel ($\Delta RH \neq 0$, $\Delta T \neq 0$ and $V_{air}=1.6m/s$). 79

Table 4.25. Coefficients (β_1, β_2) and time constants (τ_1, τ_2) in equations (4.22) and (4.23) describing transient temperature response of a 100mm thick molecular sieve wheel ($\Delta RH \neq 0$, $\Delta T \neq 0$ and $V_{air}=1.6m/s$). 81

Table 4.26. Coefficients (β_1, β_2) and time constants (τ_1, τ_2) in equations (4.22) and (4.23) describing transient temperature response of a 100mm thick silica gel wheel ($\Delta RH \neq 0$, $\Delta T \neq 0$ and $V_{air}=1.6m/s$). 82

Table 4.27. Average coefficients describing the transient humidity response of the energy wheel. 82

Table 4.28. Average coefficients describing the transient temperature response of the energy wheel. 82

Table 4.29. Coefficients (β_1, β_2) and time constants (τ_1, τ_2) in equations (4.22) and (4.23) describing transient temperature response of a 100mm thick molecular sieve wheel determined by the thermocouple measurement ($\Delta RH \neq 0$, $\Delta T \neq 0$ and $V_{air}=1.6m/s,$). 83

Table 4.30. Coefficients (β_1, β_2) and time constants (τ_1, τ_2) in equations (4.22) and (4.23) describing transient temperature response of a 100mm thickness silica gel wheel determined by the thermocouple measurement ($\Delta RH \neq 0$, $\Delta T \neq 0$ and $V_{air}=1.6m/s,$). 84

Table 4.31. Average coefficients describing the transient temperature response of energy wheels measured by the thermocouple. 84

Table 4.32. Transient humidity and temperature response of energy wheels. 85

Table 4.33. Uncertainty of each coefficient describing transient humidity response for the energy wheels plus the humidity/temperature transmitter. 87

Table 4.34. Uncertainty of each coefficient describing transient temperature response for the energy wheel plus humidity/temperature transmitter. 87

Table 4.35. Uncertainty of each coefficient describing transient temperature response for the energy wheel plus the thermocouple. 87

Table 4.36. Uncertainty of each coefficient describing the transient humidity response of energy wheels. 88

Table 4.37. Uncertainty of each coefficient describing the transient temperature response of energy wheels measured by the humidity/temperature transmitter. 89

Table 4.38. Uncertainty of each coefficient describing the transient temperature response of energy wheels measured by the thermocouple. 89

LIST OF FIGURES

Figure 1.1 Air-to-air energy wheel transferring heat and moisture between supply and exhaust air streams. (ASHRAE reference) 2

Figure 2.1 Photo of the test section for sensor transient calibration (with no wheel). 10

Figure 2.2 Schematic of the test facility showing the flow lines, instrumentation and test wheel. 10

Figure 2.3 Photo of the test section for energy wheel plus sensor test. 11

Figure 2.4 Schematic of the test section with its rapid tube rotation capability between the two inlets flow tubes. 12

Figure 2.5 Scheme for humidity/temperature sensors or an energy wheel test in parallel flow noting measurement locations (1-4) for temperature and humidity. 13

Figure 3.1 A dynamic system. 16

Figure 3.2 Schematic of the transmitters showing the nomenclature for the inlet (i) and outlet (o) humidity/temperature transmitters (RH, T) when they are exposed to hot (h), cold (c), humid (w) and dry (d) test conditions (a) before, and (b) after the switch. 18

Figure 3.3 Measured inlet and outlet relative humidity without a wheel for a transient change in humidity and no change in temperature ($\Delta RH \neq 0$, $\Delta T = 0$, V_{air}=1.6m/s and $\Delta t \approx 200s$). 19

Figure 3.4 Measured inlet and outlet RH without a wheel for a transient change in humidity, but no change in temperature at a flow rate of 100L/min ($\Delta RH \neq 0$, $\Delta T = 0$, V_{air}=0.8m/s). 19

Figure 3.5 Measured inlet and outlet RH without a wheel for a transient change in humidity, but no change in temperature at a flow rate of 50L/min ($\Delta RH \neq 0$, $\Delta T = 0$, V_{air}=0.4m/s). 20

Figure 3.6 Measured inlet and outlet relative humidity without a wheel for a transient change in humidity and temperature ($\Delta RH \neq 0$, $\Delta T \neq 0$, V_{air}=1.6m/s). 21

Figure 3.7 Measured inlet and outlet temperature without a wheel for a transient change in humidity and temperature ($\Delta RH \neq 0$, $\Delta T \neq 0$, V_{air}=1.6m/s). 21

Figure 3.8 Measured inlet and outlet temperature without a wheel for a transient change in temperature ($\Delta RH = 0$, $\Delta T \neq 0$, V_{air}=1.6m/s). 22

Figure 3.9 Measured inlet and outlet RH without a wheel for a transient change in constant humidity ratio ($\Delta RH \neq 0$, $\Delta T \neq 0$, $\Delta W = 0$, V_{air}=1.6m/s). 23

Figure 3.10 Measured inlet and outlet temperature without a wheel for a transient change in constant humidity ratio ($\Delta RH \neq 0$, $\Delta T \neq 0$, $\Delta W = 0$, V_{air}=1.6m/s). 23

Figure 3.11 Comparison between the measured RH of sensor $RH_{o,d}$ and correlation equation (3.1) (x_1=0.94, t_1=3.6s, x_2=0.06, t_2=110s) for $\Delta RH \neq 0$, $\Delta T = 0$ and V_{air}=1.6m/s (data from Figure 3.3). 26

Figure 3.12 Comparison between the measured RH of sensor RHo,w and correlation equation (3.2) (x_1=0.97, t_1=2.6s, x_2=0.03, t_2=250s) for $\Delta RH \neq 0$, $\Delta T=0$, V_{air}=1.6m/s (data from Figure 3.3). 26

Figure 3.13 Comparison between the measured RH of sensor $RH_{o,d}$ and correlation equation (3.1) with one time constant (x_1=1, t_1=4.3s, x_2=0) for $\Delta RH \neq 0$, $\Delta T=0$ and V_{air}=1.6m/s (data from Figure 3.3). 28

Figure 3.14 Comparison between the measured RH of sensor RHo,w and correlation equation (3.2) with one time constant (x_1=1, t_1=2.9s, x_2=0) for $\Delta RH \neq 0$, $\Delta T=0$, V_{air}=1.6m/s (data from Figure 3.3). 28

Figure 3.15 First time constant versus airflow rate for both adsorption and desorption with $\Delta RH \neq 0$ and $\Delta T=0$. 32

Figure 3.16 Comparison between the measured temperature of sensor $T_{o,c}$ and correlation equation (3.11) (y_1=0.89, t_1=65s, y_2=0.11, t_2=260s) for $\Delta RH \neq 0$, $\Delta T \neq 0$ and V_{air}=1.6m/s (data from Figure 3.7). 38

Figure 3.17 Comparison between the measured temperature of sensor $T_{o,h}$ and correlation equation (3.12) (y_1=0.93, t_1=72s, y_2=0.07, t_2=350s) for $\Delta RH \neq 0$, $\Delta T \neq 0$ and V_{air}=1.6m/s (data from Figure 3.7). 39

Figure 3.18 Comparison of measured outlet temperature without a wheel for a transient temperature response of the transmitters and the thermocouples for $\Delta RH \neq 0$, $\Delta T \neq 0$ and V_{air}=1.6 m/s. 44

Figure 3.19 Comparison of measured outlet temperature without a wheel for a transient temperature response of the transmitters and the thermocouples under $\Delta RH=0$, $\Delta T \neq 0$ and V_{air}=1.6 m/s. 45

Figure 3.20 Comparison of measured outlet temperature without a wheel for a transient temperature response of the transmitters and the thermocouples under $\Delta RH \neq 0$, $\Delta T \neq 0$, $\Delta W=0$ and V_{air}=1.6 m/s. 45

Figure 3.21 Determination of Correlation corrections for starting time based on r^2 value. 51

Figure 4.1 Measured inlet and outlet relative humidity for a molecular sieve energy wheel exposed to a step change in relative humidity with no change in temperature ($\Delta RH \neq 0$, $\Delta T=0$ and V_{air}=1.6m/s, wheel width=100mm). 54

Figure 4.2 Measured inlet and outlet relative humidity for a silica gel energy wheel exposed to a step change in relative humidity with no change in temperature ($\Delta RH \neq 0$, $\Delta T=0$ and V_{air}=1.6m/s, wheel width=100mm). 55

Figure 4.3 Measured inlet and outlet relative humidity for a molecular sieve energy wheel exposed to a step change in relative humidity and temperature ($\Delta RH \neq 0$, $\Delta T \neq 0$ and V_{air}=1.6m/s, wheel width=100mm). 56

Figure 4.4 Measured inlet and outlet temperature for a molecular sieve energy wheel exposed to a step change in relative humidity and temperature ($\Delta RH \neq 0$, $\Delta T \neq 0$ and V_{air}=1.6m/s, wheel width=100mm). 57

Figure 4.5 Measured inlet and outlet relative humidity for a silica gel energy wheel exposed to a step change in relative humidity and temperature ($\Delta RH \neq 0$, $\Delta T \neq 0$ and V_{air}=1.6m/s, wheel width=100mm). 57

Figure 4.6 Measured inlet and outlet temperature for a silica gel energy wheel exposed to a step change in relative humidity and temperature ($\Delta RH \neq 0$, $\Delta T \neq 0$ and V_{air}=1.6m/s, wheel width=100mm). 58

Figure 4.7 Comparison of the measured and correlated normalized outlet humidity for a molecular sieve wheel exposed to an increase in relative humidity ($\Delta RH \neq 0$, ΔT=0 and V_{air}=1.6m/s in Figure 4.1). 59

Figure 4.8 Comparison of the measured and correlated normalized outlet humidity decrease for a molecular sieve wheel exposed to a decrease in relative humidity ($\Delta RH \neq 0$, ΔT=0 and V_{air}=1.6m/s in Figure 4.1). 60

Figure 4.9 Comparison of measured and correlated outlet temperature increase for a molecular sieve wheel plus a humidity/temperature transmitter (Y_1=0.94, T_1=109s, Y_2=0.06, T_2=700s) ($\Delta RH \neq 0$, $\Delta T \neq 0$ and V_{air}=1.6m/s in Figure 4.4). 65

Figure 4.10 Comparison of measured and correlated outlet temperature decrease for a molecular sieve wheel plus a humidity/temperature transmitter (Y_1=0.96, T_1=120s, Y_2=0.04, T_2=390s) ($\Delta RH \neq 0$, $\Delta T \neq 0$ and V_{air}=1.6m/s in Figure 4.4). 65

Figure 4.11 Comparison of the measured outlet transient temperature response of a molecular sieve wheel plus the transmitters and the thermocouples ($\Delta RH \neq 0$, $\Delta T \neq 0$ and V_{air}=1.6m/s width=100mm,). 69

Figure 4.12 Comparison of the measured sensor response and the measured wheel plus sensor response with the predicted transient humidity response of the wheel alone for adsorption in a molecular sieve energy wheel ($\Delta RH \neq 0$, ΔT=0 and V_{air}=1.6m/s). 73

Figure 4.13 Comparison of the measured sensor response and the measured wheel plus sensor response with the predicted transient humidity response of the wheel alone for desorption in a molecular sieve energy wheel ($\Delta RH \neq 0$, ΔT=0 and V_{air}=1.6m/s). 74

Figure 4.14 Comparison of the measured sensor response and the measured wheel plus sensor response with the predicted transient humidity response of a molecular sieve energy wheel in adsorption ($\Delta RH \neq 0$, $\Delta T \neq 0$ and V_{air}=1.6m/s). 78

Figure 4.15. Comparison of the measured sensor response and the measured wheel plus sensor response with the predicted transient humidity response of in a molecular sieve energy wheel in desorption ($\Delta RH \neq 0$, $\Delta T \neq 0$ and V_{air}=1.6m/s). 78

Figure 4.16 Comparison of the measured sensor response and the measured wheel plus sensor response with the predicted transient temperature response of the wheel alone for temperature increase in a molecular sieve energy wheel ($\Delta RH \neq 0$, $\Delta T \neq 0$ and V_{air}=1.6m/s). 80

Figure 4.17 Comparison of the measured sensor response and the measured wheel plus sensor response with the predicted transient temperature response of the wheel alone for temperature decrease in a molecular sieve energy wheel ($\Delta RH \neq 0$, $\Delta T \neq 0$ and V_{air}=1.6m/s).81

NOMENCLATURE

ACRONYMS

ARI	The Air Conditioning and Refrigeration Institute
ASHRAE	American Society of Heating, Refrigerating and Air Conditioning Engineers Inc.
ASME	American Society of Mechanical Engineers
HVAC	Heating, Ventilating and Air Conditioning
RH	relative humidity
RTD	resistance temperature device
SEE	standard error of estimate
SSE	sum of squares due to error
SSM	sum of squares about mean

ENGLISH SYMBOLS

A	surface area [m^2]
B	bias error
C	a general constant
C_p	specific heat [J/ (kg.K)]
D	diameter [m]
F	transient response function of energy wheels
f	a function
h	convective heat transfer coefficient [W/ (m^2.K)]
h_m	convective mass transfer coefficient [m/s]
I	input
k	dummy variable, or coefficient in the correlation for the response of the energy wheel, or thermal conductivity [W/m.K]
L	length[m] or liter
M	mass
N	number of readings
n	number of readings or data
O	output

P precision error

p pressure [Pa]

q heat rate [W]

R ratio

r^2 coefficient of determination

S standard error of estimate, or fit standard error, or shape factor

s second, or "s" space in Laplace transformation

T temperature [K or ^oC]

TC measured temperature of thermocouple [K or ^oC]

T_1 first time constant of energy wheel plus humidity/temperature transmitter or thermocouple [s]

T_2 second time constant of energy wheel plus humidity/temperature transmitter or thermocouple [s]

t time [s], or the Student's multiplier for 95% confidence

t_1 first time constant of humidity/temperature transmitter or thermocouple [s]

t_2 second time constant of humidity/temperature transmitter or thermocouple [s]

U uncertainty

V velocity [m/s] or volume [m^3] or voltage [V]

W humidity ratio (mass of water vapour per mass of dry air) [g/kg]

w weighting factor in coefficient of determination, or center distance between two inlet or outlet air tubes [m]

X variable

X_1 weighting coefficient

X_2 weighting coefficient

x_1 weighting coefficient

x_2 weighting coefficient

Y_1 weighting coefficient

Y_2 weighting coefficient

y_1 weighting coefficient

y_2 weighting coefficient

z variable

GREEK SYMBOLS

α_1	weighting coefficient
α_2	weighting coefficient
β_1	weighting coefficient
β_2	weighting coefficient
Δ	difference
ε	porosity
τ	time constant [s]
τ_1	first time constant of energy wheel [s]
τ_2	second time constant of energy wheel [s]
Φ	relative humidity
Φ	relative humidity
θ	sensitivity coefficient in uncertainty analysis
ρ	density [kg/m^3]

SUBSCRIPTS

ads	adsorption
al	aluminium
c	cold
dec	decrease
des	desorption
e	effective
f	final condition
h	hot
i	initial condition or i=1,2,3…k
i,c	inlet cold side
i,h	inlet hot side
i,d	inlet dry side
i,w	inlet wet side
inc	increase
j	j=1,2,3…k

o	initial value
o,c	outlet cold side
o,h	outlet hot side
o,d	outlet dry side
o,w	outlet wet side
s	sensor
w	energy wheel

1. INTRODUCTION

1.1. Background

Energy wheels are typically made of a corrugated material (e.g., aluminium or plastic) that is coated with a thin layer desiccant (e.g., silica gel, molecular sieve or salts) through which supply and exhaust air flow in a counter flow arrangement. When warm moist air passes through the wheel on the supply side, the air transfers heat and moisture to the matrix, and then this heat and moisture are transferred from the matrix to the air on the exhaust side (see Figure 1.1). In this manner, the energy wheel transfers heat and moisture between the two air streams. Heat and moisture exchange using an energy wheel has been shown to be cost effective for ventilation air heat and moisture exchange in many new and retrofitted commercial buildings. For the energy cost concern, the HVAC industry has developed several ventilation air energy recovery devices, such as heat pipes, thermosiphons, and energy recovery wheels over the last two decades. Heating and cooling ventilation air often accounts for 20% to 40% of the total heating, ventilating, and air conditioning energy used in commercial buildings (Ciepliski, 1997). Architects and engineers make great efforts to reduce building energy costs, such as applying higher efficiency HVAC devices and so on. The air-to-air energy exchanger is one approach to recover energy exhausted from buildings and transfer it to the ventilation air. In recent years, energy wheels have been the most actively investigated by industry and researchers due to their ability to cost-effectively transfer both heat and moisture. This has resulted in several patents and many research papers.

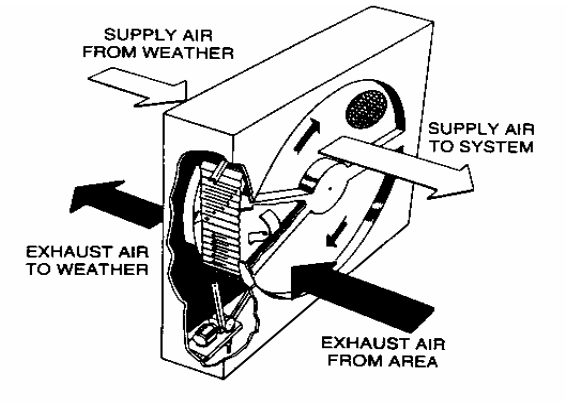

Figure 1.1 Air-to-air energy wheel transferring heat and moisture between supply and exhaust air streams. (ASHRAE HVAC Systems and Equipment, 1992)

The existing standard method of testing air-to-air energy exchangers, ASHRAE Standard 84-1991, implies that expensive laboratory equipment and a large laboratory are required to provide the large air flows, heating and cooling capacities necessary to obtain accurate test data. In the thesis work of Ciepliski (1997) and Shang (2002), this standard was followed, but the configuration of their laboratory experimental test facility was complicated. It was constructed with large air ducts, including fans, orifice plates, flow straighteners, dampers, swirl vane mixers and tracer gas ports. In the past, it took one or two people about three weeks to construct the whole experimental set-up and calibrate all the sensors. Three hours were needed to collect all experimental data for each test. All their experimental data were obtained in steady-state operating conditions. Accurate measurements of moisture transfer are difficult because the difference in supply and exhaust air absolute humidities are fairly small for ARI tests. ARI developed a certification program (ARI Test Standard 1060) based on ASHRAE Standard 84-1991. The testing and certification of commercial air-to-air energy wheels need very expensive equipment. An investment of over US$1 million in the test facility can be expected to provide the large airflows and heating and cooling capacities required to obtain accurate test data. Consequently, there are few labs that have done any testing and only one can test large equipment. Testing according to these standards is very expensive (e.g., US$5,000 per test). In order to reduce these costs and testing time and also avoid the difficulties they experienced in maintaining steady-state test conditions, a new test procedure is proposed and investigated in this thesis. The general objective of this research is to develop a small-scale test facility that can be used to accurately determine the effectiveness of large energy wheels without requiring large equipment

(fans, ducts, and heating and cooling equipment), and instrumentation systems to measure and determine the mass flow rates, bulk temperature and humidities recorded over about 30 minutes of steady-state operating conditions. Effectiveness is the most important characteristic for energy wheels. It is the main performance characteristic measured in the ASHRAE Standard and ARI Standard.

The schematic of the new test facility is much simpler than the standard one required in ASHRAE 84-1991. In the laboratory, it takes only one or two days for one person to set up the experimental equipment and one or two hours to record all the test data. The energy wheel does not rotate in the new experiment. The experimental data, such as relative humidity and temperature, are measured at inlet and outlet test sections. The inlet air conditions experience a transient step change after the equilibrium stage is reached in about 30 minutes, and the transient response of the air conditions in the outlet section are recorded. The two air streams pass through energy wheels in a parallel flow pattern. Therefore, the transient characteristics of the humidity sensors used in this new experiment are studied and the transient response of energy wheels is measured with the same sensors.

The rate of response of a temperature or humidity sensor clearly depends on the physical properties of the sensor, the physical properties of its environment, as well as the dynamical properties of its environment. The dynamic characteristics of instruments measuring the energy wheels' behaviour are to be fully investigated and understood before studying the dynamic behaviour of an energy wheel.

1.2. Research Concept

The general hypothesis of this research is that the steady-state cyclic characteristics of an energy wheel (i.e., performance characteristics such as effectiveness) will be predictable using the transient response characteristics of the wheel. The specific hypothesis of this thesis is that the humidity and temperature response of the energy wheel will require the measured transient response characteristics of the sensors used as well as the measured transient response characteristics of these same sensors downstream of an energy wheel. The expected outcome of this thesis research will be a device to achieve transient step changes in airflow properties and the methods to analyze and determine the transient response characteristics of wheels and sensors. The changes in operating conditions will be facilitated by changing the inlet temperature and

humidity conditions to the humidity sensor in a step fashion. Such a step change in operating conditions is somewhat similar to the changes that occur in a rotating energy wheel every 180 degrees of wheel rotation, where inlet conditions change every 1 to 2s for a wheel rotating at 15 to 30rpm and exposed to supply or exhaust air every half cycle.

1.3. Literature Review

Guided by the research concept, the literature on transient humidity and temperature measurement are presented in this section. Humidity measurement is the most important measurement for regenerative wheels that transfer water vapour and temperature measurement is essential when heat is transferred. Rotary regenerative heat exchangers have been in use since the 1950's. Experimental test results and numerical models of these heat exchangers have been presented in more than 30 papers (Besant 2000 and 2003, Ciepliski, 1998 and Simonson, 1999).

1.3.1. Measurement of Transient Humidity Changes

Accurate humidity measurement and control is essential in a wide range of industries including food processing and storage, fertilizer processing and storage, detergent processing and storage, horticultural and animal environments, and human environments (Ciepliski, 1997). ASHRAE Fundamentals (2001) provides an overview of humidity measurement and some of its applications.

In this research work, polymer film electronic hygrometers (capacity type humidity sensors) are used to measure transient relative humidity and temperature changes. These devices consist of a hygroscopic organic polymer deposited as a thin film on a water-permeable substrate. Both capacitance and impedance sensors are available to measure the changes in electrical properties (capacitance or resistance) caused by water vapour adsorption or desorption. These hygrometers typically have integrated circuits that provide temperature correction, signal conditioning and a display of relative and/or absolute humidity. The primary advantages of this sensor technology are small size, low cost, and good steady-state accuracy over the range of $5\%<RH<95\%$. Since other humidity measurement devices are less accurate for steady-state applications (ASHRAE Fundamentals, 2001), only one of these types of sensors will be investigated.

Several researchers for several research applications have studied the dynamic behaviour of humidity sensors. Researchers have investigated the response characteristics of sensors made of various materials with different physical geometries. These studies have shown that different humidity sensors respond to a step-like input in quite a similar fashion. Marchgraber and Grote (1963) reported that the response is characterized by a fast initial response followed by a slower drift to equilibrium. In another study on the transient behaviour of a humidity sensor, Kuse and Takahashi (2000) studied the transient behaviour of a tin oxide semiconductor humidity sensor placed inside a large vessel undergoing a step-like humidity change. They found the transitional behaviour of semiconductor sensors under a step change in humidity followed an exponential curve with two time constants. The first time constant was a few hours and the second one was at least ten times larger. In their study, the sensors were placed inside a large chamber compared to the sensor size and exposed to a maximum airflow rate of 5L/min implying that the measured time constants were most likely that of the container and not the sensor. Since the Kuse and Takahashi investigation was done under very different conditions (i.e., lower air velocity) than in many HVAC applications, a new study is needed to characterize the transient response of humidity sensors exposed to higher air velocities.

The time constant of a sensor, defined as the time necessary to reproduce 63% of its total potential reading change when subjected to a humidity step change, is approximately doubled when the sensor is protected by a dust filter, which is used for the most accurate sensors. In this case, moisture is transported in and out of space adjacent to the sensor by molecular diffusion of water vapour in air between the filter and the sensor. The time constant of the sensor is also influenced by the time necessary for the probe to adapt to temperature change in ambient temperature (Lafarie, 1985).

In some recent medical research done by Tetelin et al. (2003), a fast response humidity sensor was fabricated to equip a medical microsystem for diagnosis of pulmonary diseases. This sensor was based on a capacitor made of a divinyl siloxane benzocyclobutene (BCB) film between parallel plate electrodes. It was fabricated with compatible CMOS technology and it exhibits a short response time. Their study showed an initial rapid increase in the water adsorption in the BCB material followed by a rather slow approach to equilibrium. Their adsorption versus time curves were fitted well by an exponential correlation with two time

constants. Humidity steps from 33% to 67%RH were applied to the sensors at 40^{o}C and ambient temperature.

The above works were all done in air. The response of four different electrochemically prepared resistive conducting polymer sensors subject to exposure to various concentrations of ethanol vapour has been investigated by Ingleby et al. (1999). Their correlations for the ethanol versus time are compared with experimental results gathered when exposing the sensors to different concentrations of ethanol vapour in air at different relative humidities. For this group of polymers a double-exponential expression was used to model the generally longer time responses and the drift demonstrated during exposure. Their correlations divided the response of the sensors into two regions: the first was an initial response due to the exposure of the ethanol vapour; and the second region was a long term response either due to the ethanol vapour or of the sensor output caused by drift within the polymer.

Some other research papers have also shown that the transient response of humidity sensors can be well fitted by a double exponential model (Delpha et al. 2000).

1.3.2. Measurement of Transient Temperature Changes

There are many types of temperature sensors that are used in a wide range of applications (ASHRAE Fundamentals Handbook, 2001). Some examples are thermocouples, resistance thermometers, liquid-in-glass thermometers and radiation pyrometers. Two different temperature sensors are used in this research. One type is RTD sensor that is embedded in the humidity sensor and the other is a type-T thermocouple. Other previous research on the transient step response of temperature sensors are presented below.

Minkina (1999) recorded the step response of a NiCr-NiAl, 3mm diameter shield thermocouple during the air temperature measurement within a chamber. Minkina presented non-linear corrections to account for greater temperature changes. The non-linearity of the model was indicated by the parabolic or exponential dependence of the time constant on temperature. Minkina's experimental results confirmed that the theoretical predication of the thermocouple step responses as recorded during measurements of air temperature have a non-linear character. An identification of the nature of the non-linear heat transfer process during thermocouple unit step response measurement in an air medium is presented in Minkina's research.

A simple experimental method was developed by Shammas et al. (2002) to study the transient thermal characterization of semiconductor packages. They showed that the transient thermal response of more complex structural devices has widely separated time constants. Their results showed a very fast temperature decrease during cooling of the sensor, and these decay versus time curves were fitted well by exponential correlation equations with two time constants; the first time constant was about 0.02s and the second one was about 3s.

1.4. Research Objectives

The research objectives related to a new, small-scale test facility that is to be used with energy wheels are:

1. To develop a transient test methodology to measure the humidity and temperature downstream of an energy wheel or any other interactive device;
2. To design and construct an apparatus for this transient test;
3. To calibrate the instruments for steady-state operating conditions;
4. To test the instruments under transient operating conditions;
5. To determine the response of energy wheels to a step change in inlet air temperature and humidity using data for the transient instrument test and data from the same instrument downstream of an energy wheel;
6. To determine the uncertainty in the measured and analytically determined results.

1.5. Procedure or Methodology and Scope of Research

In this research work, a test methodology is to be developed using a small-scale test apparatus to test humidity sensors under transient operating conditions. Two energy wheels, each coated with desiccant (e.g., molecular sieve and silica gel), are to be tested using same sensors at same operating conditions. Several steps will be necessary to carry out the research to meet the objectives.

1. This research work required, as a first step, the design construction and instrumentation of a test facility that would permit a rapid step change in test conditions and the measurement of all the inlet properties and outlet temperature and humidity.

2. The second step will be the calibration of all the test sensors at equilibrium used in the test facility for steady-state conditions.
3. The third step will be the transient test of outlet humidity and temperature sensors at various conditions and correlation of the measured data along with an uncertainty analysis.
4. Two energy wheels with the same outlet sensors downstream will be tested under the same transient step change conditions, and the transient response characteristics of energy wheels alone will be derived from the measured experimental data. The uncertainties of the measured and analytical data will be determined.

The final determination of the energy wheel effectiveness from the transient response results is to be left to future work because it requires significant additional analysis of experimental data and verification with test data and numerical simulations.

This thesis is divided into five chapters and three appendices. Chapter 2 presents the new experimental test facility and instrumentation and steady-state calibration of the instruments used. The transient characteristics of the humidity sensors at various test conditions are discussed in Chapter 3. The uncertainty analysis of the test data correlations and the characteristic time constants are presented in this chapter. In Chapter 4, results are presented and discussed for the case where the same sensors are used to test two energy wheels each coated with a different desiccant. The transient response of the energy wheels is determined together with the uncertainty in wheel response. The conclusions are presented in Chapter 5 along with recommendations for future work.

2. TEST FACILITY AND INSTRUMENTATION

The process of designing a test facility to accurately test the transient response of a humidity/temperature sensor and an energy wheel begins with an apparatus that can create a step change in the inlet humidity and temperature conditions.

2.1. Design and Description of the Test Facility

A rotary switch plate was designed to allow a rapid step change switch from one set of inlet conditions to another (see Figures 2.1 and 2.2). The rotary switch plate can be operated manually by rapidly rotating two inlet tubes 180 degrees relative to the clamping plates, the energy wheel and outlet tubes which are stationary. In this way, the outlet humidity sensors and thermocouples are subject to a step change in conditions. O-ring seals are used to minimize air leakage between the inlet rotational plate and the clamping plate. Closed cell foam is used between the clamping plates and the energy wheel to prevent air leakage between the clamping plates and the energy wheel surface. Prior to each test, conditioned air is passed through the wheel for a long time (at least 30 minutes) so that the apparatus and test section would be at steady-state conditions. To initiate a transient step change in the outlet humidity, the inlet tubes are quickly rotated 180 degrees with respect to the outlet tubes. Air temperatures and humidities are measured at each inlet and outlet. The selected inlet air test conditions used in this thesis are presented in Table 2.1. Tests show that this 180 degrees rotation takes less than one second, and the step change in outlet tube humidity occurs in less than 0.2s, which is the time it takes for an inlet tube to move one diameter distance across the face of the outlet tube. The details of design are presented in Appendix A.

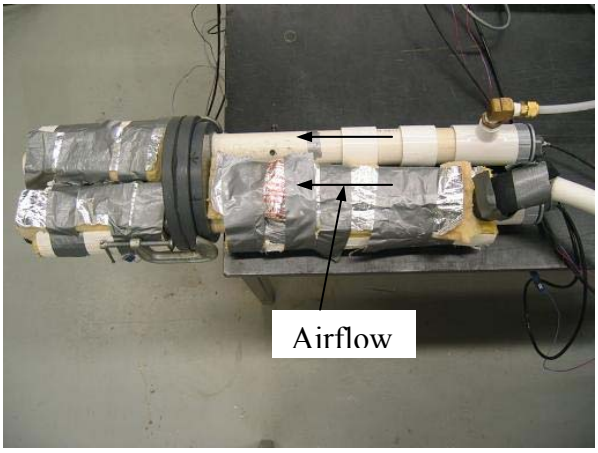

Figure 2.1 Photo of the test section for sensor transient calibration (with no wheel).

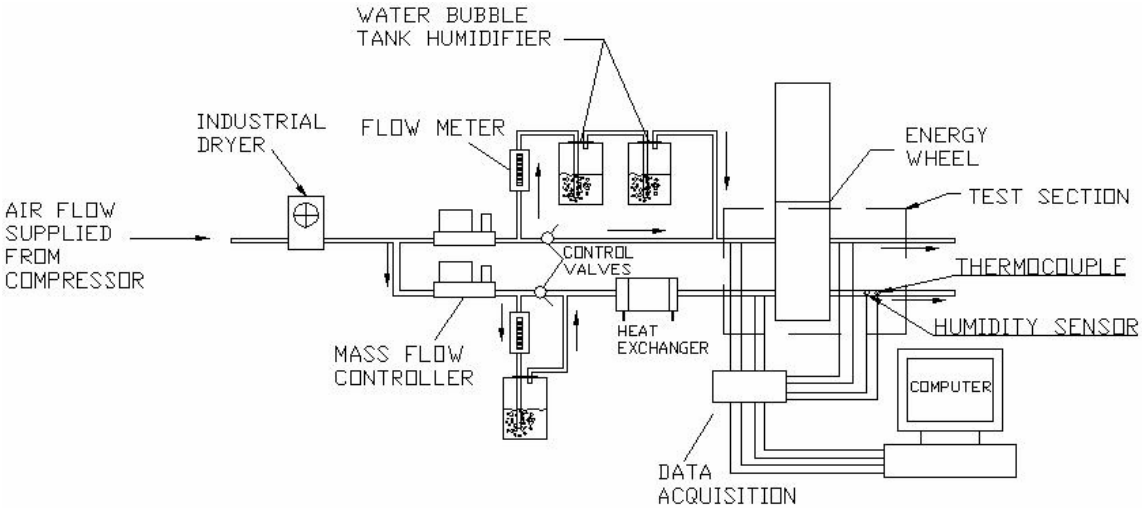

Figure 2.2 Schematic of the test facility showing the flow lines, instrumentation and test wheel.

The laboratory-experimental test facility is shown in Figure 2.2 and Figure 2.3. This test facility is significantly different than standard test facilities (e.g., ASHRAE Standard 84-1991). Testing according to ASHRAE Standard 84-1991 uses counter airflow through rotating energy wheels, while the equipment in this thesis is parallel airflow through non-rotating energy wheels.

Table 2.1. Operating conditions for the sensor or energy wheel testing.

Operating Conditions	Inlet Properties	
	Inlet #1	Inlet #2
ΔRH≠0, ΔT=0 Temperature Relative Humidity Air flow rate	≈ 23°C 3% ~ 6% 200, 100, 50L/min (V≈1.6, 0.8, 0.4m/s)	≈ 23°C 40%, 50%, 60% 200, 100, 50L/min (V≈1.6, 0.8, 0.4m/s)
ΔRH≠0, ΔT≠0 Temperature Relative Humidity Humidity Ratio Air flow rate	≈ 23°C ≈40% ≈7g/kg 200 L/min (V≈1.6m/s)	≈ 53°C ≈6% ≈5.5g/kg 200 L/min (V≈1.6m/s)
ΔRH=0, ΔT≠0 Temperature Relative Humidity Air flow rate	≈ 23°C ≈15% 200 L/min (V≈1.6m/s)	≈ 18°C, 30°C, 40°C ≈15% 200 L/min (V≈1.6m/s)
ΔRH≠0, ΔT≠0, ΔW=0 Temperature Relative Humidity Humidity Ratio Air flow rate	≈ 23°C ≈29% ≈5g/kg 200 L/min (V≈1.6m/s)	≈ 30°C, 36°C, 40°C ≈19%, 14%, 11% ≈5g/kg 200 L/min (V≈1.6m/s)

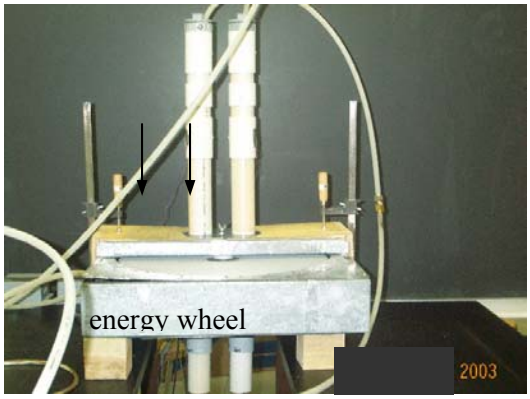

Figure 2.3 Photo of the test section for energy wheel plus sensor test.

An air compressor with a large storage tank provides air supply for the experiment. Compressed air is passed through an industrial dryer, which reduces the inlet air relative humidity to a low value, e.g., 6±1%RH. This flow is then split as in Figure 2.2 before it passes through two mass flow controllers used to get the desired dry air mass flow rate through each

tube. The maximum flow rate capacity of each mass flow controller is 200L/min with uncertainty of ±2L/min. The two air streams are humidified before they are delivered to the test section. In generating the required inlet air relative humidity for the moist air streams, three water tanks are used as shown in Figure 2.2. By regulating each flow using the bypass control valves, a portion of the dry inlet air is diverted from the main line to add a certain amount of water vapour. Recombining the humid air from the water tanks with the dry air from the compressor downstream of the control valves (Figure 2.2) results in the selected air relative humidities at each inlet flow tube. A tube-to-tube heat exchanger is used to heat or cool one of the air streams using hot water from an electrical heater or cold water directly from tap.

The test section of this experiment is shown with a wheel mounted horizontally in Figure 2.3 and without a wheel for sensor only testing in Figure 2.1. The test section is comprised of two 51mm inside diameter flow tubes (Figure 2.4) for the transmission of air at various conditions to the test section. These inlet tubes are aligned with two outlet tubes of the same size. When they are aligned about 500 flow channels (each 1 to 2mm high and 3 to 4mm wide) of a typical energy wheel allow air to flow from inlet to outlet. One of the supply inlet tubes delivers hot dry or cool humid airflow and is insulated to reduce heat loss or gain. The two outlet tubes are insulated to ensure that the properties of the air being measured are the same as the properties of the air passing through the air tubes. The other supply inlet air tube does not need to be insulated because it carries air at ambient temperature; therefore, there is minimal heat transfer between this tube and the surroundings.

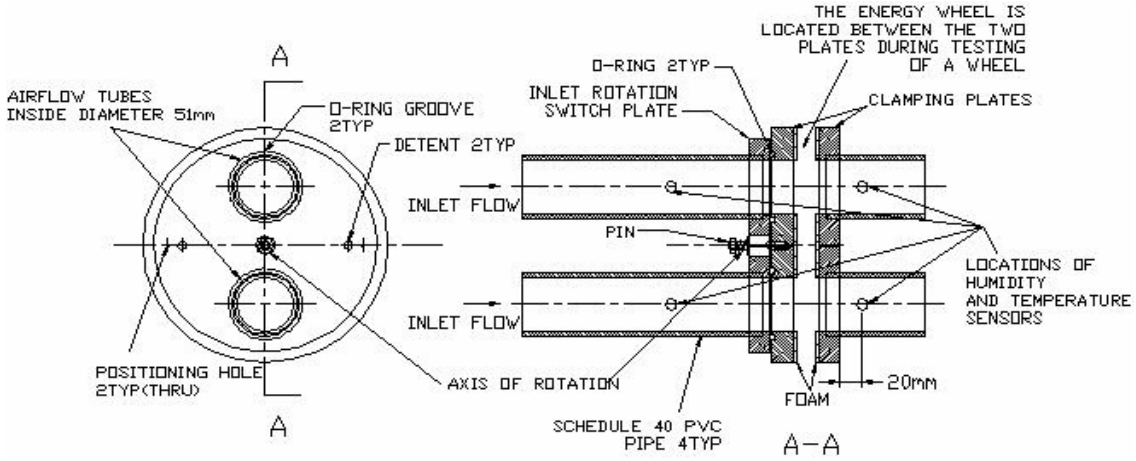

Figure 2.4 Schematic of the test section with its rapid tube rotation capability between the two inlets flow tubes.

2.2. Instrumentation and Steady-state Calibration

Experimental instrumentation is needed for four sections (Figure 2.5). Each section measures the same two quantities, temperature and relative humidity. The measurement sections shown in Figure 2.5 are:

Section 1-Supply inlet; Temperature 1, Relative humidity 1

Section 2-Supply inlet; Temperature 2, Relative humidity 2

Section 3-Exhaust outlet; Temperature 3, Relative humidity 3

Section 4-Exhaust outlet; Temperature 4, Relative humidity 4.

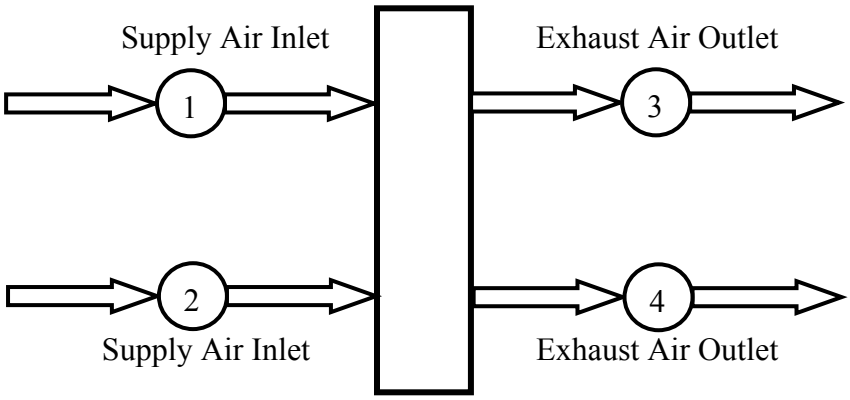

Figure 2.5 Scheme for humidity/temperature sensors or an energy wheel test in parallel flow noting measurement locations (1-4) for temperature and humidity.

2.2.1. Humidity Measurement

In this thesis, an instrument manufactured by Vaisala is used to measure relative humidity. Although, the main purpose of this instrument is to accurately measure relative humidity using a thin-film polymer sensor, the instrument also contains a RTD temperature sensor. To reflect the main function of this instrument, yet distinguish its dual function of measuring temperature and humidity, this entire instrument will be referred to as the humidity/temperature transmitter or the transmitter throughout the thesis. Therefore the humidity/temperature transmitter can measure humidity with its humidity sensor and temperature with its temperature sensor.

Humidity measurement is difficult to obtain with high accuracy because it is sensitive to temperature and airflow. The thin-film polymer humidity sensor in the humidity/temperature transmitter used in this research adsorbs or desorbs moisture with changing relative humidity.

This change in moisture content results in a change in electrical capacitance or impedance. Factory calibration relates capacitance to relative humidity and the sensor outputs 0 to 1V representing 0 to 100%RH. As noted previously, the humidity/temperature transmitter also includes a temperature sensor and can therefore simultaneously measure temperature and relative humidity. The accuracy of relative humidity measurement was claimed by Vaisala to be ±1%RH when used between 0 and 90%RH and ±2%RH when used between 90 and 100%RH. Vaisala lists the response time for 90% of at 20^{o}C in still air with a dust filter as 15 seconds.

Steady-state calibration is required for the humidity/temperature transmitters. Sensor calibration at equilibrium is necessary to determine the bias error of the transmitters at outlet section, which will be used in the uncertainty analysis. The steady-state calibration is performed with a chilled mirror sensor with a bias uncertainty of ±0.3^{o}C in dew point and ±1%RH at 20^{o}C. The steady-state calibration results are presented in Table 2.2 and they show that, after calibration, the bias uncertainties of these outlet tube transmitters are ±1.8%RH. Calibration is done for the transmitters in the range of 10% to 95%RH. The steady state calibration of each transmitter is done before and after the whole set of transient test and shows that there is essentially no change between calibrations.

Table 2.2. Steady state RH calibration for two outlet transmitters.

Chilled Mirror Sensor Reading (%)	Sensor Reading (%)	
	Sensor #A	Sensor #B
10.5	10.4	10.6
21.7	20.6	20.8
32.3	31.1	31.2
41.1	41.0	41.0
52.0	52.4	52.2
62.5	62.9	63.1
71.7	72.9	73.0
83.2	83.8	84.0
94.6	94.3	95.4

2.2.2. Temperature Measurement

Temperature is measured using both the RTD temperature sensor in the humidity/temperature transmitter and a T-type thermocouple. Previous calibration results in a

thermocouple indicated an uncertainty of ±0.1°C when the thermocouple wire is from the same roll. The RTD temperature sensors at outlet section are calibrated at steady-state condition using a dry-well calibrator with the accuracy of ±0.1°C. The steady-state calibration results are presented in Table 2.3. It is found that the bias uncertainties of these outlet tube sensors are ±3.0°C after calibration, and the bias uncertainty of these RTD temperature sensors at room temperature (20°C) is less than ±0.3°C. For most experiments operating at room temperature, the bias uncertainty is not significant for these outlet tube RTD temperature sensors.

Table 2.3. Steady-state temperature calibration for two outlet transmitters.

Calibrator Reading (°C)	Sensor Reading (°C)	
	Sensor #A	Sensor #B
-18.0	-16.2	-16.5
-10.0	-8.5	-8.9
0.0	0.8	0.6
10.0	10.7	10.2
20.0	19.7	19.7
30.0	29.3	29.3
40.0	38.9	39.0
50.0	48.5	48.7

The comparison of the two different types of temperature sensor measurement is made in Section 3.2.3. The locations of transmitters and thermocouples in the ducting for both the inlet and outlet sections are shown in Figure 2.2.

2.3. Data Acquisition

Experimental data are recorded using a computer data acquisition system with the resolution of 12 bits. Measurement signals from eight sensors are digitally converted using Sciemetric Instruments Labmate data acquisition and controller and stored on a Compaq Pentium computer using Maximon data acquisition software. The signals need to be collected are: 4 humidity signals and 8 temperature signals.

The hardware connection of the instrument and the data collection computer is done via a Labmate data acquisition board. The thermocouples are connected directly to the data board, while the humidity sensors are connected through copper paired cable.

3. TRANSIENT SENSOR RESPONSE AND DATA ANALYSIS

The word *dynamic* implies change with time. Figure 3.1 shows a schematic of a dynamic system with time variable inputs and outputs. For a heat exchanger or an energy wheel, the input variables would include fluid temperature, pressure and velocity. The temperature, humidity, heat transfer rate, pressure drop could be selected as the outputs. In this thesis, only the temperature and humidity are measured as inputs and outputs.

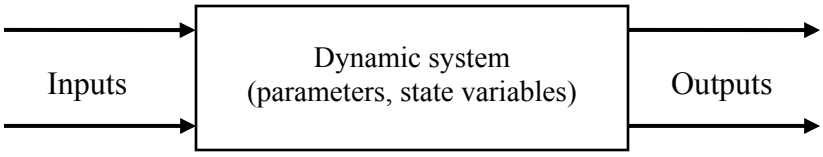

Figure 3.1 A dynamic system.

The objective of system analysis is to predict relevant performance characteristics of a system operating under specified input conditions. The type of input signal used in this research is a step function because it is one of the simplest types of inputs and because test results can be obtained very rapidly. It is also the type of disturbance caused by the steady rotation of a wheel as it cyclically switches from exhaust air to supply air exposure. To investigate the dynamic behaviour of an energy wheel, the dynamic characteristics of temperature and humidity sensors used to measure the outputs need to be studied first. In this chapter, the transient relative humidity and temperature response of the humidity/temperature transmitter are measured under various operating conditions. The transient temperature response of the thermocouples is also investigated under the same conditions to compare with the transient temperature response of the humidity/temperature transmitter. Theoretical correlations are determined to describe the transient response of these sensors, and it is discovered that the correlations fit very well with experimental data. The statistical average value of each coefficient in the theoretical correlations is calculated and their uncertainties are analyzed.

3.1. Transient Response of the Humidity/Temperature Transmitter

The transient response characteristics of the transmitter is given by its time constants for a given step change input. Any recorded humidity data that show significant changes with time must be corrected for the transient response characteristics of the humidity/temperature transmitters. The inlet transmitters are not exposed to transient property changes during the tests. The apparatus is operated at steady-state conditions for about 30 minutes prior to each test. This preconditioning period ensures that the entire facility (transmitters, tubes and the energy wheel) has reached steady state before the step change is introduced. Transient response testing of the outlet transmitters is done using the test section configuration shown in Figure 2.1 with no wheel. In this arrangement, the outlet conditions will change within 0.2s or less when the switch is done because the inlet and outlet lines are directly connected very rapidly. Therefore, the humidity/temperature transmitters in the outlet ducts will be subject to a nearly perfect step change.

Before presenting the measured results, the nomenclature used to represent the data measured by the inlet and outlet humidity/temperature transmitters must be established. During the preconditioning period (Figure 3.2(a)), the inlet (i) and outlet (o) transmitters are preconditioned to humid (w), cold(c) and dry (d), hot (h) conditions. Therefore, just before the switch the humidity reading from the humidity sensor in the humid inlet ($RH_{i,w}$) will equal the reading of the sensor in the humid outlet ($RH_{o,w}$). Similarly, $RH_{i,d}=RH_{o,d}$, $T_{i,c}=T_{o,c}$ and $T_{i,h}=T_{o,h}$ prior to the switch. Therefore, outlet transmitters are labelled according to the conditions that they are preconditioned (i.e., $RH_{o,d}$ represents the outlet humidity sensor that is preconditioned with dry air before the switch).

After the switch, the outlet sensors are interchanged so that they experience a step change (Figure 3.2(b)). For the example in Figure 3.2, the outlet humidity/temperature transmitter that is preconditioned with dry and hot air ($RH_{o,d}$, $T_{o,h}$) is exposed to the humid and cold inlet conditions ($RH_{i,w}$, $T_{i,c}$) and thus $RH_{o,d}$ will increase and $T_{o,h}$ will decrease with time after the switch. Similarly, the outlet transmitter that is humid and cold ($RH_{o,w}$, $T_{o,c}$) before the switch is exposed to dry and hot inlet conditions ($RH_{i,d}$, $T_{i,h}$) after the switch. When presenting the measured results of the inlet and outlet sensors in this thesis, a schematic of the test conditions that exist after the switch, as in Figure 3.2(b), will be included to clarify the test conditions.

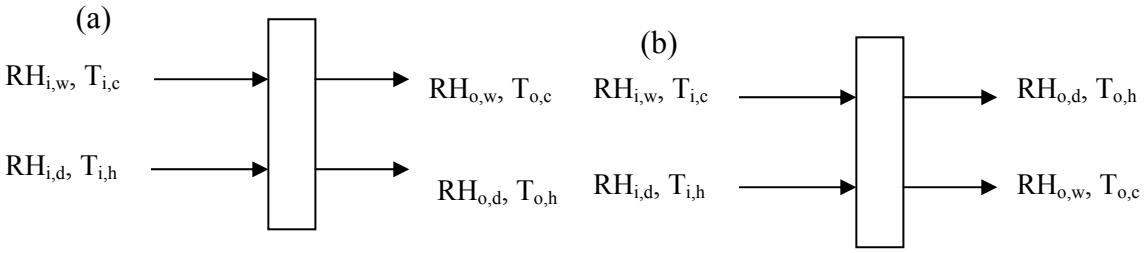

Figure 3.2 Schematic of the transmitters showing the nomenclature for the inlet (i) and outlet (o) humidity/temperature transmitters (RH, T) when they are exposed to hot (h), cold (c), humid (w) and dry (d) test conditions (a) before, and (b) after the switch.

3.1.1. Humidity Change Only ($\Delta RH \neq 0$, $\Delta T = 0$)

The transient response of the outlet humidity/temperature transmitters are measured for several step changes in relative humidity, such as 60%, 50% and 40%RH, while the airflow is close to room conditions, e.g., 23°C. The dry side is always at 6±1%RH. In these tests, one transient switch could be made every 30 to 40 minutes. Figure 3.3 shows the measured transmitters' response profile for one typical step change from 6% to 40%RH in about 2 minutes. After the switch, the transmitter, $RH_{o,w}$, undergoes a decrease in humidity or desorption and the transmitter, $RH_{o,d}$, undergoes an increase in humidity or adsorption and they approach very quickly to the inlet humidity conditions, $RH_{i,d}$ and $RH_{i,w}$. In Figure 3.3, the transmitter, $RH_{o,d}$, indicates 39%RH 2 minutes after the switch, while the transmitter, $RH_{o,w}$, indicates 6%RH or the inlet condition 2 minutes after the switch. All tests are done three times at each testing condition as given in Table 2.1. The time zero in Figures 3.3 to 3.10 is the time to start to record experimental data, and the 180 degrees switch is made in a few seconds after the data was started to be recorded.

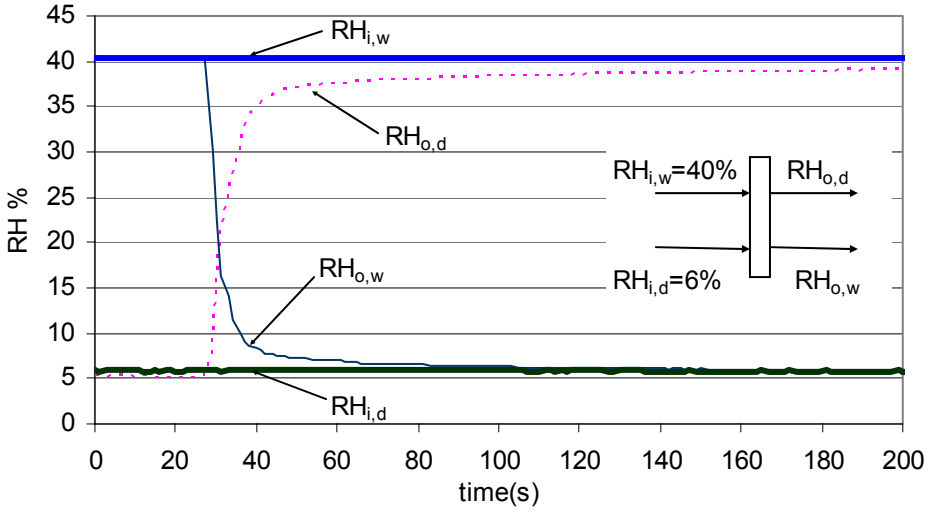

Figure 3.3 Measured inlet and outlet relative humidity without a wheel for a transient change in humidity and no change in temperature ($\Delta RH \neq 0$, $\Delta T=0$, V_{air}=1.6m/s and $\Delta t \approx 200$s).

Figures 3.4 and 3.5 show relative humidity step change from 6% to 40% at half of the airflow rate (100L/min, V_{air}=0.8m/s) and one quarter of the airflow rate (50L/min, V_{air}=0.4m/s) of the previous test (200L/min, V_{air}=1.6m/s).

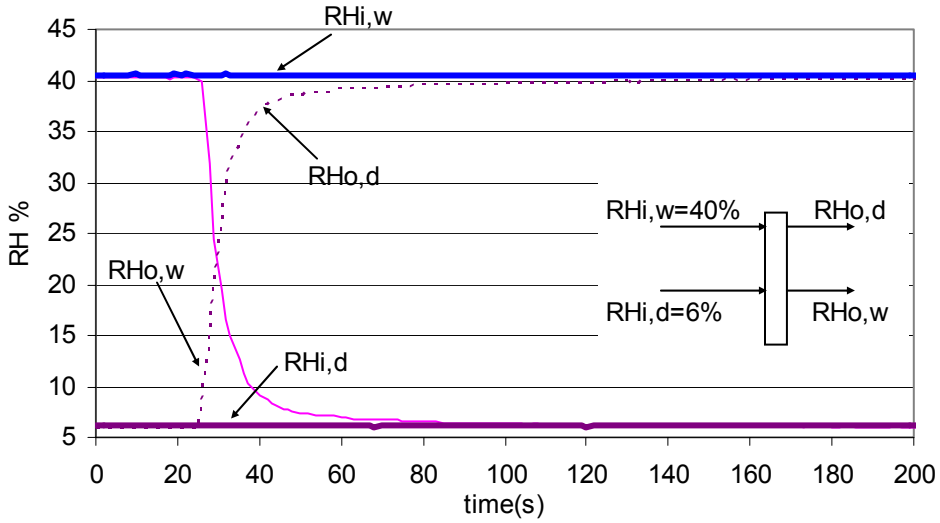

Figure 3.4 Measured inlet and outlet RH without a wheel for a transient change in humidity, but no change in temperature at a flow rate of 100L/min ($\Delta RH \neq 0$, $\Delta T=0$, V_{air}=0.8m/s).

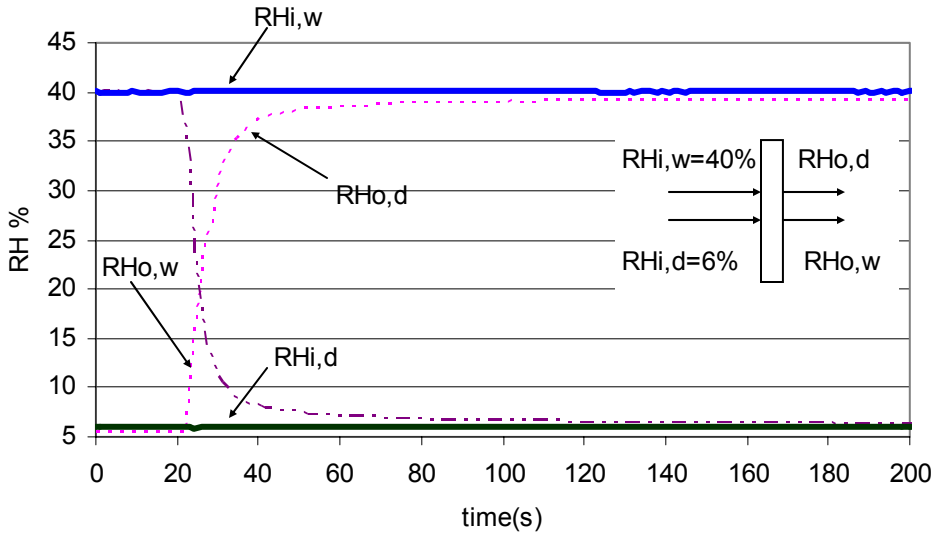

Figure 3.5 Measured inlet and outlet RH without a wheel for a transient change in humidity, but no change in temperature at a flow rate of 50L/min ($\Delta RH \neq 0$, $\Delta T = 0$, $V_{air} = 0.4$m/s).

It appears that there is no significant difference between Figures 3.3, 3.4 and 3.5, which indicates that the transient response of the transmitters is not sensitive to air flow rate in the range tested.

3.1.2. Humidity and Temperature Change ($\Delta RH \neq 0$, $\Delta T \neq 0$)

In this section, transient response of the outlet transmitters is presented for step changes in both the temperature and relative humidity. Figures 3.6 to 3.7 present the humidity sensor data with $\Delta RH \neq 0$ and $\Delta T \neq 0$, which is presented in Table 2.1.

Comparing Figure 3.6 with Figure 3.3 shows that the humidity transmitter responds much slower when there is a temperature change ($\Delta T \neq 0$) than when there is no temperature change ($\Delta T = 0$).

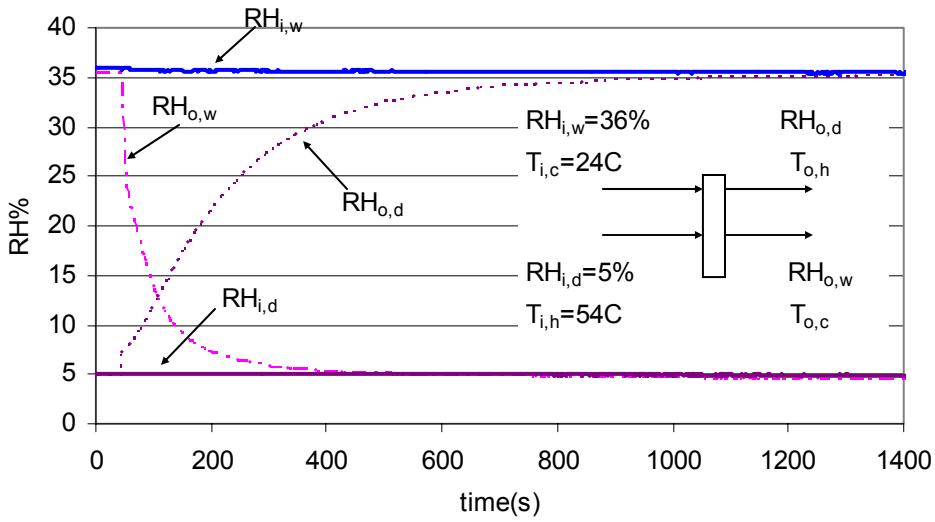

Figure 3.6 Measured inlet and outlet relative humidity without a wheel for a transient change in humidity and temperature (ΔRH≠0, ΔT≠0, V_{air}=1.6m/s).

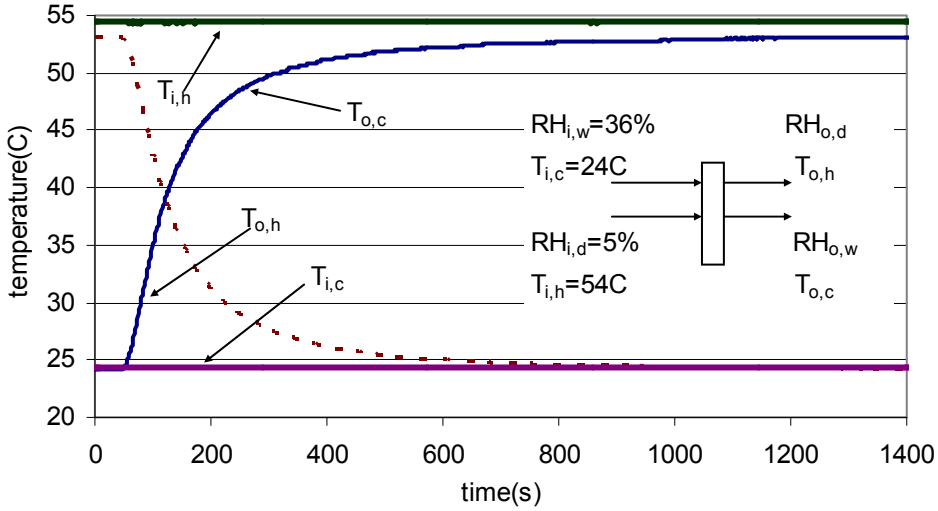

Figure 3.7 Measured inlet and outlet temperature without a wheel for a transient change in humidity and temperature (ΔRH≠0, ΔT≠0, V_{air}=1.6m/s).

3.1.3. Temperature Change Only (ΔRH=0 and ΔT≠0)

Based on the above data for the test condition, ΔRH≠0 and ΔT≠0, the response of the temperature sensor in humidity/temperature transmitter appears to have a large time constant. Therefore this sensor needs to be further investigated during a step change in temperature alone with no relative humidity change (ΔRH=0 and ΔT≠0) to check its dynamic behaviour. Figure 3.8

indicates a typical temperature response (from 21°C to 30°C) for these conditions (ΔRH=0 and ΔT≠0).

Figure 3.8 shows the response of the transmitters to a step change in temperature is quite similar to that the temperature response in Figure 3.7. The time constants of these temperature response and comparisons are presented in Section 3.2.3 and show that they have very similar transient behaviour even when the humidity is changed.

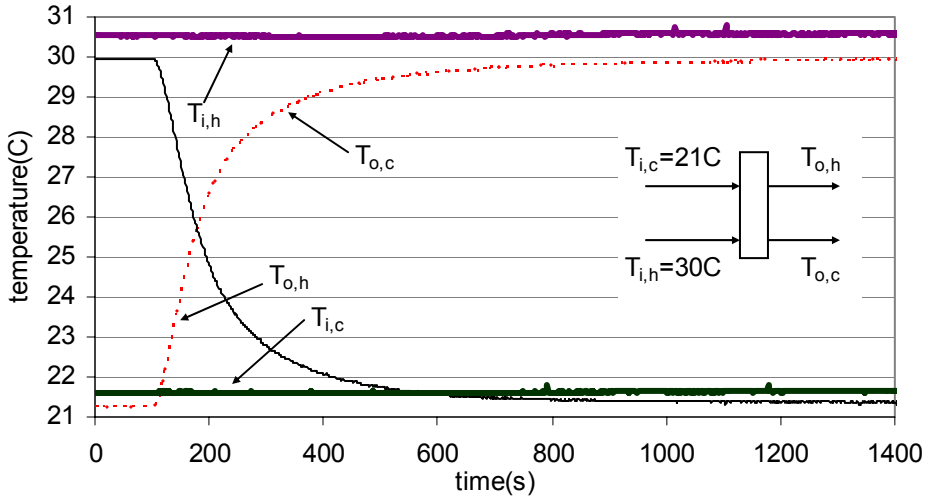

Figure 3.8 Measured inlet and outlet temperature without a wheel for a transient change in temperature (ΔRH=0, ΔT≠0, V_{air}=1.6m/s).

3.1.4. Conditions with Constant Humidity Ratio (ΔW=0)

To further explore transient performance of the transmitter, test conditions with ΔRH≠0, ΔT≠0 and ΔW=0 are also investigated in this research work. Condition ΔRH≠0, ΔT≠0 and ΔW=0 has both temperature and humidity changes but a constant humidity ratio of about 5g/kg. Figure 3.9 presents a typical measured relative humidity response at condition ΔRH≠0, ΔT≠0 and ΔW=0, which inlet conditions are $T_{i,c}$=24°C, $RH_{i,w}$=27% and $T_{i,h}$=40°C, $RH_{i,d}$=11%. The measured temperature response is shown in Figure 3.10.

Figures 3.9 and 3.10 indicate that measured the temperature and humidity dynamic response for ΔRH≠0, ΔT≠0 and ΔW=0 are very similar with their response with the other conditions (e.g., ΔRH≠0, ΔT≠0 and ΔRH=0, ΔT≠0). The detailed results will be discussed in following sections.

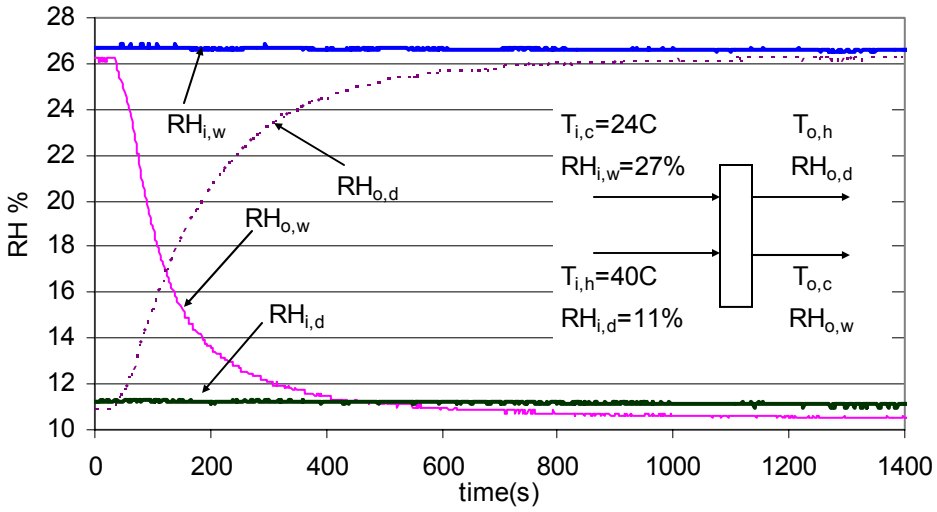

Figure 3.9 Measured inlet and outlet RH without a wheel for a transient change in constant humidity ratio ($\Delta RH \neq 0$, $\Delta T \neq 0$, $\Delta W = 0$, V_{air}=1.6m/s).

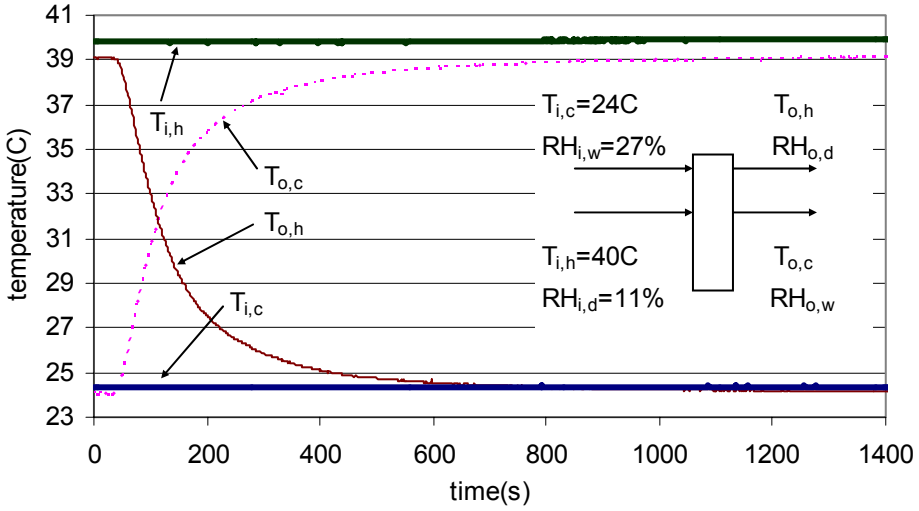

Figure 3.10 Measured inlet and outlet temperature without a wheel for a transient change in constant humidity ratio ($\Delta RH \neq 0$, $\Delta T \neq 0$, $\Delta W = 0$, V_{air}=1.6m/s).

3.2. Transient Data Correlation

Figures 3.3 to 3.10 show that the output of the outlet humidity/temperature transmitters ($RH_{o,d}$, $RH_{o,w}$, $T_{o,c}$ and $T_{o,h}$) are not instantaneous changes, even though the inlet air humidity and temperature change in a step fashion. The thermal time constant for a solid may be expressed as

$\tau = \frac{\rho V c_p}{hA}$, which is associated with the density, physical volume, surface area and specific heat capacity of the solid, and also convection heat transfer between the solid and its surrounding air. The outlet relative humidity also shows an exponential increase or decrease, which is due to the moisture capacity and diffusion resistance of the sensing material and the air surrounding the sensor. For an inlet humidity step change, two time constants are observed to give good correlations for both humidity increase and decrease as will be described in the next Section (3.2.1). For the moisture transfer, the first time constant, $t = \frac{M}{A\ h_m}$, is always the most important and it is thought to be a consequence of air diffusion resistance. The correlations in Section 3.2.1 show that the second time constant is at least an order of magnitude greater than the first one perhaps because of a slow diffusion process of water molecules into the transmitter as the transmitter approaches equilibrium. Time constants for humidity/temperature transmitters are to be determined by correlation using the exponential equations (3.1) and (3.2) for adsorption and desorption. The correlations equations that best represent the transmitter response to inlet humidity step change are presented in the Section (3.2.1).

3.2.1. Transient Relative Humidity Data Correlation

Moisture adsorption into the transmitter from the air (i.e., increasing relative humidity) is assumed to follow the correlation equation:

$$\frac{\Delta\phi_s}{\Delta\phi_{so}}(t)_{ads} = x_1(1-e^{-t/t_1}) + x_2(1-e^{-t/t_2})\,. \tag{3.1}$$

For moisture desorption from the transmitter into the air (i.e., decreasing relative humidity) the correlation equation is:

$$\frac{\Delta\phi_s}{\Delta\phi_{so}}(t)_{des} = 1 - \frac{\Delta\phi}{\Delta\phi_o}(t)_{ads} = x_1 e^{-t/t_1} + x_2 e^{-t/t_2}\,, \tag{3.2}$$

where the coefficients x_1 and x_2 satisfy the same constraint equation for both adsorption and desorption:

$$x_1 + x_2 = 1,\ x_1 \geq 0\ , x_2 \geq 0, \tag{3.3}$$

but with different values for each case. Other symbols are:

$\Delta\phi_s$ =change in relative humidity = $|\phi_s - \phi_{si}|$, where ϕ_{si} is the initial condition;

$\Delta\phi_{so}$ = maximum change in relative humidity = $|\phi_{sf} - \phi_{si}|$, where ϕ_{sf} is the final condition; and t_1 and t_2 are the first and second time constants respectively.

Figure 3.11 and Figure 3.12 show that the measured data agrees very well with the correlation data for one typical test for ΔRH≠0 and ΔT=0. The time zero in Figures 3.11 and 3.12 is not the time zero showing in previous Figures 3.3 to 3.10, it is the time point when 180 degrees switch is made. The value of each coefficient, x_1, x_2, t_1 and t_2, is obtained using a computer software, TableCurve, for both adsorption and desorption and are summarized in Tables 3.1 and 3.2. The time constants do not seem to depend on the magnitude of the step change. For every case, the r^2 values are greater than 0.978. The r^2 coefficient of determination is the most commonly used goodness of fit measure for curve-fitting data. It is TableCurve's default and defined as follows:

$$r^2 = 1 - \frac{SSE}{SSM}, \tag{3.4}$$

where $SSE = \sum_{i=1}^{n} w_i (\hat{z}_i - z_i)^2$, and (3.5)

$$SSM = \sum_{i=1}^{n} w_i (z_i - \bar{z})^2 . \tag{3.6}$$

SSE is the actual least-squares measure of fit. The weighting factor (w_i) is determined from the sum of the squared residuals. The z_i is the measured data and the estimated value of z_i value is $\hat{z}_i$. In the SSM calculation, $\bar{z}$ is the mean of all the z_i data. In equations (3.5) and (3.6), n is the total number of data points. As the value of r^2 approaches 1.0 the fit is considered to be good while a value close to zero indicate a very poor fit. In this research work the number of data points use for each correlation was 1800 unless stated otherwise.

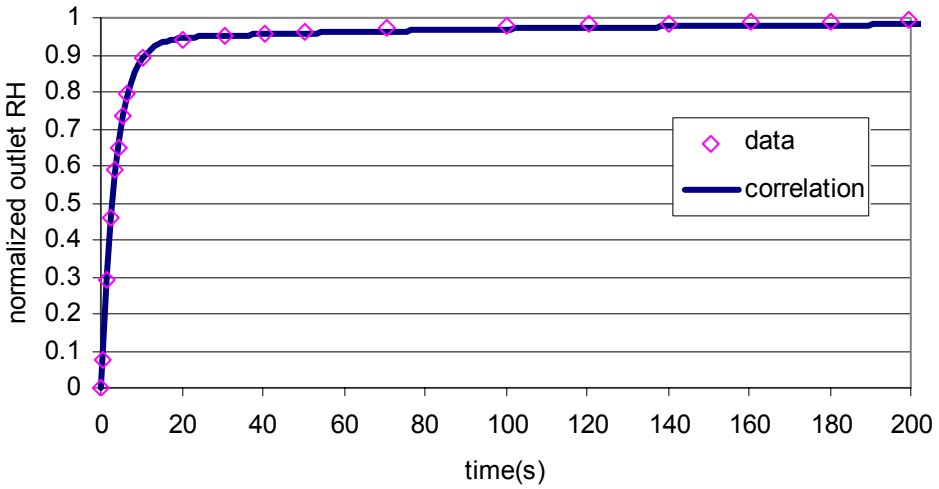

Figure 3.11 Comparison between the measured RH of sensor $RH_{o,d}$ and correlation equation (3.1) (x_1=0.94, t_1=3.6s, x_2=0.06, t_2=110s) for $\Delta RH \neq 0$, ΔT=0 and V_{air}=1.6m/s (data from Figure 3.3).

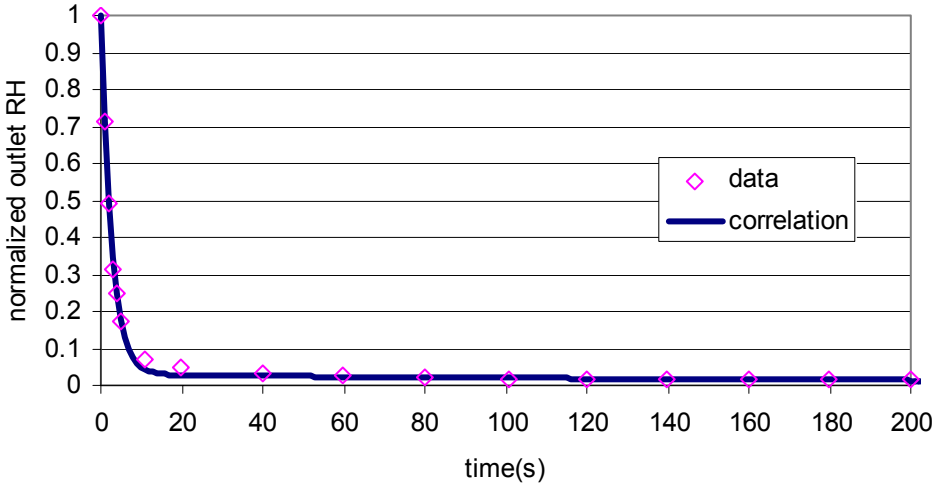

Figure 3.12 Comparison between the measured RH of sensor RHo,w and correlation equation (3.2) (x_1=0.97, t_1=2.6s, x_2=0.03, t_2=250s) for $\Delta RH \neq 0$, ΔT=0, V_{air}=1.6m/s (data from Figure 3.3).

Table 3.1. Adsorption coefficients (x_1, x_2) and time constants (t_1, t_2) in equation (3.1) that describe the transient humidity response of the humidity/temperature transmitter with $\Delta RH \neq 0$, ΔT=0, V_{air}=1.6m/s during three trials at different wet side humidity conditions.

Inlet conditions	x_1	t_1(s)	x_2	t_2(s)	r^2
dry side: $T_{i,d}$≈23°C, $\Phi_{i,d}$≈6% wet side: $T_{i,w}$≈ 23°C, $\Phi_{i,w}$≈40%	0.94	3.6	0.06	110	0.983
	0.96	2.8	0.04	70	0.987
	0.89	3.2	0.11	100	0.991
dry side: $T_{i,d}$≈23°C, $\Phi_{i,d}$≈6% wet side: $T_{i,w}$≈ 23°C, $\Phi_{i,w}$≈50%	0.95	3.5	0.05	105	0.990
	0.94	3.2	0.06	95	0.978
	0.90	3.0	0.10	80	0.994
dry side: $T_{i,d}$≈23°C, $\Phi_{i,d}$≈6% wet side: $T_{i,w}$≈ 23°C, $\Phi_{i,w}$≈60%	0.92	3.6	0.08	90	0.995
	0.88	2.4	0.12	75	0.998
	0.85	2.9	0.15	90	0.995

Table 3.2. Desorption coefficients (x_1, x_2) and time constants (t_1, t_2) in equation (3.2) that describe the transient humidity response of the humidity/temperature transmitter with $\Delta RH \neq 0$, $\Delta T=0$, V_{air}=1.6m/s during three trials at different wet side humidity conditions.

Inlet conditions	x_1	t_1(s)	x_2	t_2(s)	r^2
dry side: $T_{i,d}$≈23°C, $\Phi_{i,d}$≈6% wet side: $T_{i,w}$≈ 23°C, $\Phi_{i,w}$≈40%	0.97	2.6	0.03	250	0.988
	0.97	3.0	0.03	430	0.993
	0.96	2.9	0.04	260	0.990
dry side: $T_{i,d}$≈23°C, $\Phi_{i,d}$≈6% wet side: $T_{i,w}$≈ 23°C, $\Phi_{i,w}$≈50%	0.97	2.2	0.03	280	0.992
	0.97	2.7	0.03	190	0.992
	0.97	2.9	0.03	380	0.992
dry side: $T_{i,d}$≈23°C, $\Phi_{i,d}$≈6% wet side: $T_{i,w}$≈ 23°C, $\Phi_{i,w}$≈60%	0.96	2.3	0.04	140	0.994
	0.95	2.4	0.05	100	0.996
	0.96	2.8	0.04	180	0.990

To investigate the goodness of the experimental data agree with the correlation data with only one time constant, x_1 is set as 1 and x_2 is set as 0 in equations (1) and (2). It is found that the measured data do not agree with the correlation data as well for $\Delta RH \neq 0$ and $\Delta T=0$ because r2 is much lower with this correlation. Figures 3.13 and 3.14 show one typical test data set for both adsorption and desorption, r^2 is found to be 0.92. Therefore, the transient response of the sensor is correlated using by equations (1) and (2) with two time constants.

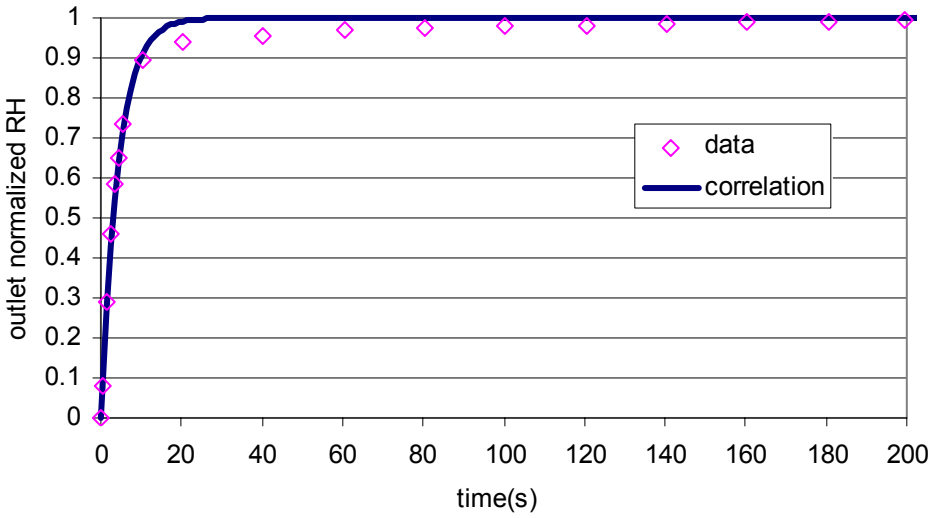

Figure 3.13 Comparison between the measured RH of sensor $RH_{o,d}$ and correlation equation (3.1) with one time constant (x_1=1, t_1=4.3s, x_2=0) for $\Delta RH \neq 0$, ΔT=0 and V_{air}=1.6m/s (data from Figure 3.3).

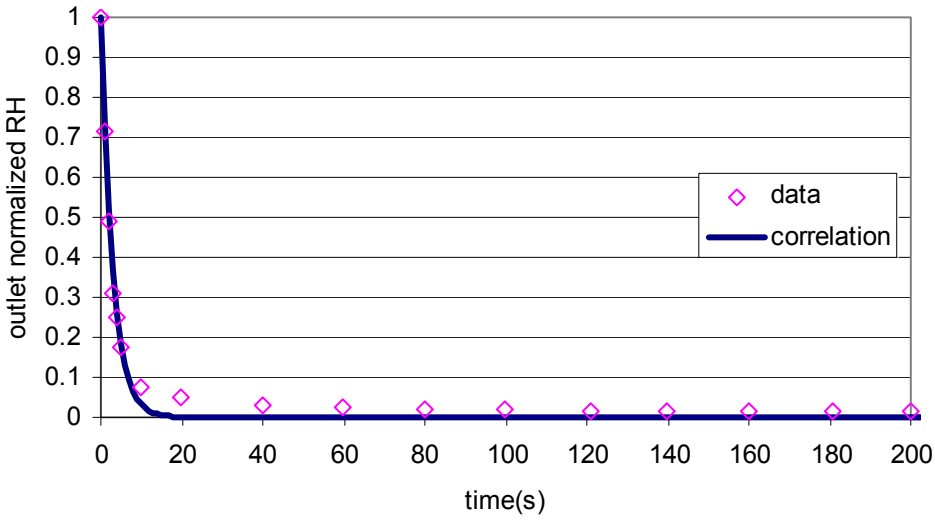

Figure 3.14 Comparison between the measured RH of sensor RHo,w and correlation equation (3.2) with one time constant (x_1=1, t_1=2.9s, x_2=0) for $\Delta RH \neq 0$, ΔT=0, V_{air}=1.6m/s (data from Figure 3.3).

Based on the information in Tables 3.1 and 3.2, it is discovered that the humidity/temperature transmitter responds quickly to a relative humidity step change. The first time constant is usually less than 4s in adsorption and less than 3s in desorption. It takes the transmitter about 15~20s (5 times the first time constant) to reach about 90% of the total step

change, which is quite similar with quotation by the manufacturer. It also shows that the first time constant plays the most important role in humidity response.

Comparing the results in Tables 3.1 and 3.2 shows that the constant coefficients (x_1, x_2) change by a maximum 0.12. The first coefficient (x_1) is larger than 0.9 and x_2 is less than 0.1 for most cases. The second time constant is much greater than the first time constant. The average value of the time constants and coefficients are needed to describe a generalized expression for the transmitter's response and it will be determined later by using the data in these tables. The results in Tables 3.1 and 3.2 confirm that the transmitter responds faster when moisture is released from the transmitter than when moisture is adsorbed in the transmitter. The results also show that the coefficients (x_1, x_2) and time constants (t_1, t_2) are nearly the same regardless of the inlet humidity.

To investigate the sensitivity of the coefficients to the test time, each coefficient, x_1, x_2, $t_1$and t_2, is determined using data over the time of $0 \le t \le 5$s, $0 \le t \le 10$s and $0 \le t \le 20$s. Table 3.3 and Table 3.4 gives one typical example of the coefficients in the three different time intervals for $\Delta RH \neq 0$, $\Delta T = 0$.

Table 3.3. Adsorption coefficients (x_1, x_2) and time constants (t_1, t_2) in equation (3.1) that describe the transient humidity response of the humidity/temperature transmitter with $\Delta RH \neq 0$, $\Delta T = 0$, V_{air}=1.6m/s during three time intervals with one wet side humidity condition.

Inlet conditions: dry side: $T_{i,d} \approx 23^oC$, $\Phi_{i,d} \approx 6\%$ wet side: $T_{i,w} \approx 23^oC$, $\Phi_{i,w} \approx 40\%$	x_1	t_1(s)	x_2	t_2(s)	r^2
$0 \le t \le 5$s	0.89	3.0	0.11	3.0	0.997
$0 \le t \le 10$s	0.97	2.8	0.03	6870	0.998
$0 \le t \le 20$s	0.96	2.8	0.04	1E20	0.999

Table 3.4. Desorption coefficients (x_1, x_2) and time constants (t_1, t_2) in equation (3.2) that describe the transient humidity response of the humidity/temperature transmitter with $\Delta RH \neq 0$, $\Delta T = 0$, V_{air}=1.6m/s during three time intervals with one wet side humidity condition.

Inlet conditions: dry side: $T_{i,d} \approx 23^oC$, $\Phi_{i,d} \approx 6\%$ wet side: $T_{i,w} \approx 23^oC$, $\Phi_{i,w} \approx 40\%$	x_1	t_1(s)	x_2	t_2(s)	r^2
$0 \le t \le 5$s	0.96	2.5	0.04	2E23	0.998
$0 \le t \le 10$s	0.97	2.5	0.03	8E19	0.995
$0 \le t \le 20$s	0.93	2.3	0.07	75	0.999

Comparing the data in Tables 3.1 and 3.2 with the data in Tables 3.3 and 3.4 indicates that the first time constant does not change significantly when the time interval (or test time) changes. The first time constant is the most important because its associated coefficient, x_1, is greater than 0.90 in most cases.

To study the sensitivity of the transmitter response to variations in the airflow rate for $\Delta RH \neq 0$, $\Delta T = 0$, the transient response coefficients are presented in Tables 3.5 to 3.8 for the airflow rates of 100L/min (V_{air}=0.8m/s) and 50L/min (V_{air}=0.4m/s).

Table 3.5. Adsorption coefficients (x_1, x_2) and time constants (t_1, t_2) in equation (3.1) that describe the transient humidity response of the humidity/temperature transmitter with $\Delta RH \neq 0$, $\Delta T = 0$, V_{air}=0.8m/s during three trials at different wet side humidity conditions.

Inlet conditions	x_1	t_1(s)	x_2	t_2(s)	r^2
dry side: $T_{i,d} \approx 23^oC$, $\Phi_{i,d} \approx 6\%$ wet side: $T_{i,w} \approx 23^oC$, $\Phi_{i,w} \approx 40\%$	0.96	3.7	0.04	160	0.993
	0.97	5.1	0.03	360	0.988
	0.93	3.1	0.07	100	0.994
dry side: $T_{i,d} \approx 23^oC$, $\Phi_{i,d} \approx 6\%$ wet side: $T_{i,w} \approx 23^oC$, $\Phi_{i,w} \approx 50\%$	0.96	5.3	0.04	210	0.989
	0.95	3.8	0.05	130	0.996
	0.94	3.0	0.06	100	0.996
dry side: $T_{i,d} \approx 23^oC$, $\Phi_{i,d} \approx 6\%$ wet side: $T_{i,w} \approx 23^oC$, $\Phi_{i,w} \approx 60\%$	0.94	3.8	0.06	130	0.993
	0.94	3.7	0.06	120	0.992
	0.96	3.1	0.04	100	0.998

Table 3.6. Desorption coefficients (x_1, x_2) and time constants (t_1, t_2) in equation (3.2) that describe the transient humidity response of the humidity/ temperature transmitter with $\Delta RH \neq 0$, $\Delta T = 0$, V_{air}=0.8m/s during three trials at different wet side humidity conditions.

Inlet conditions	x_1	t_1(s)	x_2	t_2(s)	r^2
dry side: $T_{i,d} \approx 23^oC$, $\Phi_{i,d} \approx 6\%$ wet side: $T_{i,w} \approx 23^oC$, $\Phi_{i,w} \approx 40\%$	0.97	3.7	0.03	530	0.991
	0.97	3.4	0.03	430	0.990
	0.97	3.8	0.03	440	0.992
dry side: $T_{i,d} \approx 23^oC$, $\Phi_{i,d} \approx 6\%$ wet side: $T_{i,w} \approx 23^oC$, $\Phi_{i,w} \approx 50\%$	0.96	3.2	0.04	190	0.992
	0.96	3.3	0.04	170	0.995
	0.96	3.0	0.04	160	0.994
dry side: $T_{i,d} \approx 23^oC$, $\Phi_{i,d} \approx 6\%$ wet side: $T_{i,w} \approx 23^oC$, $\Phi_{i,w} \approx 60\%$	0.96	2.5	0.04	150	0.992
	0.97	3.5	0.03	280	0.994
	0.96	2.1	0.04	150	0.986

Table 3.7. Adsorption coefficients (x_1, x_2) and time constants (t_1, t_2) in equation (3.1) that describe the transient humidity response of the humidity/ temperature transmitter with $\Delta RH \neq 0$, $\Delta T=0$, $V_{air}=0.4$m/s during three trials at different wet side humidity conditions.

Inlet conditions	x_1	t_1(s)	x_2	t_2(s)	r^2
dry side: $T_{i,d}\approx 23^oC$, $\Phi_{i,d}\approx 6\%$ wet side: $T_{i,w}\approx 23^oC$, $\Phi_{i,w}\approx 40\%$	0.97	3.9	0.03	100	0.992
	0.99	3.7	0.01	2400	0.994
	0.99	4.1	0.01	2400	0.994
dry side: $T_{i,d}\approx 23^oC$, $\Phi_{i,d}\approx 6\%$ wet side: $T_{i,w}\approx 23^oC$, $\Phi_{i,w}\approx 50\%$	0.95	3.6	0.05	70	0.988
	0.98	3.6	0.02	580	0.991
	0.96	3.2	0.04	50	0.994
dry side: $T_{i,d}\approx 23^oC$, $\Phi_{i,d}\approx 6\%$ wet side: $T_{i,w}\approx 23^oC$, $\Phi_{i,w}\approx 60\%$	0.95	3.0	0.05	50	0.997
	0.96	3.1	0.04	90	0.997
	0.96	3.0	0.04	50	0.991

Table 3.8. Desorption coefficients (x_1, x_2) and time constants (t_1, t_2) in equation (3.2) that describe the transient humidity response of the humidity/ temperature transmitter with $\Delta RH \neq 0$, $\Delta T=0$, $V_{air}=0.4$m/s during three trials at different wet side humidity conditions.

Inlet conditions	x_1	t_1(s)	x_2	t_2(s)	r^2
dry side: $T_{i,d}\approx 23^oC$, $\Phi_{i,d}\approx 6\%$ wet side: $T_{i,w}\approx 23^oC$, $\Phi_{i,w}\approx 40\%$	0.97	3.4	0.03	460	0.987
	0.97	3.0	0.03	360	0.987
	0.96	2.7	0.04	180	0.991
dry side: $T_{i,d}\approx 23^oC$, $\Phi_{i,d}\approx 6\%$ wet side: $T_{i,w}\approx 23^oC$, $\Phi_{i,w}\approx 50\%$	0.97	3.6	0.03	340	0.993
	0.97	3.3	0.03	250	0.993
	0.97	2.8	0.03	390	0.989
dry side: $T_{i,d}\approx 23^oC$, $\Phi_{i,d}\approx 6\%$ wet side: $T_{i,w}\approx 23^oC$, $\Phi_{i,w}\approx 60\%$	0.97	3.4	0.03	420	0.991
	0.97	3.2	0.03	180	0.994
	0.97	3.2	0.03	370	0.990

The first time constants in Tables 3.5 to 3.8 indicate that the airflow rate has no significant impact on the first time constant. The first time constant for adsorption ranges from 2.4 to 3.6s at 200L/min, 3.0 to 5.3s at 100L/min and 3.0 to 4.1s at 50L/min. For desorption, the ranges are 2.2 to 3.0s at 200L/min, 2.1 to 3.8s at 100L/min and 2.7 to 3.6s at 50L/min respectively. Since all the ranges overlapped, it appears that the response of these transmitters to a step change in humidity is not sensitive to the airflow rate. This agrees with the results of Brion (1986) who found that the response of a polymer humidity sensor was flow rate independent. Figure 3.15 presents the first time constant versus airflow rate for both the adsorption and desorption cases further demonstrating that the airflow rate seems to have a limited effect on the first time constant over the range of flow rate tested.

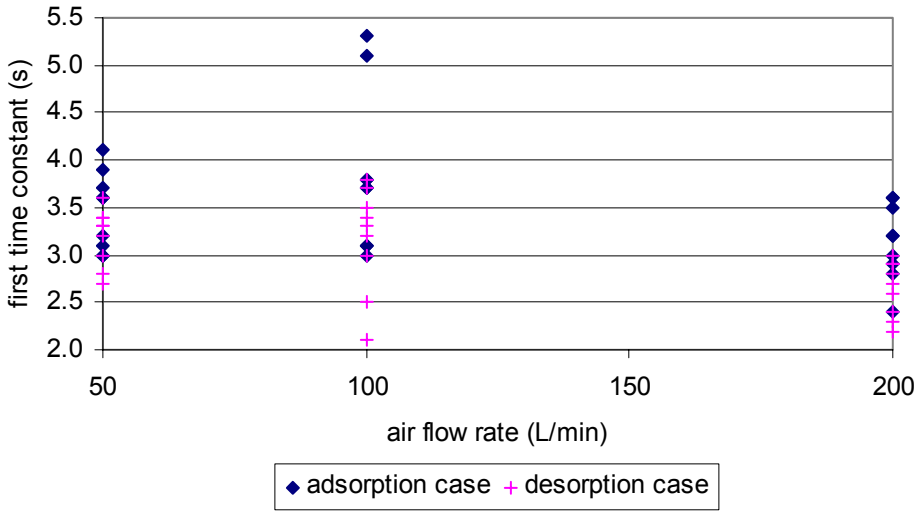

Figure 3.15 First time constant versus airflow rate for both adsorption and desorption with $\Delta RH \neq 0$ and $\Delta T = 0$.

The results presented in Tables 3.1 to 3.8 are all obtained under testing conditions with only humidity change but no temperature change; however, to fully understand the behaviour of the humidity/temperature transmitter, inlet air conditions with temperature difference need to be studied. Here, the inlet temperature conditions of 23°C to 53°C (see Table 2.1) are applied. The results presented in Tables 3.9 to 3.10 indicate that the temperature has a very large impact on the relative humidity reading. The adsorption time constants are still larger than the desorption time constants, but the time constants are much larger in the case with $\Delta T \neq 0$ (i.e., the transmitter responds to a step change in relative humidity much slower than it does with no temperature change). Comparing the adsorption cases, the first time constants in Table 3.9 (i.e., with $\Delta T \neq 0$) are about 40 times larger than those in Table 3.1 and the desorption first time constants in Table 3.10 (i.e., with $\Delta T \neq 0$) are at least 10 times larger. This indicates that the temperature plays an important role in transient relative humidity measurement. Three tests are completed in order to determine the average values of each constants, x_1, x_2, t_1 and t_2 for adsorption and desorption. The detailed results are given in Tables 3.9 and 3.10 as following. For every test, the r^2 values are equal to or greater than 0.987, which indicates correlation data agree very well with experimental data. In this situation, the humidity/temperature transmitter needs at least 10 minutes to reach the inlet condition when relative humidity increases and about 5 minutes when humidity decreases. The adsorption first time constants are at least 3 times greater than desorption first time constants.

It means the process of moisture absorbed in sensor is a much slower procedure in this circumstance. The transient temperature behaviour of the temperature sensor in the transmitter is discussed in Section 3.2.2.

Table 3.9. Adsorption coefficients (x_1, x_2) and time constants (t_1, t_2) in equation (3.1) describing the transient humidity response of the humidity/temperature transmitter with $\Delta RH \neq 0$, $\Delta T \neq 0$ and V_{air}=1.6m/s.

Inlet conditions	x_1	t_1(s)	x_2	t_2(s)	r^2
cold side: $T_{i,c} \approx 23^oC$, $\Phi_{i,w} \approx 36\%$ hot side: $T_{i,h} \approx 53^oC$, $\Phi_{i,d} \approx 5\%$	0.99	139	0.01	1800	0.997
	0.95	122	0.05	385	0.999
	0.99	136	0.01	1085	0.999

Table 3.10. Desorption coefficients (x_1, x_2) and time constants (t_1, t_2) in equation (3.2) describing the transient humidity response of the humidity/temperature transmitter with $\Delta RH \neq 0$, $\Delta T \neq 0$ and V_{air}=1.6m/s.

Inlet conditions	x_1	t_1(s)	x_2	t_2(s)	r^2
cold side: $T_{i,c} \approx 23^oC$, $\Phi_{i,w} \approx 36\%$ hot side: $T_{i,h} \approx 53^oC$, $\Phi_{i,d} \approx 5\%$	0.93	38	0.07	606	0.992
	0.91	36	0.09	398	0.987
	0.92	40	0.08	450	0.991

The operating condition of $\Delta RH \neq 0$, $\Delta T \neq 0$ and $\Delta W = 0$ is used to study the transient characteristics of the humidity/temperature transmitter exposed to both air streams are the same humidity ratio (5g/kg). The results in Tables 3.11 and 3.12 show the first time constant is about 120s, which is similar with the result in Table 3.9 ($\Delta RH \neq 0$, $\Delta T \neq 0$). Although the first time constant for desorption is greater when $\Delta W = 0$ than when $\Delta W \neq 0$, both conditions show a very similar behaviour due to the simultaneous step change in temperature.

Table 3.11. Adsorption coefficients (x_1, x_2) and time constants (t_1, t_2) in equation (3.1) describing the transient humidity response of the humidity/temperature transmitter with $\Delta RH \neq 0$, $\Delta T \neq 0$ and $\Delta W = 0$, V_{air}=1.6m/s during three trials at different wet side humidity.

Inlet conditions	x_1	t_1(s)	x_2	t_2(s)	r^2
dry side: $T_{i,c} \approx 23^oC$, $\Phi_{i,w} \approx 29\%$	0.98	96	0.02	550	0.996
wet side: $T_{i,h} \approx 30^oC$, $\Phi_{i,d} \approx 19\%$	0.98	100	0.02	3870	0.997
$W \approx 5g/kg$	0.98	103	0.02	1400	0.997
dry side: $T_{i,c} \approx 23^oC$, $\Phi_{i,w} \approx 29\%$	0.99	117	0.01	1950	0.997
wet side: $T_{i,h} \approx 36^oC$, $\Phi_{i,d} \approx 14\%$	0.99	119	0.01	1620	0.997
$W \approx 5g/kg$	0.95	103	0.05	560	0.985
dry side: $T_{i,c} \approx 24^oC$, $\Phi_{i,d} \approx 27\%$	0.99	125	0.01	2580	0.997
wet side: $T_{i,h} \approx 40^oC$, $\Phi_{i,d} \approx 11\%$	0.99	130	0.01	3860	0.996
$W \approx 5g/kg$	0.98	123	0.02	1400	0.997

Table 3.12. Desorption coefficients (x_1, x_2) and time constants (t_1, t_2) in equation (3.2) describing the transient humidity response of the humidity/temperature transmitter with $\Delta RH \neq 0$, $\Delta T \neq 0$ and $\Delta W = 0$, V_{air}=1.6m/s during three trials at different wet side humidity.

Inlet conditions	x_1	t_1(s)	x_2	t_2(s)	r^2
dry side: $T_{i,c} \approx 23^oC$, $\Phi_{i,w} \approx 29\%$	0.80	87	0.20	250	0.997
wet side: $T_{i,h} \approx 30^oC$, $\Phi_{i,d} \approx 19\%$	0.89	70	0.11	450	0.996
$W \approx 5g/kg$	0.89	78	0.11	450	0.990
dry side: $T_{i,c} \approx 23^oC$, $\Phi_{i,w} \approx 29\%$	0.88	70	0.12	530	0.996
wet side: $T_{i,h} \approx 36^oC$, $\Phi_{i,d} \approx 14\%$	0.89	67	0.11	500	0.996
$W \approx 5g/kg$	0.91	66	0.09	490	0.994
dry side: $T_{i,c} \approx 24^oC$, $\Phi_{i,d} \approx 27\%$	0.89	65	0.11	640	0.996
wet side: $T_{i,h} \approx 40^oC$, $\Phi_{i,d} \approx 11\%$	0.90	64	0.10	430	0.995
$W \approx 5g/kg$	0.92	67	0.08	750	0.996

Since the humidity/temperature transmitter response does not appear to depend on the magnitude of the relative humidity step change, the coefficients (x_1, x_2, t_1 and t_2) are statistically averaged for Gaussian distributions weighed according to the standard deviation of each coefficient, which is given by the curve fitting computer program, TableCurve. The average is calculated such that the results with the lowest uncertainty are weighted more according to equations (3.7) and (3.8) (Taylor, 1982). Using the data in Tables 3.1 to 3.12, the weighted average time constants ($\overline{t_1}$, $\overline{t_2}$) and coefficients ($\overline{x_1}$, $\overline{x_2}$) are determined using equations (3.7) to (3.10) (Taylor, 1982) and the results are presented in Table 3.13.

$$\overline{x_i} = \left\{ \frac{\sum_{j=1}^{k} \left[x_{ij}^2 \left(\frac{1}{R(S_j)} \right)^2 \right]}{\sum_{j=1}^{k} \left[\frac{1}{R(S_j)} \right]^2} \right\}^{1/2}, \tag{3.7}$$

and

$$\overline{t_i} = \left\{ \frac{\sum_{j=1}^{k} \left[t_{ij}^2 \left(\frac{1}{R(S_j)} \right)^2 \right]}{\sum_{j=1}^{k} \left[\frac{1}{R(S_j)} \right]^2} \right\}^{1/2}, \tag{3.8}$$

where $R(S_j) = S_j / x_{ij}$, (3.9)

or $R(S_j) = S_j / t_{ij}$, (3.10)

where S is the fit standard error of the curve fitting for experimental data.

The information in Table 3.13 demonstrates the generalized relative humidity response of the humidity/temperature transmitter. These results confirm that the first time constant in adsorption is greater than that in desorption and the transient response of this polymer humidity sensor is quite similar over the range of flow rates studied. The results also show that the transmitter responds very slowly to a step change in humidity when $\Delta T \neq 0$. In these causes the first time constant is about 2 minutes and the second time constant is about 10 minutes.

Table 3.13. Average coefficients describing the transient humidity response of the humidity/temperature transmitter.

Test Conditions	Coefficient	Adsorption	Desorption
ΔRH≠0 ΔT=0 V_{air}=1.6m/s	$\overline{x_1}$	0.91	0.97
	$\overline{t_1}(s)$	3.1	2.6
	$\overline{x_2}$	0.09	0.03
	$\overline{t_2}(s)$	90	290
ΔRH≠0 ΔT=0 V_{air}=0.8m/s	$\overline{x_1}$	0.95	0.97
	$\overline{t_1}(s)$	3.6	3.1
	$\overline{x_2}$	0.05	0.03
	$\overline{t_2}(s)$	140	310
ΔRH≠0 ΔT=0 V_{air}=0.4m/s	$\overline{x_1}$	0.99	0.97
	$\overline{t_1}(s)$	3.6	3.1
	$\overline{x_2}$	0.01	0.03
	$\overline{t_2}(s)$	630	340
ΔRH≠0 ΔT≠0 V_{air}=1.6m/s	$\overline{x_1}$	0.99	0.93
	$\overline{t_1}(s)$	130	40
	$\overline{x_2}$	0.01	0.07
	$\overline{t_2}(s)$	660	500
ΔRH≠0 ΔT≠0 ΔW=0 V_{air}=1.6m/s	$\overline{x_1}$	0.98	0.89
	$\overline{t_1}(s)$	120	70
	$\overline{x_2}$	0.02	0.11
	$\overline{t_2}(s)$	1800	480

The statistical average values provided in Table 3.13 indicate that the humidity/temperature transmitter has a similar exponential response with and without a temperature change, but the time constants change significantly when there is a step change in temperature. The averaged response is such that the transmitter will record at least 90% of the humidity change during the first 15s (five times the first time constant) when there is no temperature changes (ΔT=0) regardless of the airflow rate, while the remaining 10% will take at least 8 minutes (five times the second time constant). When there is a change in temperature (ΔT≠0), it takes the transmitter at least 3 minutes (five times the first time constant) to record

about 90% of the humidity change, the remaining 10% change will take about 30 minutes (five times the second time constant). It is found that the humidity/temperature transmitter needs at least a 10 times longer time period to respond a step change in relative humidity when $\Delta T \neq 0$ than when $\Delta T = 0$.

3.2.2. Transient Temperature Data Correlation

In the previous section, the transient humidity data correlation is studied based on three operating conditions. These results show the strong interaction between transient temperature and humidity measurements. Since the humidity/temperature transmitter also has the ability to record temperature, this section will present the transient characteristics of this RTD temperature sensor that is part of the humidity/temperature transmitter. Figure 3.8 indicates that the temperature sensor follows an exponential function with two time constants similarly as the capacitance based humidity sensor that is characterized in Section 3.2.1. Thus, equations similar to equations (3.1) and (3.2) are applied to transient temperature data.

First, based on heat transfer into the transmitter from the air (increasing temperature),

$$\frac{\Delta T_s}{\Delta T_{so}}(t)_{inc} = y_1(1 - e^{-t/t_1}) + y_2(1 - e^{-t/t_2}), \tag{3.11}$$

and secondly for heat transfer from the transmitter into the air (decreasing temperature),

$$\frac{\Delta T_s}{\Delta T_{so}}(t)_{dec} = y_1 e^{-t/t_1} + y_2 e^{-t/t_2}, \tag{3.12}$$

where the coefficients y_1 and y_2 satisfy the same equation for both temperature increasing and decreasing,

$$y_1 + y_2 = 1,\ y_1 \geq 0,\ y_2 \geq 0, \tag{3.13}$$

but with different values for each case. Other symbols are:

ΔT_s =change in temperature $= |T_s - T_{si}|$, where T_{si} is the initial temperature;

ΔT_{so} = maximum change in temperature $= |T_{sf} - T_{si}|$, where T_{sf} is the final temperature; and t_1 and t_2 are the first and second time constants respectively.

The experimental data obtained at conditions of $\Delta RH \neq 0$, $\Delta T \neq 0$ and the curve fit shown in Figures 3.16 and 3.17 agree very well. In all cases $r^2 \geq 0.996$ as can be seen in Tables 3.14 and 3.15 where the transient coefficients and r^2 are presented for all tests. These data show that the transient response of the RTD temperature sensor in the humidity/temperature transmitter is much slower than the transient response of the humidity sensor in the transmitter presented in Section 3.2.1. The first time constants of the RTD temperature sensor are about 70s for both temperature increasing and decreasing compared to about 3s for the humidity sensor in the transmitter when $\Delta T = 0$.

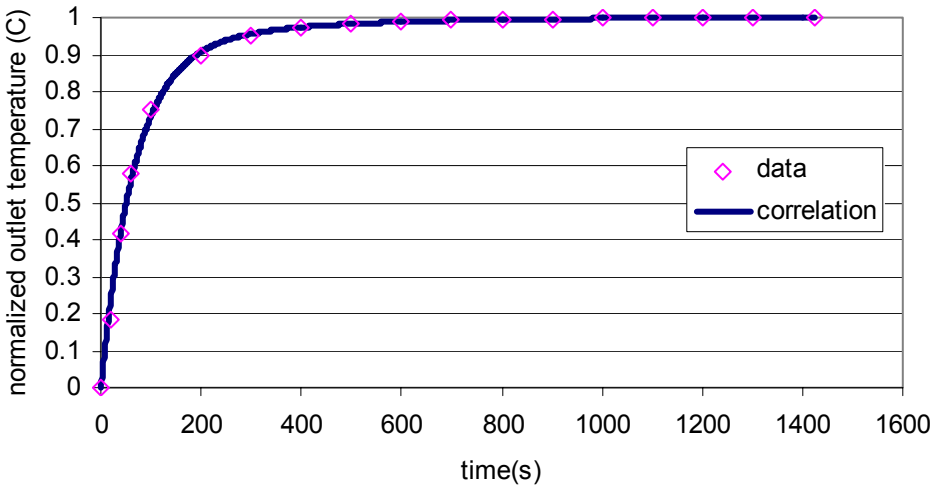

Figure 3.16 Comparison between the measured temperature of sensor $T_{o,c}$ and correlation equation (3.11) (y_1=0.89, t_1=65s, y_2=0.11, t_2=260s) for $\Delta RH \neq 0$, $\Delta T \neq 0$ and V_{air}=1.6m/s (data from Figure 3.7).

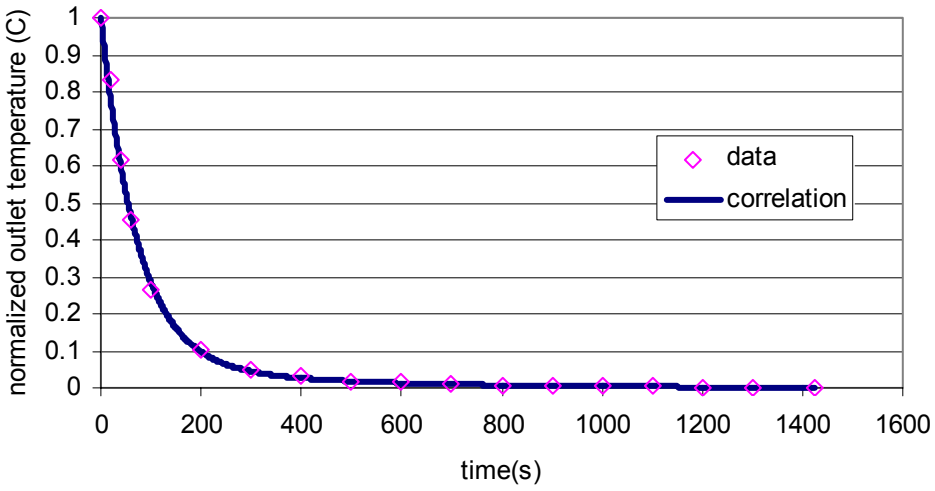

Figure 3.17 Comparison between the measured temperature of sensor $T_{o,h}$ and correlation equation (3.12) (y_1=0.93, t_1=72s, y_2=0.07, t_2=350s) for $\Delta RH \neq 0$, $\Delta T \neq 0$ and V_{air}=1.6m/s (data from Figure 3.7).

Table 3.14. Increasing coefficients (y_1, y_2) and time constants (t_1, t_2) in equation (3.11) that present the transient temperature response of the humidity/temperature transmitter with $\Delta RH \neq 0$, $\Delta T \neq 0$, V_{air}=1.6m/s.

Inlet conditions	y_1	t_1(s)	y_2	t_2(s)	r^2
cold side:$T_{i,c} \approx 24^oC$, $\Phi_{i,w} \approx 36$ % hot side:$T_{i,h} \approx 54^oC$,$\Phi_{i,d} \approx 5\%$	0.91	74	0.09	890	0.996
	0.89	65	0.11	260	0.996
	0.91	71	0.09	470	0.997

Table 3.15. Decreasing coefficients (y_1, y_2) and time constants (t_1, t_2) in equation (3.12) that present the transient temperature response of the humidity/temperature transmitter with $\Delta RH \neq 0$, $\Delta T \neq 0$, V_{air}=1.6m/s.

Inlet conditions	y_1	t_1(s)	y_2	t_2(s)	r^2
cold side:$T_{i,c} \approx 24^oC$, $\Phi_{i,w} \approx 36$ % hot side:$T_{i,h} \approx 54^oC$,$\Phi_{i,d} \approx 5\%$	0.92	67	0.08	410	0.996
	0.93	72	0.07	350	0.996
	0.91	64	0.09	310	0.997

Further experiments are completed with no relative humidity change, but with a step change in temperature ($\Delta RH=0$, $\Delta T \neq 0$). These conditions are tested in nine tests with three different temperature differences as shown below, in Tables 3.16 to 3.19.

Table 3.16. Increasing coefficients (y_1, y_2) and time constants (t_1, t_2) in equation (3.11) that present the transient temperature response of the humidity/temperature transmitter with $\Delta RH=0$, $\Delta T\neq 0$, V_{air}=1.6m/s.

Inlet conditions	y_1	t_1(s)	y_2	t_2(s)	r^2
cold side:$T_{i,c}\approx 23^oC$, $\Phi_{i,w}\approx 15\%$ hot side:$T_{i,h}\approx 40^oC$,$\Phi_{i,d}\approx 15\%$	0.94	78	0.06	410	0.995
	0.90	70	0.10	380	0.991
	0.96	81	0.04	560	0.993
cold side:$T_{i,c}\approx 21^oC$, $\Phi_{i,w}\approx 15\%$ hot side:$T_{i,h}\approx 30^oC$,$\Phi_{i,d}\approx 15\%$	0.91	68	0.09	350	0.996
	0.94	77	0.06	570	0.997
	0.93	72	0.07	560	0.997
cold side:$T_{i,c}\approx 22^oC$, $\Phi_{i,w}\approx 15\%$ hot side:$T_{i,h}\approx 18^oC$,$\Phi_{i,d}\approx 15\%$	0.95	66	0.05	780	0.998
	0.95	70	0.05	710	0.996
	0.90	62	0.10	440	0.994

Table 3.17. Decreasing coefficients (y_1, y_2) and time constants (t_1, t_2) in equation (3.12) that present the transient temperature response of the humidity/temperature transmitter with $\Delta RH=0$, $\Delta T\neq 0$, V_{air}=1.6m/s.

Inlet conditions	y_1	t_1(s)	y_2	t_2(s)	r^2
cold side:$T_{i,c}\approx 23^oC$, $\Phi_{i,w}\approx 15\%$ hot side:$T_{i,h}\approx 40^oC$,$\Phi_{i,d}\approx 15\%$	0.92	68	0.08	320	0.996
	0.94	75	0.06	450	0.995
	0.94	71	0.06	400	0.995
cold side:$T_{i,c}\approx 21^oC$, $\Phi_{i,w}\approx 15\%$ hot side:$T_{i,h}\approx 30^oC$,$\Phi_{i,d}\approx 15\%$	0.96	73	0.06	770	0.997
	0.92	65	0.08	360	0.997
	0.94	73	0.06	430	0.997
cold side:$T_{i,c}\approx 22^oC$, $\Phi_{i,w}\approx 15\%$ hot side:$T_{i,h}\approx 18^oC$,$\Phi_{i,d}\approx 15\%$	0.97	78	0.03	520	0.991
	0.92	69	0.08	430	0.997
	0.93	76	0.07	580	0.998

Table 3.18. Increasing coefficients (y_1, y_2) and time constants (t_1, t_2) in equation (3.11) that present the transient temperature response of the humidity/temperature transmitter with $\Delta RH\neq 0$, $\Delta T\neq 0$, $\Delta W=0$, V_{air}=1.6m/s.

Inlet conditions	y_1	t_1(s)	y_2	t_2(s)	r^2
dry side: $T_{i,c}\approx 23^oC$, $\Phi_{i,w}\approx 29\%$ wet side: $T_{i,h}\approx 30^oC$, $\Phi_{i,d}\approx 19\%$ $W\approx 5g/kg$	0.90	68	0.10	540	0.997
	0.93	78	0.07	510	0.997
	0.90	71	0.10	400	0.996
dry side: $T_{i,c}\approx 23^oC$, $\Phi_{i,w}\approx 29\%$ wet side: $T_{i,h}\approx 36^oC$, $\Phi_{i,d}\approx 14\%$ $W\approx 5g/kg$	0.89	66	0.11	360	0.999
	0.93	79	0.07	400	0.995
	0.92	66	0.08	410	0.994
dry side: $T_{i,c}\approx 24^oC$, $\Phi_{i,d}\approx 27\%$ wet side: $T_{i,h}\approx 40^oC$, $\Phi_{i,d}\approx 11\%$ $W\approx 5g/kg$	0.90	70	0.10	440	0.996
	0.89	77	0.11	450	0.995
	0.90	71	0.10	570	0.996

Table 3.19. Decreasing coefficients (y_1, y_2) and time constants (t_1, t_2) in equation (3.12) that present the transient temperature response of the humidity/temperature transmitter with $\Delta RH \neq 0$, $\Delta T \neq 0$, $\Delta W = 0$, V_{air}=1.6m/s.

Inlet conditions	y_1	t_1(s)	y_2	t_2(s)	r^2
dry side: $T_{i,c} \approx 23^oC$, $\Phi_{i,w} \approx 29\%$	0.95	74	0.10	500	0.990
wet side: $T_{i,h} \approx 30^oC$, $\Phi_{i,d} \approx 19\%$	0.96	75	0.07	690	0.993
$W \approx 5g/kg$	0.94	73	0.10	480	0.996
dry side: $T_{i,c} \approx 23^oC$, $\Phi_{i,w} \approx 29\%$	0.93	73	0.11	340	0.998
wet side: $T_{i,h} \approx 36^oC$, $\Phi_{i,d} \approx 14\%$	0.92	69	0.07	400	0.995
$W \approx 5g/kg$	0.92	69	0.08	420	0.994
dry side: $T_{i,c} \approx 24^oC$, $\Phi_{i,d} \approx 27\%$	0.94	76	0.10	450	0.995
wet side: $T_{i,h} \approx 40^oC$, $\Phi_{i,d} \approx 11\%$	0.93	72	0.11	400	0.996
$W \approx 5g/kg$	0.94	76	0.10	440	0.998

The data in Tables 3.14 to 3.19 show that the first coefficient (y_1) is usually slightly larger than 0.9 and y_2 is less than 0.1. The first time constant is about 70s and second time constant is about 450s for both a temperature increase and decrease. Since the temperature response does not appear to depend on the magnitude of the step change, the coefficients (y_1, y_2, t_1 and t_2) are statistically averaged by same method using equations (3.7) to (3.10). Using the data in Tables 3.14 to 3.19, the weighted average time constants ($\overline{t_1}$, $\overline{t_2}$) and coefficients ($\overline{y_1}$, $\overline{y_2}$) for each parameter are determined and the results are presented in Table 3.20. The average temperature response in each case is such that the sensor will record 90% of the humidity change in about 350s (five times the first time constant), while the remaining 10% will take more than 30 minutes to be recorded.

Table 3.20. Average coefficients describing transient temperature response of the temperature sensor in the humidity/temperature transmitter.

Test Conditions	Coefficient	Increase	Decrease
ΔRH≠0 ΔT≠0 V_{air}=1.6m/s	$\overline{y_1}$	0.94	0.90
	$\overline{t_1}$ (s)	69	70
	$\overline{y_2}$	0.06	0.10
	$\overline{t_2}$ (s)	630	620
ΔRH=0 ΔT≠0 V_{air}=1.6m/s	$\overline{y_1}$	0.91	0.92
	$\overline{t_1}$ (s)	72	67
	$\overline{y_2}$	0.09	0.08
	$\overline{t_2}$ (s)	750	370
ΔRH≠0 ΔT≠0 ΔW=0 V_{air}=1.6m/s	$\overline{y_1}$	0.91	0.94
	$\overline{t_1}$ (s)	72	73
	$\overline{y_2}$	0.09	0.06
	$\overline{t_2}$ (s)	470	460

According to the discussion in the previous sections, the transient humidity and temperature response of the humidity/temperature transmitter can be described in equations based on various operating conditions, which are listed in Table 3.21. These equations express the generalized dynamic behaviour of this humidity/temperature transmitter when it is exposed to airflow with a step change in relative humidity and temperature simultaneously or independently.

Table 3.21. Transient characteristics of the humidity/temperature transmitter under various operating conditions.

Operating Conditions	Transient Response of The Transmitter
ΔRH≠0, ΔT=0, V_{air}=1.6m/s	$\frac{\Delta\phi_s}{\Delta\phi_{so}}(t)_{ads} = 0.91(1-e^{-t/3.1}) + 0.09(1-e^{-t/90})$ $\frac{\Delta\phi_s}{\Delta\phi_{so}}(t)_{des} = 0.97(1-e^{-t/2.6}) + 0.03(1-e^{-t/290})$
ΔRH≠0, ΔT=0, V_{air}=0.8m/s	$\frac{\Delta\phi_s}{\Delta\phi_{so}}(t)_{ads} = 0.95(1-e^{-t/3.6}) + 0.05(1-e^{-t/140})$ $\frac{\Delta\phi_s}{\Delta\phi_{so}}(t)_{des} = 0.97(1-e^{-t/3.1}) + 0.03(1-e^{-t/310})$
ΔRH≠0, ΔT=0, V_{air}=0.4m/s	$\frac{\Delta\phi_s}{\Delta\phi_{so}}(t)_{ads} = 0.99(1-e^{-t/3.6}) + 0.09(1-e^{-t/630})$ $\frac{\Delta\phi_s}{\Delta\phi_{so}}(t)_{des} = 0.97(1-e^{-t/3.1}) + 0.03(1-e^{-t/340})$
ΔRH≠0, ΔT≠0 V_{air}=1.6m/s	$\frac{\Delta\phi_s}{\Delta\phi_{so}}(t)_{ads} = 0.99(1-e^{-t/130}) + 0.09(1-e^{-t/660})$ $\frac{\Delta\phi_s}{\Delta\phi_{so}}(t)_{des} = 0.93(1-e^{-t/40}) + 0.07(1-e^{-t/500})$ $\frac{\Delta T_s}{\Delta T_{so}}(t)_{inc} = 0.94(1-e^{-t/69}) + 0.06(1-e^{-t/630})$ $\frac{\Delta T_s}{\Delta T_{so}}(t)_{dec} = 0.90(1-e^{-t/70}) + 0.10(1-e^{-t/620})$
ΔRH=0, ΔT≠0 V_{air}=1.6m/s	$\frac{\Delta T_s}{\Delta T_{so}}(t)_{inc} = 0.91(1-e^{-t/72}) + 0.09(1-e^{-t/750})$ $\frac{\Delta T_s}{\Delta T_{so}}(t)_{dec} = 0.92(1-e^{-t/67}) + 0.08(1-e^{-t/370})$
ΔRH≠0, ΔT≠0, ΔW=0 V_{air}=1.6m/s	$\frac{\Delta\phi_s}{\Delta\phi_{so}}(t)_{ads} = 0.98(1-e^{-t/120}) + 0.02(1-e^{-t/1800})$ $\frac{\Delta\phi_s}{\Delta\phi_{so}}(t)_{des} = 0.89(1-e^{-t/70}) + 0.11(1-e^{-t/480})$ $\frac{\Delta T_s}{\Delta T_{so}}(t)_{inc} = 0.91(1-e^{-t/72}) + 0.09(1-e^{-t/470})$ $\frac{\Delta T_s}{\Delta T_{so}}(t)_{inc} = 0.94(1-e^{-t/73}) + 0.06(1-e^{-t/460})$

3.2.3. Comparison of Transient Temperature Measurement

In this section, the transient response of the RTD temperature sensor, which is integral to the humidity measurement device manufactured by Vaisala, is compared to that of a Type-T thermocouple. It is expected that the thermocouple will have a faster response than the RTD temperature sensor in the humidity/temperature transmitter because the thermocouple has less capacitance than the RTD temperature sensor. Figures 3.18 to 3.20 compare the transient thermal response of the RTD temperature sensor and the thermocouple during three different test conditions. In these figures, the curves $TC_{o,c}$ and $TC_{o,h}$ represent the thermocouple temperature response. These figures confirm that the temperature sensor in the humidity/temperature transmitter responds slower than the thermocouple.

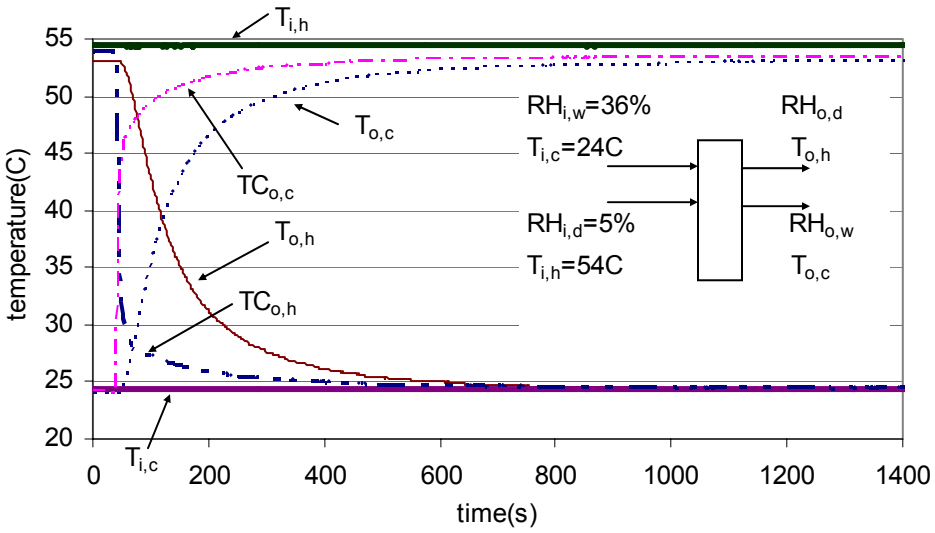

Figure 3.18 Comparison of measured outlet temperature without a wheel for a transient temperature response of the transmitters and the thermocouples for $\Delta RH \neq 0$, $\Delta T \neq 0$ and V_{air}=1.6 m/s.

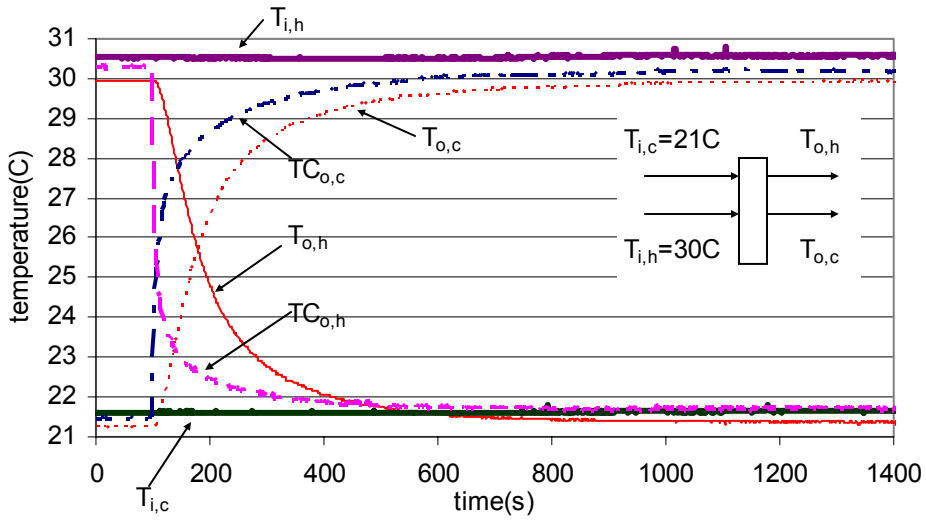

Figure 3.19 Comparison of measured outlet temperature without a wheel for a transient temperature response of the transmitters and the thermocouples under $\Delta RH=0$, $\Delta T\neq 0$ and $V_{air}=1.6$ m/s.

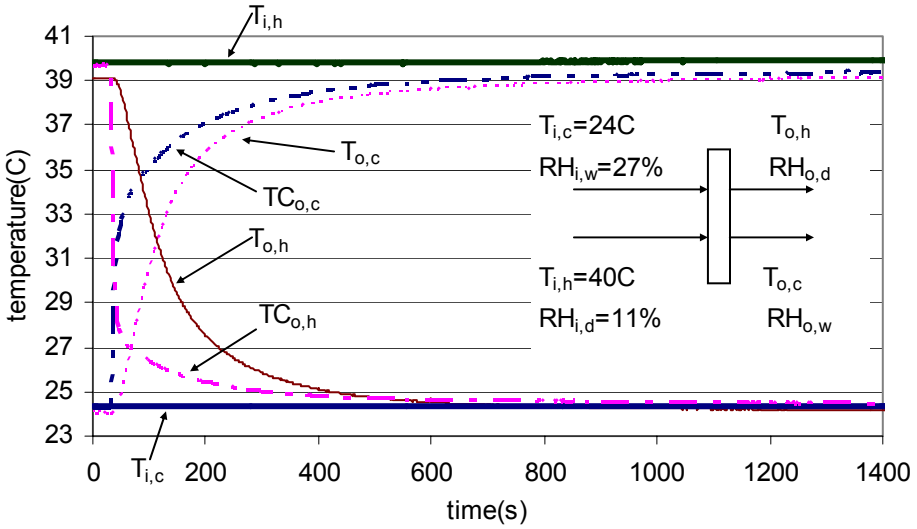

Figure 3.20 Comparison of measured outlet temperature without a wheel for a transient temperature response of the transmitters and the thermocouples under $\Delta RH\neq 0$, $\Delta T\neq 0$, $\Delta W=0$ and $V_{air}=1.6$ m/s.

Since Figures 3.18 to 3.20 indicate that the transient response of the thermocouple follows an exponential function with two time constants, equations (3.11) and (3.12) can be used again. The time constants obtained using TableCurve are presented in Tables 3.22 to 3.27. The first time constants for both an increasing and decreasing temperature are about 4s, which is about 15 times

smaller than the first time constant of the RTD temperature sensor for the same operating conditions. However, the coefficient y_1 is for the thermocouple and is usually less than 0.9.

Table 3.22. Increasing coefficients (y_1, y_2) and time constants (t_1, t_2) in equation (3.11) that represent the transient temperature response of the thermocouple with $\Delta RH \neq 0$, $\Delta T \neq 0$, V_{air}=1.6m/s.

Inlet conditions	y_1	t_1(s)	y_2	t_2(s)	r^2
cold side:$T_{i,c} \approx 24^oC$, $\Phi_{i,w} \approx 36$ % hot side:$T_{i,h} \approx 54^oC$,$\Phi_{i,d} \approx 5$%	0.91	3.5	0.09	720	0.980
	0.78	3.6	0.22	100	0.981
	0.87	3.3	0.13	210	0.975

Table 3.23. Decreasing coefficients (y_1, y_2) and time constants (t_1, t_2) in equation (3.12) that represent the transient temperature response of the thermocouple with $\Delta RH \neq 0$, $\Delta T \neq 0$, V_{air}=1.6m/s.

Inlet conditions	y_1	t_1(s)	y_2	t_2(s)	r^2
cold side:$T_{i,c} \approx 24^oC$, $\Phi_{i,w} \approx 36$ % hot side:$T_{i,h} \approx 54^oC$,$\Phi_{i,d} \approx 5$%	0.84	4.4	0.16	110	0.982
	0.86	3.3	0.14	130	0.987
	0.86	3.5	0.14	110	0.985

Table 3.24. Increasing coefficients (y_1, y_2) and time constants (t_1, t_2) in equation (3.11) that represent the transient temperature response of the thermocouple with $\Delta RH = 0$, $\Delta T \neq 0$, V_{air}=1.6m/s.

Inlet conditions	y_1	t_1(s)	y_2	t_2(s)	r^2
cold side:$T_{i,c} \approx 23^oC$, $\Phi_{i,w} \approx 15$% hot side:$T_{i,h} \approx 40^oC$,$\Phi_{i,d} \approx 15$%	0.81	2.7	0.19	170	0.977
	0.68	4.9	0.32	150	0.970
	0.73	2.3	0.27	110	0.992
cold side:$T_{i,c} \approx 21^oC$, $\Phi_{i,w} \approx 15$% hot side:$T_{i,h} \approx 30^oC$,$\Phi_{i,d} \approx 15$%	0.67	7.1	0.33	140	0.970
	0.78	3.1	0.22	150	0.960
	0.64	4.1	0.36	120	0.982
cold side:$T_{i,c} \approx 22^oC$, $\Phi_{i,w} \approx 15$% hot side:$T_{i,h} \approx 18^oC$,$\Phi_{i,d} \approx 15$%	0.56	5.1	0.44	120	0.950
	0.84	8.1	0.16	210	0.970
	0.59	5.3	0.41	140	0.950

Table 3.25. Decreasing coefficients (y_1, y_2) and time constants (t_1, t_2) in equation (3.12) that represent the transient temperature response of the thermocouple with $\Delta RH=0$, $\Delta T\neq 0$, V_{air}=1.6m/s.

Inlet conditions	y_1	t_1(s)	y_2	t_2(s)	r^2
cold side:$T_{i,c}\approx 23^oC$, $\Phi_{i,w}\approx 15\%$ hot side:$T_{i,h}\approx 40^oC$,$\Phi_{i,d}\approx 15\%$	0.61	5.4	0.39	100	0.984
	0.83	3.4	0.17	150	0.975
	0.65	5.8	0.35	110	0.988
cold side:$T_{i,c}\approx 21^oC$, $\Phi_{i,w}\approx 15\%$ hot side:$T_{i,h}\approx 30^oC$,$\Phi_{i,d}\approx 15\%$	0.81	5.6	0.19	140	0.978
	0.59	5.2	0.41	100	0.990
	0.81	4.0	0.19	130	0.975
cold side:$T_{i,c}\approx 22^oC$, $\Phi_{i,w}\approx 15\%$ hot side:$T_{i,h}\approx 18^oC$,$\Phi_{i,d}\approx 15\%$	0.80	4.8	0.20	200	0.970
	0.66	7.3	0.34	160	0.977
	0.87	5.8	0.13	560	0.960

Table 3.26. Increasing coefficients (y_1, y_2) and time constants (t_1, t_2) in equation (3.11) that represent the transient temperature response of the thermocouple with $\Delta RH\neq 0$, $\Delta T\neq 0$, $\Delta W=0$, V_{air}=1.6m/s.

Inlet conditions	y_1	t_1(s)	y_2	t_2(s)	r^2
dry side: $T_{i,c}\approx 23^oC$, $\Phi_{i,w}\approx 29\%$ wet side: $T_{i,h}\approx 30^oC$, $\Phi_{i,d}\approx 19\%$ W≈5g/kg	0.83	4.1	0.17	180	0.982
	0.63	6.0	0.37	180	0.980
	0.88	3.7	0.12	320	0.990
dry side: $T_{i,c}\approx 23^oC$, $\Phi_{i,w}\approx 29\%$ wet side: $T_{i,h}\approx 36^oC$, $\Phi_{i,d}\approx 14\%$ W≈5g/kg	0.65	9.6	0.35	140	0.982
	0.85	3.1	0.15	170	0.987
	0.61	5.5	0.39	120	0.985
dry side: $T_{i,c}\approx 24^oC$, $\Phi_{i,d}\approx 27\%$ wet side: $T_{i,h}\approx 40^oC$, $\Phi_{i,d}\approx 11\%$ W≈5g/kg	0.63	6.2	0.37	160	0.986
	0.86	3.1	0.14	270	0.985
	0.64	7.7	0.36	180	0.992

Table 3.27. Decreasing coefficients (y_1, y_2) and time constants (t_1, t_2) in equation (3.12) that represent the transient temperature response of the thermocouple with $\Delta RH\neq 0$, $\Delta T\neq 0$, $\Delta W=0$, V_{air}=1.6m/s.

Inlet conditions	y_1	t_1(s)	y_2	t_2(s)	r^2
dry side: $T_{i,c}\approx 23^oC$, $\Phi_{i,w}\approx 29\%$ wet side: $T_{i,h}\approx 30^oC$, $\Phi_{i,d}\approx 19\%$ W≈5g/kg	0.82	3.3	0.18	140	0.980
	0.83	3.8	0.17	170	0.990
	0.50	3.3	0.50	140	0.991
dry side: $T_{i,c}\approx 23^oC$, $\Phi_{i,w}\approx 29\%$ wet side: $T_{i,h}\approx 36^oC$, $\Phi_{i,d}\approx 14\%$ W≈5g/kg	0.83	3.2	0.17	130	0.992
	0.54	7.9	0.46	120	0.985
	0.83	2.9	0.17	170	0.995
dry side: $T_{i,c}\approx 24^oC$, $\Phi_{i,d}\approx 27\%$ wet side: $T_{i,h}\approx 40^oC$, $\Phi_{i,d}\approx 11\%$ W≈5g/kg	0.82	3.6	0.18	130	0.980
	0.49	7.5	0.51	120	0.988
	0.81	3.4	0.19	130	0.982

The statistically averaged values of the coefficients (y_1, y_2, t_1 and t_2) describing the transient response of the thermocouple are obtained using equations (3.7) to (3.10), and are given in Table 3.28. These results also show that the transient temperature response of the thermocouple is much faster than the response of the temperature sensor in the humidity/temperature transmitter. The first time constant of the thermocouple is about 3 to 5s, which is at least 15 times smaller than that of the RTD temperature sensor in humidity/temperature transmitter.

Table 3.28. Average coefficients describing the transient temperature response of the thermocouple.

Test Conditions	Coefficient	Increase	Decrease
ΔRH≠0 ΔT≠0 ΔW≠0 V_{air}=1.6m/s	$\overline{y_1}$	0.86	0.87
	$\overline{t_1}$ (s)	3.5	3.6
	$\overline{y_2}$	0.14	0.13
	$\overline{t_2}$ (s)	330	120
ΔRH=0 ΔT≠0 V_{air}=1.6m/s	$\overline{y_1}$	0.76	0.80
	$\overline{t_1}$ (s)	5.1	5.1
	$\overline{y_2}$	0.24	0.20
	$\overline{t_2}$ (s)	130	160
ΔRH≠0 ΔT≠0 ΔW=0 V_{air}=1.6m/s	$\overline{y_1}$	0.83	0.82
	$\overline{t_1}$ (s)	4.1	3.3
	$\overline{y_2}$	0.17	0.18
	$\overline{t_2}$ (s)	180	140

3.3. Uncertainty Analysis

There is no such thing as a perfect measurement and this all measurements contain inaccuracies. The word accuracy refers to the closeness of agreement between a measured value and the true value. The degree of inaccuracy or the total measurement error is the difference between the measured value and the true value. The total error (or uncertainty) is the sum of the systematic (or bias) error and random (or precision) error. The bias error (B) is the fixed or constant of the total error. Bias errors are often more difficult to quantify because they depend on the entire sequence of calibration for each instrument used in an experiment. The random

component (P) of the total error is sometimes called the repeatability, repeatability error, or precision error. It is observed in repeated measurements that do not and are not expected to agree exactly.

According to ASME PTC 19.1-1998, bias errors and precision errors are both assumed to be independent with respect to each independent variable X_i, i=1, 2, 3, … j. Bias and precision uncertainty limits are kept separate for each measurement so that the two values can be reported separately. The bias, B, is combined with the total precision, P, at the 95% confidence level to form the root-sum-square uncertainty, U:

$$U = [B^2 + P^2]^{1/2}, \tag{3.14}$$

which is reported with all results for any experiment aimed at obtaining a specified result, X, or average result that is derived from several samples, $\overline{X}$, i.e.,

$$\overline{X} \pm U(\overline{X}). \tag{3.15}$$

Variations in instrument readings, X_i, tend to follow a random distribution. The sample standard deviation of a large number of readings, N, characterizes this distribution and is called the precision index, S:

$$S = \left[\frac{\sum_{i=1}^{N} (X_i - \overline{X})^2}{N-1} \right]^{1/2}, \tag{3.16}$$

where the mean value is defined by

$$\overline{X} = \frac{1}{N} \sum_{i=1}^{N} X_i . \tag{3.17}$$

The precision index can be reduced by using this average in place of individual measurements giving the precision index of the average as

$$S_{\overline{X}} = S / \sqrt{N} . \tag{3.18}$$

Consider a general case in which an experimental result, f, is a function of *n* measured variables X_i:

$$f = f(X_1, X_2, ..., X_n), \tag{3.19}$$

then the equivalent of (3.16) is

$$S_f = \left[\sum_{i=1}^{n} (\theta_i S_{\overline{X}_i})^2 \right]^{1/2}, \tag{3.20}$$

where

$$\theta_i = \partial f / \partial X_i \tag{3.21}$$

is the sensitivity coefficient.

The precision error is defined as

$$P = tS_{\overline{X}}, \tag{3.22}$$

where t is the student t for the 95% confidence level.

Therefore, the uncertainty is given as

$$U = [B^2 + (tS_{\overline{X}})^2]^{1/2}. \tag{3.23}$$

The relative humidity calibration correction is investigated because the inlet air tubes are operated manually and the data acquisition program records data every second, therefore it is difficult to determine the exact time that the conditions change. These have a large effect on the humidity/temperature transmitter because it has a small first time constant (3s) for $\Delta RH \neq 0$ and $\Delta T = 0$. Therefore, it is necessary to estimate the switch time to reduce the uncertainty of the first time constant. It is known that the correction of the starting time is between 0 and 1s because the data are recorded every second and the starting time is selected to be 1s prior to the first data point that begins to change from the previous steady-state conditions. During any test, the starting time (or switch time) may be from 0.1 to 1s prior to this first detected change. To determine the best estimate for this starting time offset, the starting time is increased from the normally assumed value in the range of 0.1 to 1s. These data are then curve-fitted to the exponential equations and the offset that gives the best curve fit (i.e., highest r^2) represents the best estimate of the starting time. TableCurve and equations (3.1) and (3.2) are used to obtain the value of r^2 for each set of test data. Figure 3.21 shows three test examples used to determine the starting time corrections for the transmitter humidity response measurement. The peak value of r^2 for test 1 is

99.6% corresponding to a start time of 0.6s, which is greater than the normal start time or 0.4s prior to the first noticed change in the outlet humidity. For test 2, the greatest r^2 is 99.3% at 0.5s, while r^2=99.4% at 0.1s for test 3. These data imply that the starting time correction is different for each test. Once the greatest value of r^2 is found for each test, the correction is applied for each test. As well, this same method of starting time correction is applied to the wheel plus sensor data.

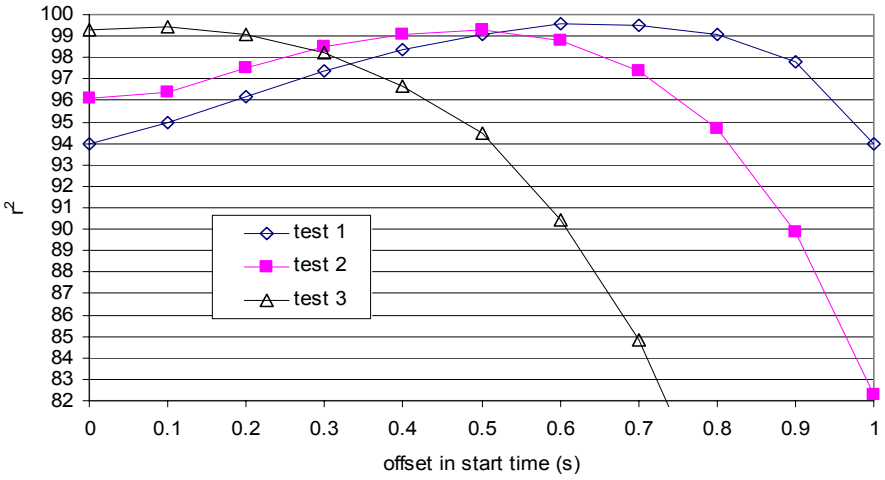

Figure 3.21 Determination of Correlation corrections for starting time based on r^2 value.

The results in Figure 3.21 indicate an uncertainty in the switch time of less than 0.2s. This offset and associated uncertainty has a larger effect on the first time constants, which is about 3s for $\Delta RH \neq 0$ and $\Delta T = 0$, than on the larger second time constants. This uncertainty of the response start time is considered to be the bias error in the starting time of the step change for each test. This is used to compute total uncertainty of time constant. Hence, the total uncertainty of time constants is computed using equation (3.23).

Based on the discussion above, the uncertainties of time constants and coefficients for sensor's humidity and temperature reading are calculated and presented in Tables 3.29 to 3.30.

Table 3.29. Uncertainty of each coefficient describing the transient humidity response of the humidity/temperature transmitter.

Test Conditions	Coefficient	Adsorption	Desorption
ΔRH≠0 ΔT=0 V_{air}=1.6m/s	$\overline{x_1} \pm U(\overline{x_1})$	0.91±0.03	0.97±0.01
	$\overline{t_1} \pm U(\overline{t_1})(s)$	3.1±0.4	2.6±0.3
	$\overline{x_2} \pm U(\overline{x_2})$	0.09±0.03	0.03±0.01
	$\overline{t_2} \pm U(\overline{t_2})(s)$	90±10	290±90
ΔRH≠0 ΔT=0 V_{air}=0.8m/s	$\overline{x_1} \pm U(\overline{x_1})$	0.95±0.01	0.97±0.01
	$\overline{t_1} \pm U(\overline{t_1})(s)$	3.6±0.6	3.1±0.4
	$\overline{x_2} \pm U(\overline{x_2})$	0.05±0.01	0.03±0.01
	$\overline{t_2} \pm U(\overline{t_2})(s)$	140±60	310±110
ΔRH≠0 ΔT=0 V_{air}=0.4m/s	$\overline{x_1} \pm U(\overline{x_1})$	0.99±0.01	0.97±0.003
	$\overline{t_1} \pm U(\overline{t_1})(s)$	3.6±0.4	3.1±0.3
	$\overline{x_2} \pm U(\overline{x_2})$	0.01±0.01	0.03±0.003
	$\overline{t_2} \pm U(\overline{t_2})(s)$	630±130	340±80
ΔRH≠0 ΔT≠0 V_{air}=1.6m/s	$\overline{x_1} \pm U(\overline{x_1})$	0.99±0.06	0.93±0.02
	$\overline{t_1} \pm U(\overline{t_1})(s)$	130±23	40±5
	$\overline{x_2} \pm U(\overline{x_2})$	0.01±0.06	0.07±0.02
	$\overline{t_2} \pm U(\overline{t_2})(s)$	660±180	500±270
ΔRH≠0 ΔT≠0 ΔW=0 V_{air}=1.6m/s	$\overline{x_1} \pm U(\overline{x_1})$	0.98±0.01	0.89±0.03
	$\overline{t_1} \pm U(\overline{t_1})(s)$	120±10	70±6
	$\overline{x_2} \pm U(\overline{x_2})$	0.02±0.01	0.11±0.03
	$\overline{t_2} \pm U(\overline{t_2})(s)$	1800±950	480±110

Table 3.30. Uncertainty of each coefficient describing the transient temperature response of the humidity/temperature transmitter and the thermocouple.

Test Conditions	Coefficient	Humidity/Temperature Transmitter		Thermocouple	
		Increase	Decrease	Increase	Decrease
ΔRH≠0 ΔT≠0 V_{air}=1.6m/s	$\overline{y_1} \pm U(\overline{y_1})$	0.94±0.03	0.90±0.02	0.86±0.17	0.87±0.03
	$\overline{t_1} \pm U(\overline{t_1})(s)$	69±11	70±10	3.5±0.4	3.6±1.5
	$\overline{y_2} \pm U(\overline{y_2})$	0.06±0.03	0.10±0.02	0.14±0.17	0.13±0.03
	$\overline{t_2} \pm U(\overline{t_2})(s)$	630±80	620±130	330±80	120±30
ΔRH=0 ΔT≠0 V_{air}=1.6m/s	$\overline{y_1} \pm U(\overline{y_1})$	0.91±0.02	0.92±0.01	0.76±0.07	0.80±0.08
	$\overline{t_1} \pm U(\overline{t_1})(s)$	72±5	67±3	5.1±1.5	5.1±0.8
	$\overline{y_2} \pm U(\overline{y_2})$	0.09±0.02	0.08±0.01	0.24±0.07	0.20±0.08
	$\overline{t_2} \pm U(\overline{t_2})(s)$	750±110	370±100	130±20	160±110
ΔRH≠0 ΔT≠0 ΔW=0 V_{air}=1.6m/s	$\overline{y_1} \pm U(\overline{y_1})$	0.91±0.01	0.94±0.01	0.83±0.09	0.82±0.12
	$\overline{t_1} \pm U(\overline{t_1})(s)$	72±4	73±2	4.1±1.7	3.3±1.5
	$\overline{y_2} \pm U(\overline{y_2})$	0.09±0.01	0.06±0.01	0.17±0.09	0.18±0.12
	$\overline{t_2} \pm U(\overline{t_2})(s)$	470±50	460±70	180±50	140±20

The information in Table 3.29 and Table 3.30 demonstrates the average value of each coefficient and its uncertainty to describe transient temperature and humidity response characteristics of the humidity/temperature transmitter and the thermocouple. For the transient humidity response of the transmitter, the relative uncertainty of first time constant (Table 3.29) is from ±8% to ±18%; for the transient temperature response of the transmitter, the relative uncertainty of first time constant is from ±3% to ±16%, but the relative uncertainty of the first time constant for the thermocouple response is greater, e.g., ±11% to ±45% (Table 3.30).

In this chapter, the transient characteristics of the humidity/temperature transmitter and the thermocouple have been studied. It is found that the humidity/temperature transmitter responds very fast (the first time constant is about 3s) to a step change in relative humidity with no temperature change but very slowly (the first time constant is about 2 minutes) with a temperature change. Hence, the humidity/temperature transmitter is recommended to measurement transient humidity change without a temperature change. The thermocouple responds very quickly to a step change in temperature and its first time constant is about 4s, but the humidity/temperature transmitter responds slowly to a step change in temperature and the first time constant is about 70s.

4. TESTS ON ENERGY WHEELS

In this chapter, the humidity/temperature transmitters, characterized for transient response alone, are used to measure the transient response of energy wheels using these transmitters downstream of the wheel. Two energy wheels (both 100 mm thick) coated with different desiccants are tested. All tests are done under the first two operating conditions as shown in Table 2.1 (i.e., $\Delta RH \neq 0$, $\Delta T = 0$ and $\Delta RH \neq 0$, $\Delta T \neq 0$). Three tests are presented at three different positions on each wheel face and three typical sets of data are obtained without and with a temperature change. In the experiment in this thesis the wheel is stationary and the conditions of the supply air entering the wheel are changed in a step fashion. Therefore, the wheel matrix releases or stores heat and moisture following the step change in inlet air conditions.

A secondary purpose of the chapter is the evaluation of the accuracy of the experimentally determined energy wheel transient humidity and temperature response considering the accuracy of each inlet and outlet air property measurements including the transient response characteristics of the outlet sensors as quantified in Chapter 3. Typical test data are shown graphically in Figures 4.1 to 4.6.

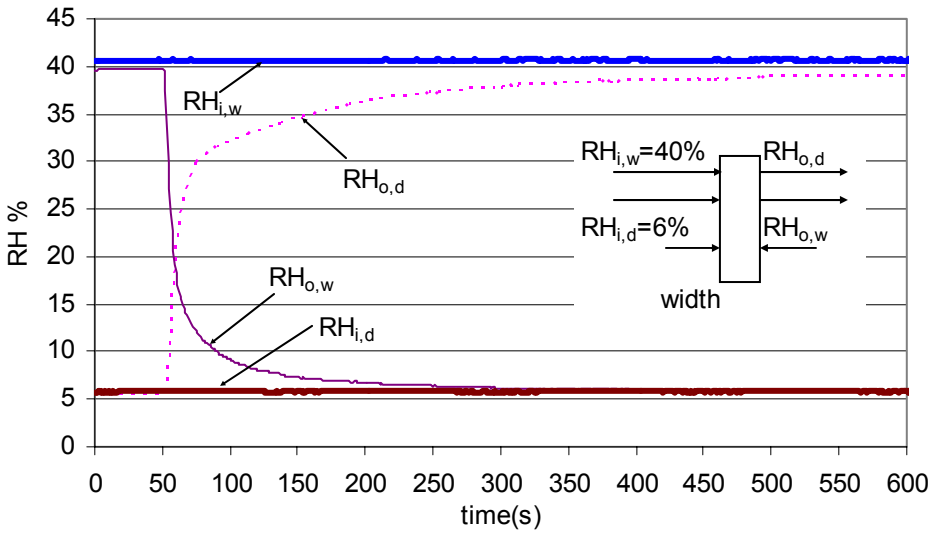

Figure 4.1 Measured inlet and outlet relative humidity for a molecular sieve energy wheel exposed to a step change in relative humidity with no change in temperature ($\Delta RH \neq 0$, $\Delta T = 0$ and V_{air}=1.6m/s, wheel width=100mm).

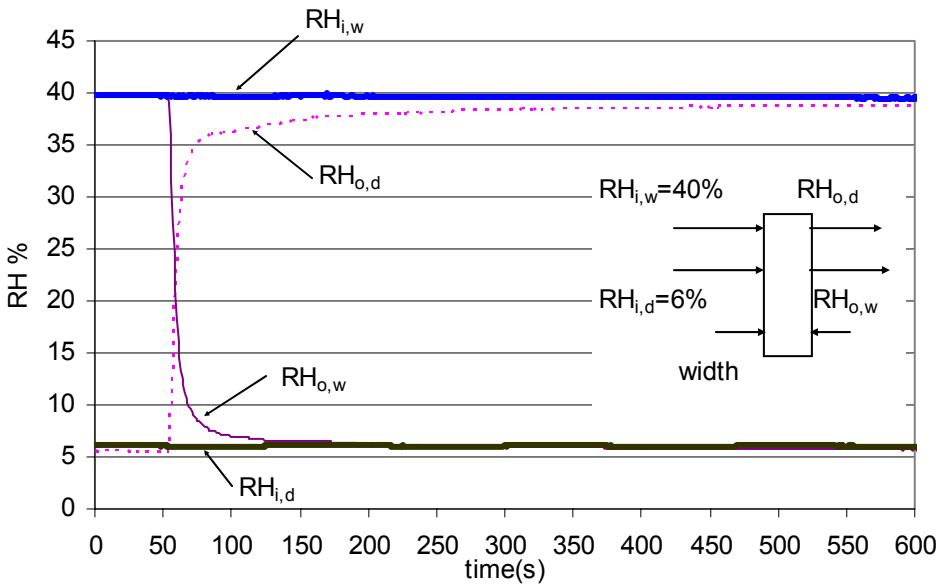

Figure 4.2 Measured inlet and outlet relative humidity for a silica gel energy wheel exposed to a step change in relative humidity with no change in temperature ($\Delta RH \neq 0$, $\Delta T = 0$ and V_{air}=1.6m/s, wheel width=100mm).

Figure 4.1 and Figure 4.2 are one set of measured data on a molecular sieve wheel and a silica gel wheel and present the measured relative humidity downstream of the energy wheel following a step change in inlet humidity under isothermal conditions ($\Delta RH \neq 0$, $\Delta T = 0$). The results show that the data from sensors ($RH_{o,d}$ and $RH_{o,w}$) are slightly different for the two wheels. For instance, the $RH_{o,d}$ sensor reads 29%RH 30s after the step change for the molecular sieve wheel; while the sensor reads 35%RH for the silica gel wheel at the same time. The $RH_{o,w}$ sensor reads 12% and 8%RH for the molecular sieve wheel and the silica gel wheel respectively, 30s after the step change. This shows that the desiccant, molecular sieve and silica gel desiccant have different characteristics of absorbing and desorbing moisture.

Figures 4.3 to 4.6 show the measured inlet and outlet humidity and temperature conditions that demonstrate the transient response of the two energy wheels for $\Delta RH \approx 34\%$ and $\Delta T \approx 30^{o}C$. The measured transient temperature response of the molecular sieve wheel is very similar to the response of the silica gel wheel. However, the measured humidity data in Figure 4.3 is significantly different from that presented in Figure 4.1. First of all, the transient humidity response is very slow when $\Delta T \neq 0$; secondly, the measured outlet data ($RH_{o,w}$ and $RH_{o,d}$) does not reach the inlet conditions ($RH_{i,w}$ and $RH_{i,d}$) at steady-state conditions, especially for the adsorption case. The measured temperature data in Figures 4.4 and 4.6 also show a difference

between the inlet and outlet readings at steady state. This temperature difference is due to heat conduction through the wheel matrix. Further analysis of the heat conduction is presented in Appendix B. This analysis shows that the heat conduction through the matrix will result in a temperature difference between the inlet and outlet conditions of about 5 to 6°C when the temperature difference between the inlet air streams is 30°C. This agrees reasonably well with the measured data in Figures 4.4 and 4.6. This temperature difference also causes the RH difference between the inlet and outlet conditions because relative humidity is associated with temperature.

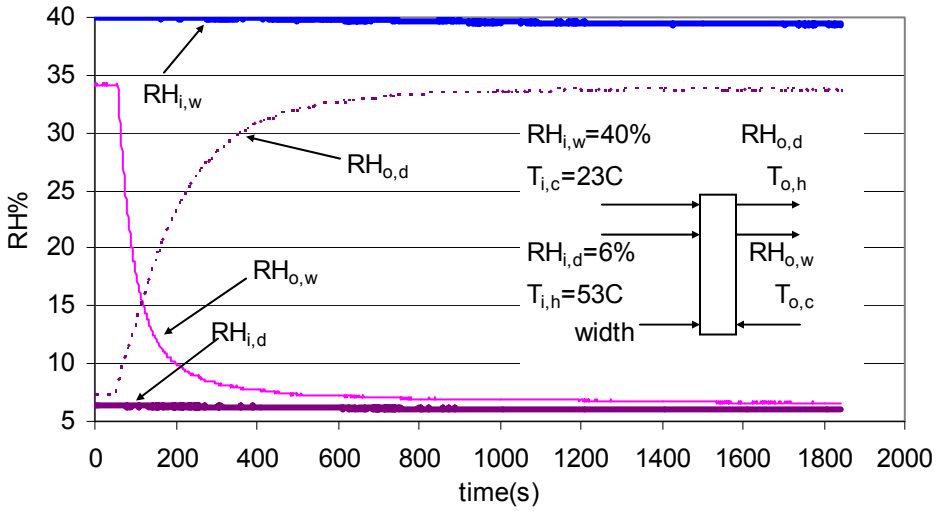

Figure 4.3 Measured inlet and outlet relative humidity for a molecular sieve energy wheel exposed to a step change in relative humidity and temperature ($\Delta RH \neq 0$, $\Delta T \neq 0$ and V_{air}=1.6m/s, wheel width=100mm).

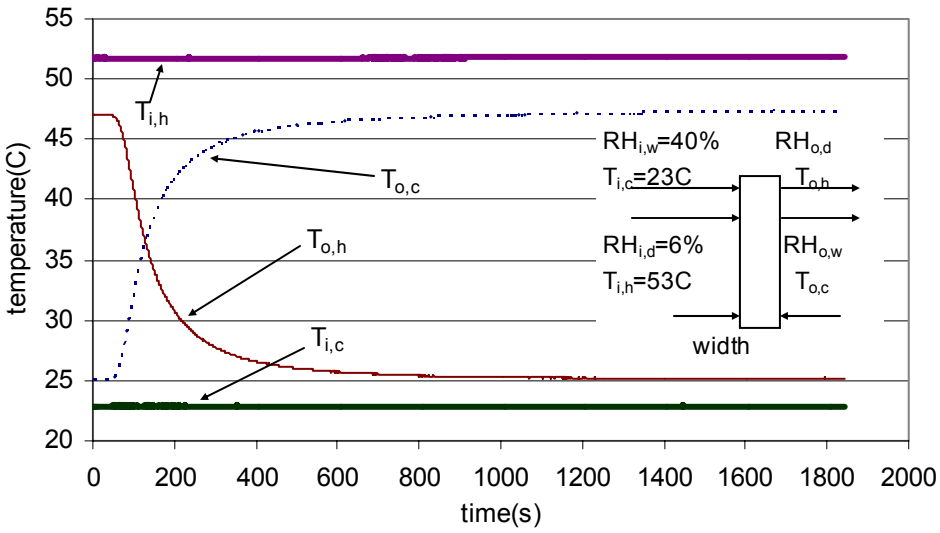

Figure 4.4 Measured inlet and outlet temperature for a molecular sieve energy wheel exposed to a step change in relative humidity and temperature ($\Delta RH \neq 0$, $\Delta T \neq 0$ and V_{air}=1.6m/s, wheel width=100mm).

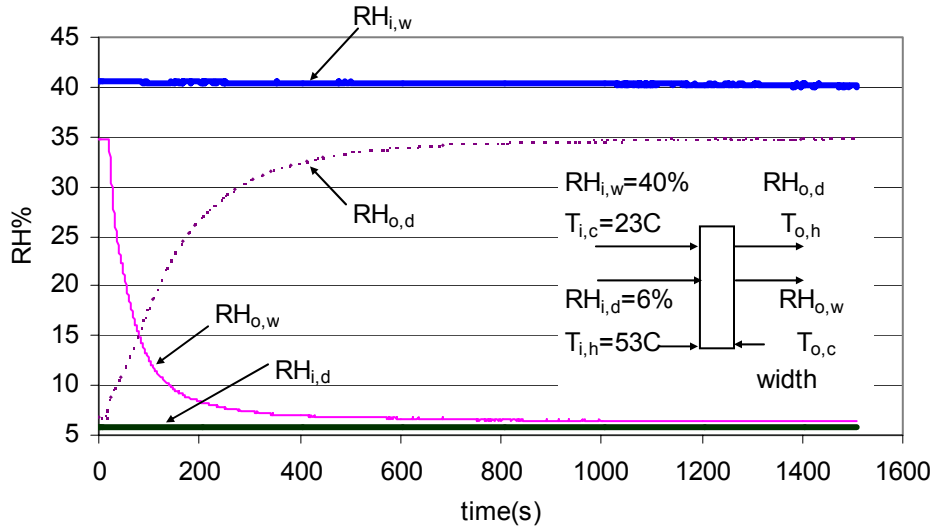

Figure 4.5 Measured inlet and outlet relative humidity for a silica gel energy wheel exposed to a step change in relative humidity and temperature ($\Delta RH \neq 0$, $\Delta T \neq 0$ and V_{air}=1.6m/s, wheel width=100mm).

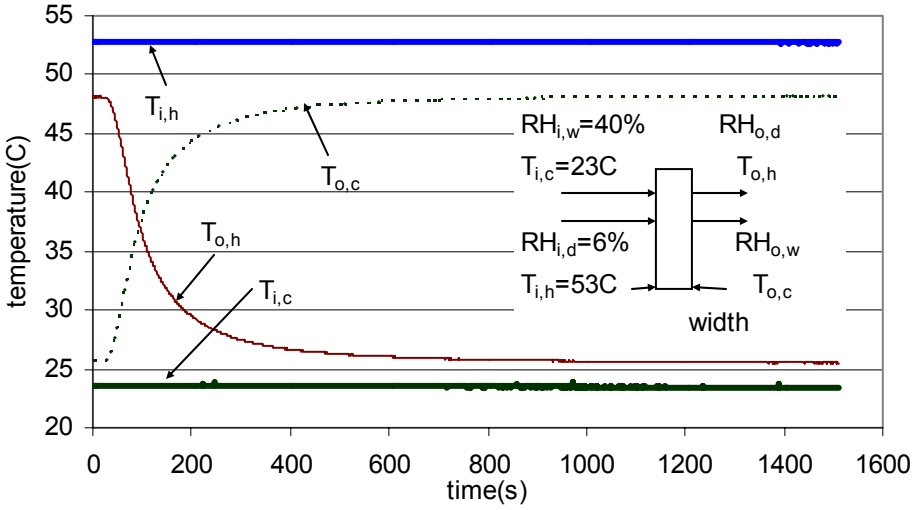

Figure 4.6 Measured inlet and outlet temperature for a silica gel energy wheel exposed to a step change in relative humidity and temperature ($\Delta RH \neq 0$, $\Delta T \neq 0$ and V_{air}=1.6m/s, wheel width=100mm).

4.1. Measured Outlet Relative Humidity Response of Energy Wheels

The measured outlet conditions are presented and calculated using exponential functions similar to the functions used to calculate the response of the sensor alone. To distinguish between the correlations for the sensor alone, the subscript symbol w+s is used for the correlations of the wheel and sensor and upper case symbols are applied for each coefficient. The relative humidity transient data correlations presented below are based on the tests of the two energy wheels presented previously. The correlation equation for the normalized outlet humidity ($\frac{\Delta\phi_{w+s}}{\Delta\phi_{(w+s)o}}$) during moisture adsorption into the wheel from the air (i.e. increasing relative humidity) is:

$$\frac{\Delta\phi_{w+s}}{\Delta\phi_{(w+s)o}}(t)_{ads} = X_1(1-e^{-t/T_1}) + X_2(1-e^{-t/T_2}), \tag{4.1}$$

and the correlation equation used for the normalized outlet humidity ($\frac{\Delta\phi_{w+s}}{\Delta\phi_{(w+s)o}}$) during moisture desorption from the wheel into the air (i.e. decreasing relative humidity) is:

$$\frac{\Delta\phi_{w+s}}{\Delta\phi_{(w+s)o}}(t)_{des} = X_1 e^{-t/T_1} + X_2 e^{-t/T_2}, \tag{4.2}$$

where the coefficients X_1 and X_2 have different values of adsorption and desorption and satisfy the equation:

$$X_1 + X_2 = 1,\ X_1 \geq 0 \text{ and } X_2 \geq 0, \qquad 4.3)$$

the other symbols are:

$\Delta\phi_{w+s} = \left|\phi_{w+s} - \phi_{(w+s)i}\right|$, where $\phi_{(w+s)i}$ is the initial condition;

$\Delta\phi_{(w+s)o} = \left|\phi_{(w+s)f} - \phi_{(w+s)i}\right|$, where $\phi_{(w+s)f}$ is the final condition; and T_1 and T_2 are the first and second time constants of wheel plus sensor response respectively.

Figures 4.7 and 4.8 show a typical comparison between the adsorption and desorption data and the correlation equation (4.1) for a molecular sieve energy wheel. The time constants (T_1, T_2), coefficients (X_1, X_2) and r^2 values are summarized in Tables 4.1 to 4.4 for three random measurement positions on wheel face with test conditions of $\Delta RH \neq 0$ and $\Delta T = 0$. The coefficients and time constants obtained from the mathematic computer software, TableCurve, are nearly the same at all three measurement locations. This suggests that the number of flow tubes of the wheel matrix in each test is large enough to get a reasonable representative average response of the wheel regardless of where the switch plate device is placed on the wheel.

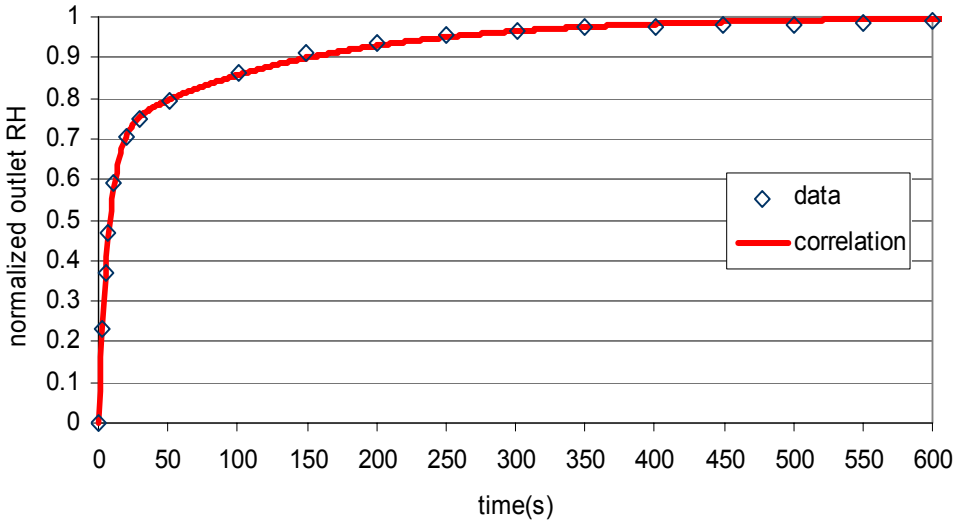

Figure 4.7 Comparison of the measured and correlated normalized outlet humidity for a molecular sieve wheel exposed to an increase in relative humidity ($\Delta RH \neq 0$, $\Delta T = 0$ and V_{air}=1.6m/s in Figure 4.1).

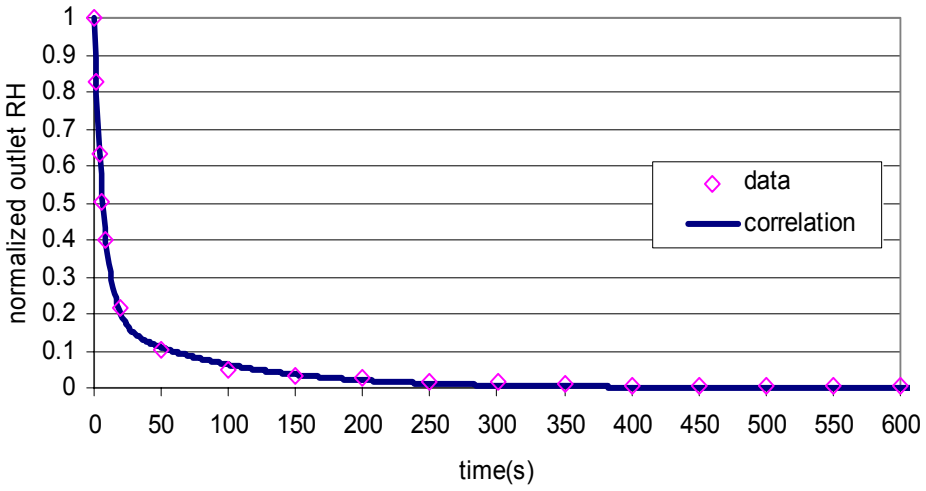

Figure 4.8 Comparison of the measured and correlated normalized outlet humidity decrease for a molecular sieve wheel exposed to a decrease in relative humidity ($\Delta RH \neq 0$, $\Delta T = 0$ and $V_{air} = 1.6$m/s in Figure 4.1).

In order to determine the exact switching time, the procedure outlined in Section 3.3 is used in this chapter to analyze the measured data. This analysis shows that the uncertainty for t=0 is ±0.2s. This uncertainty is included in the uncertainty analysis for the time constants that will be presented in Section 4.4.

Table 4.1. Adsorption coefficients (X_1, X_2) and time constants (T_1, T_2) in equation (4.1) describing the transient humidity response of a 100mm thick molecular sieve wheel plus the humidity/temperature transmitter ($\Delta RH \neq 0$, $\Delta T = 0$, and $V_{air} = 1.6$m/s).

Inlet conditions	X_1	T_1(s)	X_2	T_2(s)	r^2
dry side: $T_{i,d} \approx 23^oC$, $\Phi_{i,d} \approx 6\%$ wet side: $T_{i,w} \approx 23^oC$, $\Phi_{i,w} \approx 40\%$	0.71	7.1	0.29	140	0.994
	0.77	6.8	0.23	110	0.992
	0.78	7.8	0.22	120	0.993
dry side: $T_{i,d} \approx 23^oC$, $\Phi_{i,d} \approx 6\%$ wet side: $T_{i,w} \approx 23^oC$, $\Phi_{i,w} \approx 50\%$	0.68	6.6	0.32	130	0.997
	0.68	7.2	0.32	140	0.996
	0.68	6.5	0.32	140	0.991
dry side: $T_{i,d} \approx 23^oC$, $\Phi_{i,d} \approx 6\%$ wet side: $T_{i,w} \approx 23^oC$, $\Phi_{i,w} \approx 60\%$	0.67	6.3	0.33	130	0.997
	0.67	5.7	0.33	130	0.997
	0.66	7.3	0.34	140	0.993

Table 4.2. Desorption coefficients (X_1, X_2) and time constants (T_1, T_2) in equation (4.2) describing the transient humidity response of a 100mm thick molecular sieve wheel plus the humidity/temperature transmitter ($\Delta RH \neq 0$, $\Delta T=0$, and $V_{air}=1.6$m/s).

Inlet conditions	X_1	T_1(s)	X_2	T_2(s)	r^2
dry side: $T_{i,d}\approx 23^oC$, $\Phi_{i,d}\approx 6\%$ wet side: $T_{i,w}\approx 23^oC$, $\Phi_{i,w}\approx 40\%$	0.81	7.0	0.19	90	0.991
	0.86	8.5	0.14	120	0.988
	0.90	8.6	0.10	190	0.980
dry side: $T_{i,d}\approx 23^oC$, $\Phi_{i,d}\approx 6\%$ wet side: $T_{i,w}\approx 23^oC$, $\Phi_{i,w}\approx 50\%$	0.83	7.2	0.17	100	0.988
	0.84	7.7	0.16	100	0.990
	0.84	8.1	0.16	100	0.989
dry side: $T_{i,d}\approx 23^oC$, $\Phi_{i,d}\approx 6\%$ wet side: $T_{i,w}\approx 23^oC$, $\Phi_{i,w}\approx 60\%$	0.83	6.4	0.17	90	0.989
	0.86	7.7	0.14	100	0.991
	0.83	7.0	0.17	90	0.988

Table 4.3. Adsorption coefficients (X_1, X_2) and time constants (T_1, T_2) in equation (4.1) describing the transient humidity response of a 100mm thick silica gel wheel plus the humidity/temperature transmitter ($\Delta RH \neq 0$, $\Delta T=0$, and $V_{air}=1.6$m/s).

Inlet conditions	X_1	T_1(s)	X_2	T_2(s)	r^2
dry side: $T_{i,d}\approx 23^oC$, $\Phi_{i,d}\approx 6\%$ wet side: $T_{i,w}\approx 23^oC$, $\Phi_{i,w}\approx 40\%$	0.90	5.9	0.10	120	0.982
	0.87	5.5	0.13	100	0.991
	0.88	8.0	0.12	150	0.991
dry side: $T_{i,d}\approx 23^oC$, $\Phi_{i,d}\approx 6\%$ wet side: $T_{i,w}\approx 23^oC$, $\Phi_{i,w}\approx 50\%$	0.88	5.9	0.12	120	0.975
	0.89	5.4	0.11	120	0.973
	0.85	6.1	0.15	110	0.973
dry side: $T_{i,d}\approx 23^oC$, $\Phi_{i,d}\approx 6\%$ wet side: $T_{i,w}\approx 23^oC$, $\Phi_{i,w}\approx 60\%$	0.84	5.8	0.16	110	0.989
	0.80	5.4	0.20	120	0.986
	0.78	7.0	0.22	140	0.995

Table 4.4. Desorption coefficients (X_1, X_2) and time constants (T_1, T_2) in equation (4.2) describing the transient humidity response of a 100mm thick silica gel wheel plus the humidity/temperature transmitter ($\Delta RH \neq 0$, $\Delta T=0$, and $V_{air}=1.6$m/s).

Inlet conditions	X_1	T_1(s)	X_2	T_2(s)	r^2
dry side: $T_{i,d}\approx 23^oC$, $\Phi_{i,d}\approx 6\%$ wet side: $T_{i,w}\approx 23^oC$, $\Phi_{i,w}\approx 40\%$	0.96	6.2	0.04	300	0.992
	0.95	6.7	0.05	200	0.986
	0.93	7.3	0.07	120	0.985
dry side: $T_{i,d}\approx 23^oC$, $\Phi_{i,d}\approx 6\%$ wet side: $T_{i,w}\approx 23^oC$, $\Phi_{i,w}\approx 50\%$	0.96	6.2	0.04	400	0.989
	0.96	7.3	0.04	260	0.980
	0.96	7.5	0.04	100	0.990
dry side: $T_{i,d}\approx 23^oC$, $\Phi_{i,d}\approx 6\%$ wet side: $T_{i,w}\approx 23^oC$, $\Phi_{i,w}\approx 60\%$	0.92	4.7	0.08	210	0.992
	0.95	7.4	0.05	210	0.991
	0.93	8.4	0.07	170	0.991

Comparing the results in Tables 4.1 to 4.4 and Tables 3.1 to 3.2, which are all obtained with no temperature change ($\Delta RH \neq 0$ and $\Delta T=0$), it can be seen that the first time constant of the combined energy wheel and sensor is about 2 to 3 times larger than the first time constant of the sensors alone. The reason for this is that the moisture storage capacity of the energy wheel is large, while the moisture storage capacity of the humidity/temperature transmitter is quite small.

The effect of the measurement time interval (e.g., $0 \leq t \leq 5s$, $0 \leq t \leq 10s$, and $0 \leq t \leq 20s$) on the best-fit value of each coefficient, X_1, X_2, T_1 and T_2, is investigated in this chapter using the same analysis presented in Section 3.2.1. Table 4.5 and Table 4.6 contain one typical example of each coefficient for a silica gel wheel analyzed over the three different time intervals for $\Delta RH \neq 0$, $\Delta T=0$. The data in Tables 4.5 and 4.6 indicate that the first time constant does not change significantly when the time interval changes when comparing to data in Tables 4.3 and 4.4.

Table 4.5. Adsorption coefficients (X_1, X_2) and time constants (T_1, T_2) in equation (4.1) describing the transient humidity response of a 100mm thick silica gel wheel plus humidity/temperature transmitter in different time intervals ($\Delta RH \neq 0$, $\Delta T=0$ and V_{air}=1.6m/s).

Inlet conditions: dry side: $T_{i,d} \approx 23^oC$, $\Phi_{i,d} \approx 6\%$ wet side: $T_{i,w} \approx 23^oC$, $\Phi_{i,w} \approx 40\%$	X_1	T_1(s)	X_2	T_2(s)	r^2
$0 \leq t \leq 5s$	0.56	7.9	0.44	7.9	0.966
$0 \leq t \leq 10s$	0.65	7.1	0.35	7.2	0.983
$0 \leq t \leq 20s$	0.98	6.8	0.02	6E20	0.989

Table 4.6. Desorption coefficients (X_1, X_2) and time constants (T_1, T_2) in equation (4.2) describing the transient humidity response of a 100mm thick silica gel wheel plus humidity/temperature transmitter in different time intervals ($\Delta RH \neq 0$, $\Delta T=0$ and V_{air}=1.6m/s).

Inlet conditions: dry side: $T_{i,d} \approx 23^oC$, $\Phi_{i,d} \approx 6\%$ wet side: $T_{i,w} \approx 23^oC$, $\Phi_{i,w} \approx 40\%$	X_1	T_1(s)	X_2	T_2(s)	r^2
$0 \leq t \leq 5s$	0.60	7.0	0.40	7.1	0.987
$0 \leq t \leq 10s$	0.94	7.4	0.07	7.5	0.993
$0 \leq t \leq 20s$	0.98	6.2	0.02	2E20	0.991

Tables 4.7 and 4.8 include time constants and coefficients for these two energy wheels exposed to a simultaneous change in relative humidity and temperature ($\Delta RH \neq 0$, $\Delta T \neq 0$). Comparing the time constants in Tables 4.7 and 4.8 with those in Tables 4.1 to 4.4 shows that the first time constants are much greater with $\Delta T \neq 0$, especially for the first time constant in

adsorption, which is at least 20 times greater than that obtained with $\Delta T=0$. As discussed previously, it is believed heat conduction through the energy wheel affects the relative humidity response reading.

Table 4.7. Coefficients (X_1, X_2) and time constants (T_1, T_2) in equations (4.1) and (4.2) describing the transient humidity response of a 100mm thick molecular sieve wheel plus the humidity/temperature transmitter ($\Delta RH\neq0$, $\Delta T\neq0$ and V_{air}=1.6m/s,).

Molecular sieve wheel	Inlet conditions: hot, dry side:$T_{i,h}\approx53^oC$, $\Phi_{i,d}\approx6\%$ cool, wet side:$T_{i,c}\approx23^oC$, $\Phi_{i,w}\approx40\%$				
	X_1	T_1(s)	X_2	T_2(s)	r^2
Adsorption	0.99	170	0.01	2400	0.998
	0.98	160	0.02	1000	0.999
	0.99	160	0.01	2300	0.999
Desorption	0.89	43	0.11	290	0.999
	0.80	38	0.20	170	0.999
	0.86	42	0.14	300	0.999

Table 4.8. Coefficients (X_1, X_2) and time constants (T_1, T_2) in equations (4.1) and (4.2) describing the transient humidity response of a 100mm thick silica gel wheel plus the humidity/temperature transmitter ($\Delta RH\neq0$, $\Delta T\neq0$ and V_{air}=1.6m/s).

Silica gel wheel	Inlet conditions: hot, dry side:$T_{i,h}\approx53^oC$, $\Phi_{i,d}\approx6\%$ cool, wet side:$T_{i,c}\approx23^oC$, $\Phi_{i,w}\approx40\%$				
	X_1	T_1(s)	X_2	T_2(s)	r^2
Adsorption	0.99	150	0.01	1100	0.998
	0.98	160	0.02	1500	0.997
	0.98	150	0.02	1400	0.998
Desorption	0.82	38	0.18	180	0.998
	0.87	45	0.13	250	0.999
	0.86	43	0.14	240	0.999

4.2. Measured Outlet Temperature Response of Energy Wheels

In this section, the outlet temperature response of the two energy wheels is measured using the humidity/temperature transmitter and an independent thermocouple. It is expected that the transient temperature response of the energy wheel plus sensor will be slower than a sensor alone, because of the larger heat capacity of the energy wheel. Also, heat conduction losses or gains through the matrix core will occur for these test conditions causing very long time delay

effects. Heat conduction inside the energy wheel is discussed in Appendix B. The equations used to fit the measured temperature data are:

a) for heat transfer from the air to the wheel (increasing temperature)

$$\frac{\Delta T_{w+s}}{\Delta T_{(w+s)o}}(t)_{inc} = Y_1(1-e^{-t/t_1}) + Y_2(1-e^{-t/t_2}), \tag{4.4}$$

and b) for heat transfer from the wheel to the air (decreasing relative humidity)

$$\frac{\Delta T_{w+s}}{\Delta T_{(w+s)o}}(t)_{dec} = Y_1 e^{-t/t_1} + Y_2 e^{-t/t_2}, \tag{4.5}$$

where the coefficients Y_1 and Y_2 satisfy the same equation for both temperature increasing and decreasing,

$$Y_1 + Y_2 = 1,\ Y_1 \geq 0\ , Y_2 \geq 0, \tag{4.6}$$

but with different values for each case. Other symbols are:

ΔT_{w+s} =change in temperature $= \left| T_{w+s} - T_{(w+s)i} \right|$, where $T_{(w+s)i}$ is the initial condition;

$\Delta T_{(w+s)o}$ = maximum change in temperature $= \left| T_{(w+s)f} - T_{(w+s)i} \right|$, where $T_{(w+s)f}$ is the final condition,

and t_1 and t_2 are the first and second time constants respectively.

4.2.1. Humidity/Temperature Transmitter Temperature Data

This section presents the measured temperature data by the humidity/temperature transmitter. These measured data include the transient response of the sensor and the wheel. Figures 4.9 and 4.10 contain one example of the curve fitting for the molecular sieve wheel and Table 4.9 quantifies the agreement demonstrating that r^2 is 0.988 or greater for all cases. The first time constant is around 100s, which is greater than the first time constant of both the temperature sensors as determined in Section 3.2.2 (i.e., 70s for the transmitter and 4s for the thermocouple). Heat capacity effects inside the matrix of the energy wheel are the prime reason for these larger time constants.

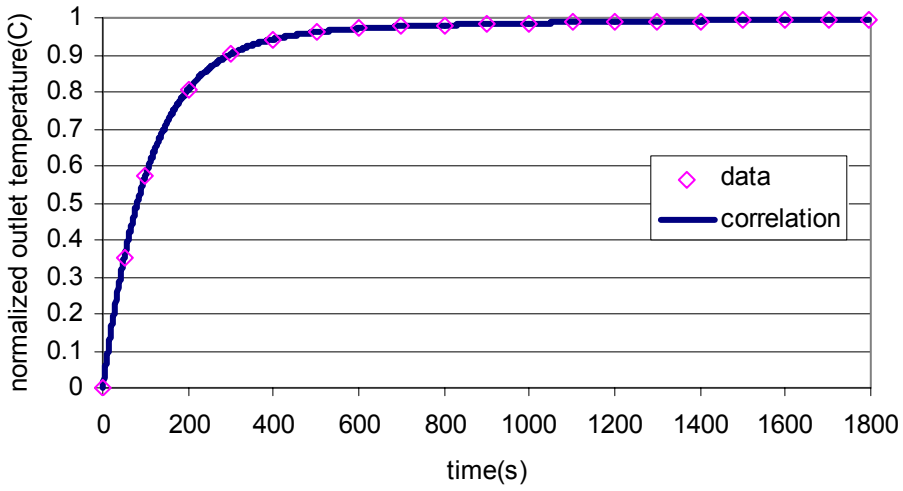

Figure 4.9 Comparison of measured and correlated outlet temperature increase for a molecular sieve wheel plus a humidity/temperature transmitter (Y_1=0.94, T_1=109s, Y_2=0.06, T_2=700s) ($\Delta RH \neq 0$, $\Delta T \neq 0$ and V_{air}=1.6m/s in Figure 4.4).

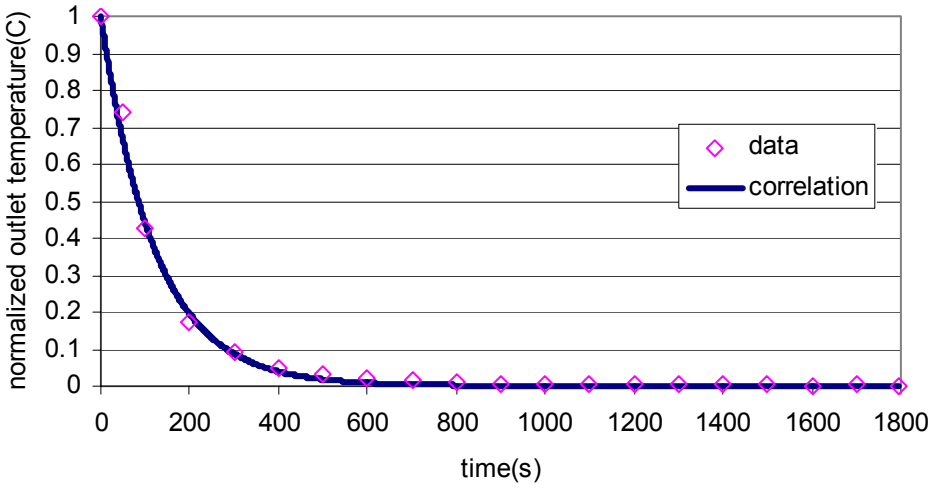

Figure 4.10 Comparison of measured and correlated outlet temperature decrease for a molecular sieve wheel plus a humidity/temperature transmitter (Y_1=0.96, T_1=120s, Y_2=0.04, T_2=390s) ($\Delta RH \neq 0$, $\Delta T \neq 0$ and V_{air}=1.6m/s in Figure 4.4).

Table 4.9. Coefficients (Y_1, Y_2) and time constants (T_1, T_2) in equations (4.4) and (4.5) describing the transient temperature response of a 100mm thick molecular sieve wheel plus the humidity/temperature transmitter ($\Delta RH \neq 0$, $\Delta T \neq 0$ and V_{air}=1.6m/s,).

Molecular Sieve wheel	Inlet conditions: hot, dry side:$T_{i,h} \approx 53^oC$, $\Phi_{i,d} \approx 6\%$ cool, wet side:$T_{i,c} \approx 23^oC$, $\Phi_{i,w} \approx 40\%$				
	Y_1	T_1(s)	Y_2	T_2(s)	r^2
Increasing	0.94	109	0.06	700	0.994
	0.94	103	0.06	610	0.993
	0.94	101	0.06	620	0.991
Decreasing	0.96	120	0.04	390	0.994
	0.95	100	0.05	590	0.996
	0.99	104	0.01	700	0.988

For the wheel coated with silica gel, the temperature response is very close to that of the molecular sieve wheel. The coefficients are summarized in Table 4.10 and show that the first time constants are all slightly less than 100s. It is thought that silica gel wheel has different overall heat conductivity than the molecular sieve wheel.

Table 4.10. Coefficients (Y_1, Y_2) and time constants (T_1, T_2) in equations (4.4) and (4.5) describing the transient temperature response of a 100mm thick silica gel wheel plus the humidity/temperature transmitter ($\Delta RH \neq 0$, $\Delta T \neq 0$ and V_{air}=1.6m/s).

Silica Gel wheel	Inlet conditions: hot, dry side:$T_{i,h} \approx 53^oC$, $\Phi_{i,d} \approx 6\%$ cool, wet side:$T_{i,c} \approx 23^oC$, $\Phi_{i,w} \approx 40\%$				
	Y_1	T_1(s)	Y_2	T_2(s)	r^2
Increasing	0.96	98	0.04	560	0.991
	0.96	97	0.04	620	0.992
	0.93	92	0.07	480	0.992
Decreasing	0.95	95	0.05	550	0.993
	0.95	97	0.05	570	0.993
	0.95	94	0.05	510	0.994

The average value of each parameter (X_1, X_2, Y_1, Y_2, T_1 and T_2) is computed because the wheel plus sensor response does not seem to depend on the magnitude of the relative humidity and temperature change and these are summarized in Tables 4.11 and Table 4.12.

Table 4.11. Average coefficients describing the transient humidity response of a molecular sieve and a silica gel energy wheel plus humidity/temperature transmitter.

Test Conditions	Coefficient	Molecular Sieve Wheel		Silica Gel Wheel	
		Adsorption	Desorption	Adsorption	Desorption
ΔRH≠0 ΔT=0 V_{air}=1.6m/s	$\overline{X_1}$	0.70	0.85	0.85	0.95
	$\overline{T_1}(s)$	6.8	7.7	6.4	6.9
	$\overline{X_2}$	0.30	0.15	0.15	0.05
	$\overline{T_2}(s)$	120	110	120	230
ΔRH≠0 ΔT≠0 V_{air}=1.6m/s	$\overline{X_1}$	0.99	0.87	0.98	0.86
	$\overline{T_1}(s)$	163	41	156	44
	$\overline{X_2}$	0.01	0.13	0.02	0.14
	$\overline{T_2}(s)$	1100	240	1300	230

Table 4.12. Average coefficients describing the transient temperature response of a molecular sieve and a silica gel energy wheel plus humidity/temperature transmitter.

Test Conditions	Coefficient	Molecular Sieve Wheel		Silica Gel Wheel	
		Increase	Decrease	Increase	Decrease
ΔRH≠0 ΔT≠0 V_{air}=1.6m/s	$\overline{Y_1}$	0.94	0.96	0.95	0.95
	$\overline{T_1}(s)$	104	103	96	95
	$\overline{Y_2}$	0.06	0.03	0.05	0.05
	$\overline{T_2}(s)$	640	580	530	540

Based on the information in Tables 4.9 to 4.10, the transient humidity and temperature response expressions for the energy wheels plus humidity/temperature transmitter are summarized in Table 4.13.

Table 4.13. Transient characteristics of the energy wheel plus the humidity/temperature transmitter.

Operating Conditions	Transient Response of Wheel plus Transmitter
ΔRH≠0, ΔT=0, V_{air}=1.6m/s	<u>A molecular sieve wheel plus the transmitter:</u> $\frac{\Delta\phi_{w+s}}{\Delta\phi_{(w+s)o}}(t)_{ads} = 0.70(1-e^{-t/6.8}) + 0.30(1-e^{-t/120})$ $\frac{\Delta\phi_{w+s}}{\Delta\phi_{(w+s)o}}(t)_{des} = 0.85(1-e^{-t/7.7}) + 0.15(1-e^{-t/100})$ <u>A silica gel wheel plus the transmitter:</u> $\frac{\Delta\phi_{w+s}}{\Delta\phi_{(w+s)o}}(t)_{ads} = 0.85(1-e^{-t/6.4}) + 0.15(1-e^{-t/120})$ $\frac{\Delta\phi_{w+s}}{\Delta\phi_{(w+s)o}}(t)_{des} = 0.95(1-e^{-t/6.9}) + 0.30(1-e^{-t/230})$
ΔRH≠0, ΔT≠0, V_{air}=1.6m/s	<u>A molecular sieve wheel plus the transmitter:</u> $\frac{\Delta\phi_{w+s}}{\Delta\phi_{(w+s)o}}(t)_{ads} = 0.99(1-e^{-t/163}) + 0.01(1-e^{-t/1100})$ $\frac{\Delta\phi_{w+s}}{\Delta\phi_{(w+s)o}}(t)_{des} = 0.87(1-e^{-t/41}) + 0.13(1-e^{-t/240})$ $\frac{\Delta T_{w+s}}{\Delta T_{(w+s)o}}(t)_{inc} = 0.94(1-e^{-t/104}) + 0.06(1-e^{-t/640})$ $\frac{\Delta T_{w+s}}{\Delta T_{(w+s)o}}(t)_{dec} = 0.96(1-e^{-t/103}) + 0.04(1-e^{-t/580})$ <u>A silica gel wheel plus the transmitter:</u> $\frac{\Delta\phi_{w+s}}{\Delta\phi_{(w+s)o}}(t)_{ads} = 0.98(1-e^{-t/156}) + 0.02(1-e^{-t/1300})$ $\frac{\Delta\phi_{w+s}}{\Delta\phi_{(w+s)o}}(t)_{des} = 0.86(1-e^{-t/44}) + 0.14(1-e^{-t/230})$ $\frac{\Delta T_{w+s}}{\Delta T_{(w+s)o}}(t)_{inc} = 0.95(1-e^{-t/96}) + 0.05(1-e^{-t/530})$ $\frac{\Delta T_{w+s}}{\Delta T_{(w+s)o}}(t)_{dec} = 0.95(1-e^{-t/95}) + 0.05(1-e^{-t/540})$

4.2.2. Thermocouple Temperature Data

The T-type thermocouple is also used to measure the transient temperature data of the energy wheel in order to study the difference with the data measured by the temperature transmitter. It is found that combined response of the wheel plus sensor is faster with a thermocouple downstream of the wheel than with the temperature transmitter downstream. Figure 4.11 presents a comparison between the temperature data measured with thermocouples and transmitters for $\Delta RH \neq 0$ and $\Delta T \neq 0$. The curves $TC_{o,c}$ and $TC_{o,h}$ indicate thermocouples response, and $T_{o,c}$ and $T_{o,h}$ are temperature response of transmitters.

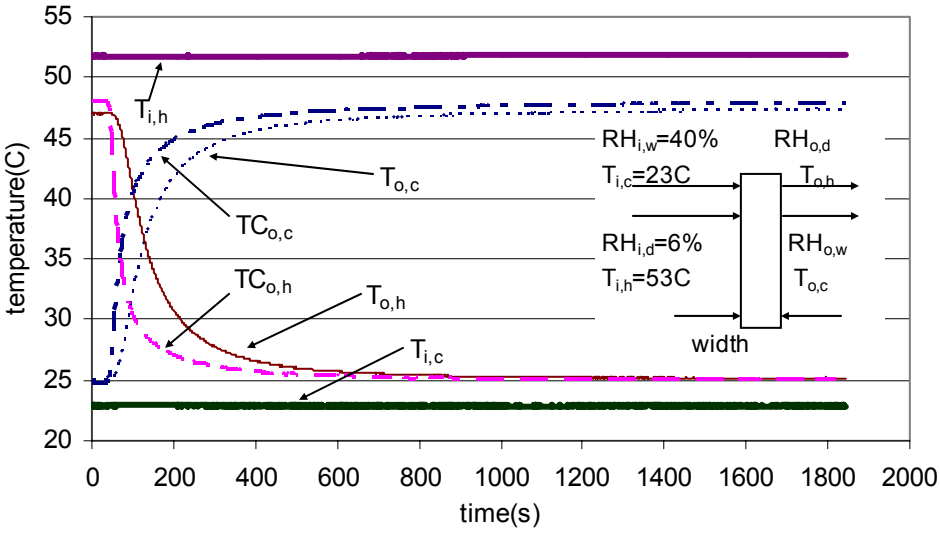

Figure 4.11 Comparison of the measured outlet transient temperature response of a molecular sieve wheel plus the transmitters and the thermocouples ($\Delta RH \neq 0$, $\Delta T \neq 0$ and V_{air}=1.6m/s width=100mm,).

The response of the energy wheel with a thermocouple follows the correlation equations (4.4) and (4.5). The time constants and coefficients are obtained by curve fitting and presented in Tables 4.14 and 4.15 for three measurement locations, the statistically averaged values are in Table 4.16.

Table 4.14. Coefficients (Y_1, Y_2) and time constants (T_1, T_2) in equations (4.4) and (4.5) describing the transient temperature response of a 100mm thick molecular sieve wheel plus a thermocouple with $\Delta RH \neq 0$, $\Delta T \neq 0$ and V_{air}=1.6m/s.

Wheel+ Thermocouple	Inlet conditions: hot, dry side:$T_{i,h}\approx 53^oC$, $\Phi_{i,d}\approx 6\%$ cool, wet side:$T_{i,c}\approx 23^oC$, $\Phi_{i,w}\approx 40\%$				
	Y_1	T_1(s)	Y_2	T_2(s)	r^2
Increasing	0.85	29	0.15	250	0.996
	0.87	40	0.13	320	0.995
	0.82	43	0.18	320	0.996
Decreasing	0.82	32	0.18	210	0.997
	0.86	30	0.14	250	0.991
	0.87	35	0.13	250	0.992

Table 4.15. Coefficients (Y_1, Y_2) and time constants (T_1, T_2) in equations (4.4) and (4.5) describing the transient temperature response of a 100mm thick silica gel wheel plus a thermocouple with $\Delta RH \neq 0$, $\Delta T \neq 0$ and V_{air}=1.6m/s.

Wheel+ Thermocouple	Inlet conditions: hot, dry side:$T_{i,h}\approx 53^oC$, $\Phi_{i,d}\approx 6\%$ cool, wet side:$T_{i,c}\approx 23^oC$, $\Phi_{i,w}\approx 40\%$				
	Y_1	T_1(s)	Y_2	T_2(s)	r^2
Increasing	0.72	26	0.28	170	0.998
	0.81	28	0.19	210	0.996
	0.74	29	0.26	200	0.997
Decreasing	0.80	25	0.20	220	0.996
	0.71	25	0.29	180	0.997
	0.80	26	0.20	210	0.996

Table 4.16. Average coefficients describing the transient temperature response of the energy wheel plus the thermocouple.

Test Conditions	Coefficient	Molecular Sieve Wheel		Silica Gel Wheel	
		Increase	Decrease	Increase	Decrease
$\Delta RH \neq 0$ $\Delta T \neq 0$ V_{air}=1.6m/s	$\overline{Y_1}$	0.85	0.84	0.76	0.79
	$\overline{T_1}(s)$	37	32	28	25
	$\overline{Y_2}$	0.15	0.16	0.24	0.21
	$\overline{T_2}(s)$	300	230	190	200

The average first time constant for the transient temperature response of the energy wheel plus the thermocouple is about 30 to 40s, which is about 10 times greater than that for the thermocouple alone (3.5~3.6s).

4.3. Analysis of Energy Wheel Data

The data and correlations in the previous section include both the wheel and sensor response, but determination of wheel response alone is desired. To determine the transient response of the wheel alone, the measured data are corrected to account for the transient response of the sensor using Duhamel's equation (Wylie, 1975) written in the form:

$$y(t) = \int_0^t A'(t-t')F(t')dt', \tag{4.7}$$

where for this application

$$y(t) = \frac{\Delta\phi_{w+s}}{\Delta\phi_{(w+s)_o}}(t), \tag{4.8}$$

is the normalized response of the wheel and sensor, and

$$A'(t-t') = \frac{\partial}{\partial t}[\frac{\Delta\phi_s}{\Delta\phi_{so}}(t-t')], \tag{4.9}$$

is normalized time derivative of the sensor response alone and F(t') is the response of the wheel alone. Therefore F(t') is considered to be the unknown characteristic while $\frac{\Delta\phi_{w+s}}{\Delta\phi_{(w+s)o}}(t)$ and $\frac{\Delta\phi_s}{\Delta\phi_{so}}(t)$ are known from the correlation equations. Equation (4.7) can be written as,

$$\frac{\Delta\phi_{w+s}}{\Delta\phi_{(w+s)o}}(t) = \int_0^t \frac{\partial}{\partial t}[\frac{\Delta\phi_s}{\Delta\phi_{so}}(t-t')]F(t')dt'. \tag{4.10}$$

To solve equation (4.10) for F(t) (i.e., the response of the wheel alone), the Laplace transform, $\mathcal{L}$, is applied. Using the convolution properties of this equation, the following equation results (Wylie, 1975):

$$\mathcal{L}[\,y(t)\,] = \mathcal{L}[\int_0^t A'(t-t')F(t')dt'\,] = \mathcal{L}[\,A'(t)\,]\mathcal{L}[\mathrm{F(t)}]. \tag{4.11}$$

This allows $\mathcal{L}$ [F(t)] to be obtained as

$$\mathcal{L}[\mathrm{F(t)}] = \mathcal{L}[\,y(t)\,]/\mathcal{L}[\,A'(t)\,]. \tag{4.12}$$

The Laplace transform results in a solution in the transformed "s" space that must be transformed back into real time using the inverse transform equation:

$$F(t)= \mathcal{L}^{-1}\{\mathcal{L}[\, y(t)\,]/\mathcal{L}[\, A'(t)\,]\}. \tag{4.13}$$

These transformations are quite complicated and therefore the commercial math package, Maple, is used. The details are in Appendix C. The final equations for the time response of the wheel during adsorption is

$$F(t)_{ads} = X_1(1-\frac{T_1-k_1+\frac{k_2}{T_1}}{T_1-k_3}e^{-t/T_1}) + X_2(1-\frac{k_1-T_2-\frac{k_2}{T_2}}{k_3-T_2}e^{-t/T_2}) + \\ [\frac{k_1}{k_3}-\frac{k_2}{k_3^2}-X_1(1+\frac{\frac{T_1k_1}{k_3}-\frac{T_1k_2}{k_3^2}-T_1}{T_1-k_3})-X_2(1+\frac{T_2-\frac{T_2k_1}{k_3}+\frac{T_2k_2}{k_3^2}}{k_3-T_2})]e^{-t/k_3}, \tag{4.14}$$

and during desorption is

$$F(t)_{des} = X_1\frac{(k_1-T_1-\frac{k_2}{T_1})}{T_1-k_3}e^{-t/T_1} + X_2\frac{(k_1-T_2-\frac{k_2}{T_2})}{T_2-k_3}e^{-t/T_2} + \\ (1-\frac{k_1}{k_3}+\frac{k_2}{k_3^2})(\frac{X_1T_1}{T_1-k_3}+\frac{X_2T_2}{T_2-k_3})e^{-t/k_3}, \tag{4.15}$$

where:

$$k_1 = \overline{t_1}+\overline{t_2}\,, \tag{4.16}$$

$$k_2 = \overline{t_1}\,\overline{t_2}\,, \text{ and} \tag{4.17}$$

$$k_3 = \overline{x_1}\,\overline{t_2}+\overline{x_2}\,\overline{t_1} \tag{4.18}$$

are characteristic constants used in (4.14) and (4.15).

In Appendix C, an analytical verification of these equations is presented for the simplified case of $\overline{t_1}$=0, $\overline{x_1}$=0, $\overline{x_2}$=1.0, which corresponds to a humidity sensor with only one time constant. It shows that when $k_1=\overline{t_2}$, k_2=0 and k_3=0, the equations (C.22) and (C.28) are identical with equations (4.14) and (4.15). The equations are also verified for the case of $\overline{x_1}$=X_1, $\overline{x_2}$=X_2, $\overline{t_1}$=T_1 and $\overline{t_2}$=T_2. This represents the case of no energy wheel and therefore the response, F(t), should

be the unit step for all times greater than zero. As shown in Appendix C, submitting $\overline{x_1}$ =X_1, $\overline{x_2}$ =X_2, $\overline{t_1}$ =T_1 and $\overline{t_2}$ =T_2 in equations (4.14) to (4.18) results in F(t)=1, this confirms that these equations are correct at least for this special case.

Each coefficient in equations (4.14) and (4.15) can be replaced by its average value, $\overline{X_1}$, $\overline{X_2}$, $\overline{T_1}$, and $\overline{T_2}$, to describe a generalized dynamic response of an energy wheel. Applying equations (4.14) and (4.15) the response of the wheel alone can be calculated directly from the coefficients, $\overline{x_1}$, $\overline{x_2}$, $\overline{t_1}$, $\overline{t_2}$, $\overline{X_1}$, $\overline{X_2}$, $\overline{T_1}$, and $\overline{T_2}$. The results are presented Figures 4.12 and 4.13 for the normalized transient relative humidity response for adsorption (Figure 4.12) and desorption (Figure 4.13) of a 100mm thick molecular sieve wheel.

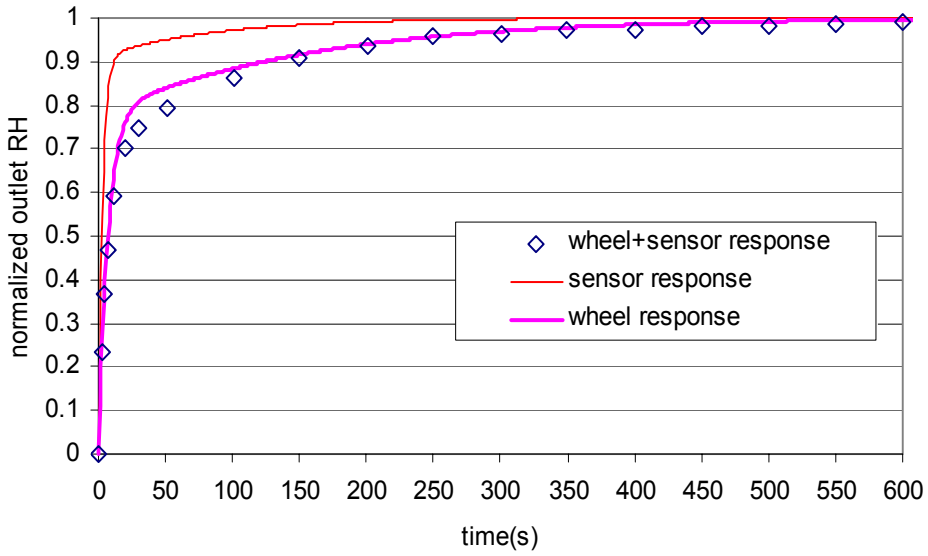

Figure 4.12 Comparison of the measured sensor response and the measured wheel plus sensor response with the predicted transient humidity response of the wheel alone for adsorption in a molecular sieve energy wheel ($\Delta RH \neq 0$, $\Delta T=0$ and V_{air}=1.6m/s).

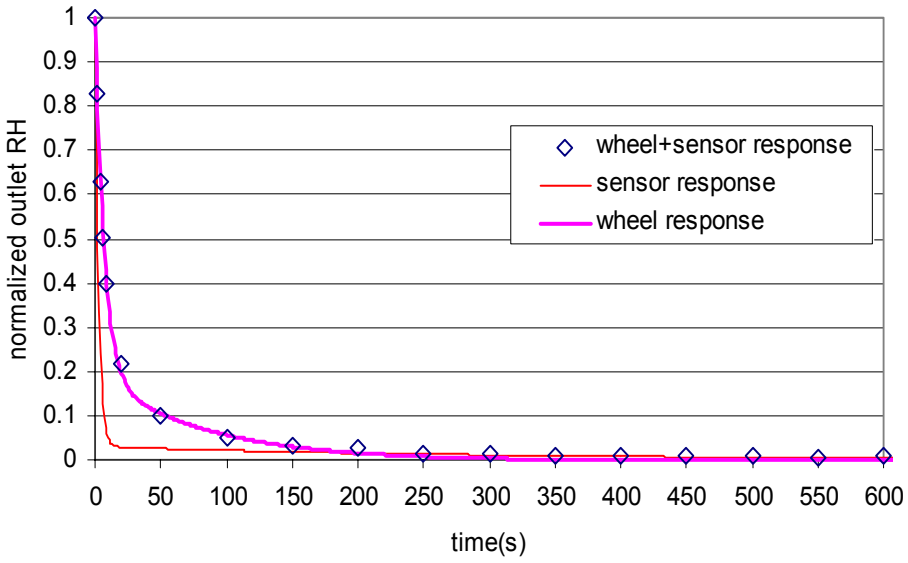

Figure 4.13 Comparison of the measured sensor response and the measured wheel plus sensor response with the predicted transient humidity response of the wheel alone for desorption in a molecular sieve energy wheel ($\Delta RH \neq 0$, $\Delta T=0$ and $V_{air}=1.6$m/s).

Figures 4.12 and 4.13 show that the sensor responds the fastest and that the wheel plus sensor response is very close to the wheel alone, because the sensor has little impact on wheel response. Equations (4.12) and (4.13) provide the relationship between the wheel response, sensor response, and sensor plus wheel response. They do not indicate the time constants of energy wheel response alone. To determine this, the computer program, TableCurve, is used again to curve fit the data from equation (4.14) and (4.15) to find time constants (τ_1 and τ_2) for each energy wheel response as described as Equations (4.19) and (4.20):

$$\frac{\Delta\phi_w}{\Delta\phi_{wo}}(t)_{ads} = \alpha_1(1-e^{-t/\tau_1}) + \alpha_2(1-e^{-t/\tau_2}), \tag{4.19}$$

$$\frac{\Delta\phi_w}{\Delta\phi_{wo}}(t)_{des} = \alpha_1 e^{-t/\tau_1} + \alpha_2 e^{-t/\tau_2}, \tag{4.20}$$

where the coefficient α_1 and α_2 satisfy the equation,

$$\alpha_1 + \alpha_2 = 1,\ \alpha_1 \geq 0 \text{ and } \alpha_2 \geq 0, \tag{4.21}$$

τ_1 and τ_2 are the first and second time constants respectively.

Tables 4.17 to 4.20 summarizes the time constants and coefficients obtained for these two energy wheels with $\Delta RH \neq 0$ and $\Delta T = 0$.

Table 4.17. Adsorption coefficients (α_1, α_2) and time constants (τ_1, τ_2) in equations (4.19) describing the transient humidity response of a 100mm thick molecular sieve wheel ($\Delta RH \neq 0$, $\Delta T = 0$, V_{air}=1.6m/s).

Inlet conditions	α_1	τ_1 (s)	α_2	τ_2 (s)	r^2
dry side: $T_{i,d} \approx 23^oC$, $\Phi_{i,d} \approx 6\%$ wet side: $T_{i,w} \approx 23^oC$, $\Phi_{i,w} \approx 40\%$	0.78	7.0	0.22	150	0.999
	0.85	6.8	0.15	120	0.999
	0.86	7.7	0.14	130	0.999
dry side: $T_{i,d} \approx 23^oC$, $\Phi_{i,d} \approx 6\%$ wet side: $T_{i,w} \approx 23^oC$, $\Phi_{i,w} \approx 50\%$	0.75	6.5	0.25	130	0.999
	0.75	7.1	0.25	140	0.999
	0.74	6.4	0.26	150	0.999
dry side: $T_{i,d} \approx 23^oC$, $\Phi_{i,d} \approx 6\%$ wet side: $T_{i,w} \approx 23^oC$, $\Phi_{i,w} \approx 60\%$	0.74	6.3	0.26	130	0.999
	0.73	5.7	0.27	130	0.999
	0.73	7.2	0.27	150	0.999

Table 4.18. Desorption coefficients (α_1, α_2) and time constants (τ_1, τ_2) in equations (4.20) describing the transient humidity response of a 100mm thick molecular sieve wheel ($\Delta RH \neq 0$, $\Delta T = 0$, V_{air}=1.6m/s).

Inlet conditions	α_1	τ_1 (s)	α_2	τ_2 (s)	r^2
dry side: $T_{i,d} \approx 23^oC$, $\Phi_{i,d} \approx 6\%$ wet side: $T_{i,w} \approx 23^oC$, $\Phi_{i,w} \approx 40\%$	0.80	6.9	0.20	80	0.999
	0.85	8.5	0.15	110	0.999
	0.90	8.7	0.10	180	0.999
dry side: $T_{i,d} \approx 23^oC$, $\Phi_{i,d} \approx 6\%$ wet side: $T_{i,w} \approx 23^oC$, $\Phi_{i,w} \approx 50\%$	0.82	7.2	0.18	100	0.999
	0.83	7.7	0.17	90	0.999
	0.83	8.1	0.17	100	0.999
dry side: $T_{i,d} \approx 23^oC$, $\Phi_{i,d} \approx 6\%$ wet side: $T_{i,w} \approx 23^oC$, $\Phi_{i,w} \approx 60\%$	0.82	6.4	0.18	90	0.999
	0.85	7.7	0.15	100	0.999
	0.82	7.0	0.18	90	0.999

Table 4.19. Adsorption coefficients (α_1, α_2) and time constants (τ_1, τ_2) in equation (4.19) describing the transient humidity response of a 100mm thickness silica gel wheel ($\Delta RH \neq 0$, $\Delta T=0$ and V_{air}=1.6m/s).

Inlet conditions	α_1	τ_1 (s)	α_2	τ_2 (s)	r^2
dry side: $T_{i,d}\approx 23^oC$, $\Phi_{i,d}\approx 6\%$ wet side: $T_{i,w}\approx 23^oC$, $\Phi_{i,w}\approx 40\%$	0.98	6.9	0.02	220	0.999
	0.96	5.5	0.04	130	0.999
	0.95	7.7	0.05	230	0.999
dry side: $T_{i,d}\approx 23^oC$, $\Phi_{i,d}\approx 6\%$ wet side: $T_{i,w}\approx 23^oC$, $\Phi_{i,w}\approx 50\%$	0.96	5.8	0.04	170	0.999
	0.97	5.3	0.03	190	0.999
	0.93	6.0	0.07	130	0.999
dry side: $T_{i,d}\approx 23^oC$, $\Phi_{i,d}\approx 6\%$ wet side: $T_{i,w}\approx 23^oC$, $\Phi_{i,w}\approx 60\%$	0.92	5.8	0.08	130	0.999
	0.88	5.3	0.12	130	0.999
	0.85	6.9	0.15	160	0.999

Table 4.20. Desorption coefficients (α_1, α_2) and time constants (τ_1, τ_2) in equation (4.20) describing the transient humidity response of a 100mm thickness silica gel wheel ($\Delta RH \neq 0$, $\Delta T=0$ and V_{air}=1.6m/s).

Inlet conditions	α_1	τ_1 (s)	α_2	τ_2 (s)	r^2
dry side: $T_{i,d}\approx 23^oC$, $\Phi_{i,d}\approx 6\%$ wet side: $T_{i,w}\approx 23^oC$, $\Phi_{i,w}\approx 40\%$	0.96	6.2	0.04	290	0.999
	0.95	6.7	0.05	190	0.999
	0.93	7.3	0.07	120	0.999
dry side: $T_{i,d}\approx 23^oC$, $\Phi_{i,d}\approx 6\%$ wet side: $T_{i,w}\approx 23^oC$, $\Phi_{i,w}\approx 50\%$	0.96	6.2	0.04	200	0.999
	0.96	7.3	0.04	400	0.999
	0.96	7.5	0.04	250	0.999
dry side: $T_{i,d}\approx 23^oC$, $\Phi_{i,d}\approx 6\%$ wet side: $T_{i,w}\approx 23^oC$, $\Phi_{i,w}\approx 60\%$	0.91	7.5	0.09	100	0.999
	0.95	7.4	0.05	200	0.999
	0.93	8.4	0.07	160	0.999

Comparing the coefficients and time constants for the wheel alone (Tables 4.17 to 4.20) with those for the sensor plus wheel (Tables 4.1 to 4.4) shows that they are very similar. The first time constants are particularly close and some of them are even equal. This confirms that the dynamic response of the energy wheels is not altered by the use of a sensor with a very fast response. If a sensor responds slower than an energy wheel, the result will be totally different and thus a slow sensor will not be of much use in this research work. Similarly analyzed for each coefficient, X_1, X_2, $T_1$and T_2, changing with different time interval (e.g., $0\leq t\leq 5s$, $0\leq t\leq 10s$, $0\leq t\leq 20s$), the coefficients (α_1, α_2, τ_1 and τ_2), are also investigated as well in these time intervals. The values are presented in Table 4.21 and Table 4.22 for one typical example of a silica gel

wheel in the three different time intervals for $\Delta RH \neq 0$, $\Delta T = 0$. It is discovered that the first time constant did not change much in this circumstance.

Table 4.21. Adsorption coefficients (α_1, α_2) and time constants (τ_1 and τ_2) in equation (4.19) describing the transient humidity response of a silica gel wheel in different time intervals ($\Delta RH \neq 0$, $\Delta T = 0$, V_{air}=1.6m/s).

Inlet conditions: dry side: $T_{i,d} \approx 23^oC$, $\Phi_{i,d} \approx 6\%$ wet side: $T_{i,w} \approx 23^oC$, $\Phi_{i,w} \approx 40\%$	α_1	τ_1 (s)	α_2	τ_2 (s)	r^2
$0 \leq t \leq 5s$	0.93	6.7	0.07	13.7	0.999
$0 \leq t \leq 10s$	0.89	6.8	0.11	12.0	0.999
$0 \leq t \leq 20s$	0.92	6.8	0.08	14.9	0.999

Table 4.22. Desorption coefficients (α_1, α_2) and time constants (τ_1 and τ_2) in equation (4.20) describing the transient humidity response of a silica gel wheel in different time intervals ($\Delta RH \neq 0$, $\Delta T = 0$, V_{air}=1.6m/s).

Inlet conditions: dry side: $T_{i,d} \approx 23^oC$, $\Phi_{i,d} \approx 6\%$ wet side: $T_{i,w} \approx 23^oC$, $\Phi_{i,w} \approx 40\%$	α_1	τ_1 (s)	α_2	τ_2 (s)	r^2
$0 \leq t \leq 5s$	0.94	6.1	0.06	48	0.999
$0 \leq t \leq 10s$	0.95	6.1	0.05	51	0.999
$0 \leq t \leq 20s$	0.95	6.1	0.05	77	0.999

The transient response of the two energy wheels during a simultaneous change in humidity and temperature ($\Delta RH \neq 0$ and $\Delta T \neq 0$) is presented in Figures 4.14 and 4.15. These graphs show a comparison of measured humidity and temperature response of the sensor alone, sensor plus energy wheel and the energy wheel alone for this operating condition.

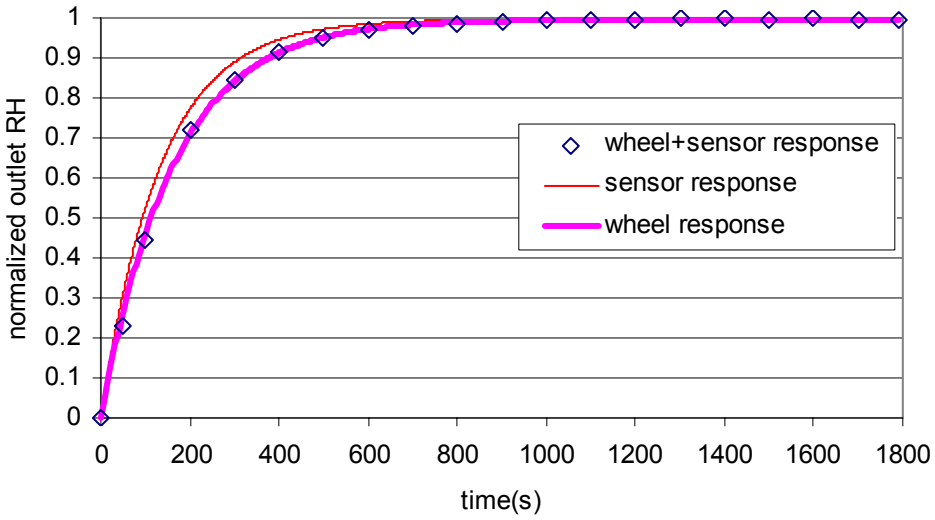

Figure 4.14 Comparison of the measured sensor response and the measured wheel plus sensor response with the predicted transient humidity response of a molecular sieve energy wheel in adsorption ($\Delta RH \neq 0$, $\Delta T \neq 0$ and V_{air}=1.6m/s).

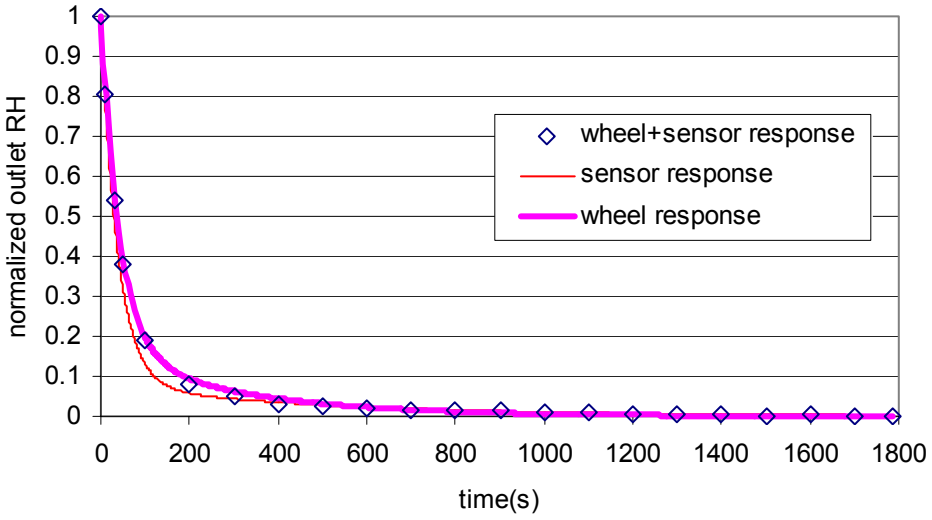

Figure 4.15. Comparison of the measured sensor response and the measured wheel plus sensor response with the predicted transient humidity response of in a molecular sieve energy wheel in desorption ($\Delta RH \neq 0$, $\Delta T \neq 0$ and V_{air}=1.6m/s).

Similarly as in the case with $\Delta T \neq 0$, Figures 4.16 and 4.17 show that the molecular sieve energy wheel responds slower than the sensor and the energy wheel's response is very close to the wheel plus sensor response. It confirms that the transmitter has little effect on wheel response under this test condition. The information in Tables 4.23 and 4.24 present the coefficients

obtained by fitting the data using TableCurve. The first time constants in Tables 4.23 and 4.24 are very close or equal to those in Tables 4.7 and 4.8 (i.e., for the sensor plus wheel).

Table 4.23. Coefficients (α_1, α_2) and time constants (τ_1, τ_2) in equations (4.19) and (4.20) describing transient humidity response of a 100mm thick molecular sieve wheel ($\Delta RH \neq 0$, $\Delta T \neq 0$ and V_{air}=1.6m/s,).

Molecular Sieve wheel	Inlet conditions: hot, dry side:$T_{i,h}\approx 53^oC$, $\Phi_{i,d}\approx 6\%$ cool, wet side:$T_{i,c}\approx 23^oC$, $\Phi_{i,w}\approx 40\%$				
	α_1	τ_1(s)	α_2	τ_2(s)	r^2
Adsorption	0.99	167	0.01	6800	0.999
	0.99	160	0.01	1400	0.999
	0.99	161	0.01	6600	0.999
Desorption	0.87	43	0.13	290	0.999
	0.60	38	0.40	180	0.999
	0.83	42	0.17	300	0.999

Table 4.24. Coefficients (α_1, α_2) and time constants (τ_1, τ_2) in equations (4.19) and (4.20) describing transient humidity response of a 100mm thickness silica gel wheel ($\Delta RH \neq 0$, $\Delta T \neq 0$ and V_{air}=1.6m/s).

Silica gel wheel	Inlet conditions: hot, dry side:$T_{i,h}\approx 53^oC$, $\Phi_{i,d}\approx 6\%$ cool, wet side:$T_{i,c}\approx 23^oC$, $\Phi_{i,w}\approx 40\%$				
	α_1	τ_1(s)	α_2	τ_2(s)	r^2
Adsorption	0.99	150	0.01	3500	0.999
	0.99	162	0.01	2400	0.999
	0.99	150	0.01	2300	0.999
Desorption	0.58	36	0.42	170	0.999
	0.83	44	0.17	220	0.999
	0.81	43	0.19	220	0.999

Figures 4.16 and 4.17 present the temperature response comparison between the RTD temperature sensor, wheel plus sensor and the wheel for a molecular sieve wheel. The energy wheel responds to an inlet temperature step change slower than the sensor during 300s, but faster after 300s. In these conditions, the wheel responds a little faster than wheel plus sensor for both the temperature increase and decrease cases. The energy wheel responds to a step change in temperature as slow as the energy wheel plus the RTD temperature sensor, and the first time constant is usually greater than 90s, while the first time constant obtained with the same condition is about 70s for the RTD temperature sensor alone. The transient temperature response

of the energy wheel also follows the exponential function with two time constants. The following equations describe the responses. For the temperature increase (heat transferred from the wheel matrix to the air):

$$\frac{\Delta T_w}{\Delta T_{wo}}(t)_{inc} = \beta_1(1-e^{-t/\tau_1}) + \beta_2(1-e^{-t/\tau_2}), \tag{4.22}$$

and for the temperature decrease (heat transferred from the air to the wheel matrix):

$$\frac{\Delta T_w}{\Delta T_{wo}}(t)_{dec} = \beta_1 e^{-t/\tau_1} + \beta_2 e^{-t/\tau_2}, \tag{4.23}$$

where the coefficient β_1 and β_2 satisfy the equation:

$$\beta_1 + \beta_2 = 1,\ \beta_1 \geq 0 \text{ and } \beta_2 \geq 0, \tag{4.24}$$

τ_1 and τ_2 are the first and second time constants respectively.

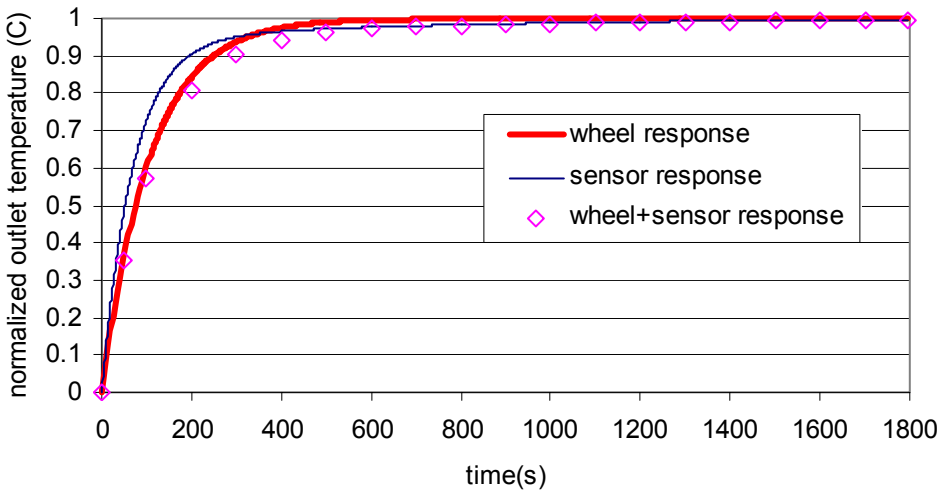

Figure 4.16 Comparison of the measured sensor response and the measured wheel plus sensor response with the predicted transient temperature response of the wheel alone for temperature increase in a molecular sieve energy wheel ($\Delta RH \neq 0$, $\Delta T \neq 0$ and V_{air}=1.6m/s).

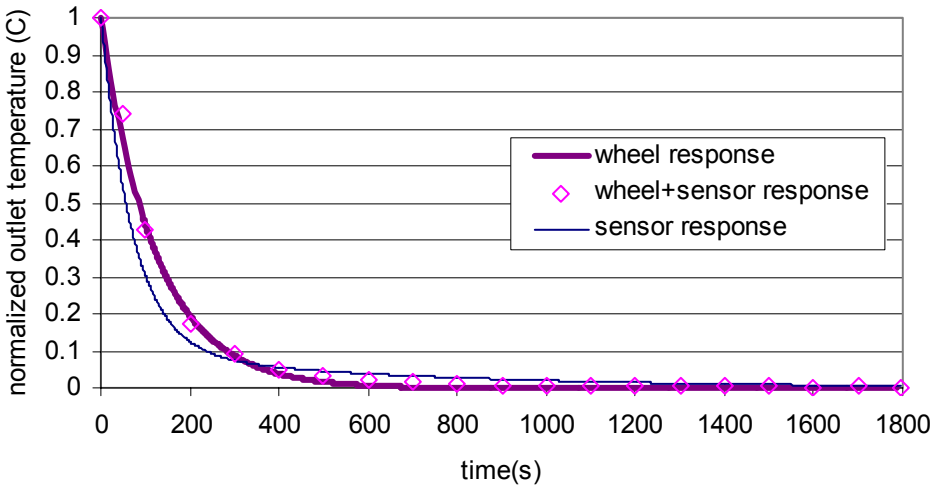

Figure 4.17 Comparison of the measured sensor response and the measured wheel plus sensor response with the predicted transient temperature response of the wheel alone for temperature decrease in a molecular sieve energy wheel ($\Delta RH \neq 0$, $\Delta T \neq 0$ and V_{air}=1.6m/s).

The time constants and coefficients are listed in Tables 4.25 and 4.26 for the correlations in equations (4.22) and (4.23). The statistically averaged time constants and coefficients of energy wheel humidity and temperature response are presented in Tables 4.27 and 4.28.

Table 4.25. Coefficients (β_1, β_2) and time constants (τ_1, τ_2) in equations (4.22) and (4.23) describing transient temperature response of a 100mm thick molecular sieve wheel ($\Delta RH \neq 0$, $\Delta T \neq 0$ and V_{air}=1.6m/s).

Molecular Sieve wheel	Inlet conditions: hot, dry side:$T_{i,h} \approx 53^oC$, $\Phi_{i,d} \approx 6\%$ cool, wet side:$T_{i,c} \approx 23^oC$, $\Phi_{i,w} \approx 40\%$				
	β_1	τ_1(s)	β_2	τ_2(s)	r^2
Temperature Increase	0.92	99	0.08	101	0.999
	0.93	102	0.07	103	0.999
	0.89	105	0.11	129	0.999
Temperature Decrease	0.74	101	0.26	103	0.999
	0.96	100	0.04	520	0.999
	0.76	122	0.24	123	0.999

Table 4.26. Coefficients (β_1, β_2) and time constants (τ_1, τ_2) in equations (4.22) and (4.23) describing transient temperature response of a 100mm thick silica gel wheel ($\Delta RH \neq 0$, $\Delta T \neq 0$ and V_{air}=1.6m/s).

Silica gel wheel	Inlet conditions: hot, dry side:$T_{i,h}\approx 53^oC$, $\Phi_{i,d}\approx 6\%$ cool, wet side:$T_{i,c}\approx 23^oC$, $\Phi_{i,w}\approx 40\%$				
	β_1	τ_1(s)	β_2	τ_2(s)	r^2
Temperature Increase	0.99	90	0.01	90	0.998
	0.97	92	0.03	92	0.997
	0.98	92	0.02	92	0.999
Temperature Decrease	0.96	95	0.04	470	0.999
	0.96	97	0.04	490	0.999
	0.96	94	0.04	400	0.999

Table 4.27. Average coefficients describing the transient humidity response of the energy wheel.

Test Conditions	Coefficient	Molecular Sieve Wheel		Silica Gel Wheel	
		Adsorption	Desorption	Adsorption	Desorption
$\Delta RH \neq 0$ $\Delta T=0$ V_{air}=1.6m/s	$\overline{\alpha_1}$	0.78	0.84	0.93	0.95
	$\overline{\tau_1}(s)$	6.6	7.6	5.7	6.8
	$\overline{\alpha_2}$	0.22	0.16	0.07	0.05
	$\overline{\tau_2}(s)$	130	140	140	290
$\Delta RH \neq 0$ $\Delta T \neq 0$ V_{air}=1.6m/s	$\overline{\alpha_1}$	0.99	0.87	0.99	0.81
	$\overline{\tau_1}(s)$	161	43	157	41
	$\overline{\alpha_2}$	0.01	0.13	0.01	0.19
	$\overline{\tau_2}(s)$	2800	280	2300	200

Table 4.28. Average coefficients describing the transient temperature response of the energy wheel.

Test Conditions	Wheel	Molecular Sieve Wheel		Silica Gel Wheel	
		Increase	Decrease	Increase	Decrease
$\Delta RH \neq 0$ $\Delta T \neq 0$ V_{air}=1.6m/s	$\overline{\beta_1}$	0.91	0.82	0.98	0.96
	$\overline{\tau_1}(s)$	102	108	91	95
	$\overline{\beta_2}$	0.09	0.18	0.02	0.04
	$\overline{\tau_2}(s)$	111	250	91	450

Table 4.27 shows that the molecular sieve wheel has greater time constants and smaller values of $\overline{\alpha_1}$ than the silica gel wheel. This means that the molecular sieve wheel responds slower to a step change in humidity than the silica gel wheel for the same operating conditions.

The transient temperature response of the wheel determined from the thermocouple measurements are presented in Tables 4.29 and 4.30. These results show that the predicted energy wheel response has a first time constant of about 30s, which is much less than the first time constant, 70s, of the temperature response of humidity/temperature transmitter for the same test condition (see Table 3.34). According to the information in Tables 4.29 and 4.30, it is thought that the temperature response of an energy wheel derived from measured thermocouple data is much more convincible than that of measured date using the transmitter. Therefore, the temperature response characteristics of an energy wheel would be expressed using the data based on the thermocouple measurements. The average time constants and coefficients are calculated and presented in Table 4.31.

Table 4.29. Coefficients (β_1, β_2) and time constants (τ_1, τ_2) in equations (4.22) and (4.23) describing transient temperature response of a 100mm thick molecular sieve wheel determined by the thermocouple measurement ($\Delta RH \neq 0$, $\Delta T \neq 0$ and V_{air}=1.6m/s,).

Molecular Sieve wheel	Inlet conditions: hot, dry side:$T_{i,h}\approx 53^oC$, $\Phi_{i,d}\approx 6\%$ cool, wet side:$T_{i,c}\approx 23^oC$, $\Phi_{i,w}\approx 40\%$				
	β_1	τ_1(s)	β_2	τ_2(s)	r^2
Temperature Increase	0.89	37	0.11	38	0.996
	0.91	28	0.09	29	0.990
	0.97	43	0.03	200	0.999
Temperature Decrease	0.86	34	0.14	220	0.999
	0.89	31	0.11	270	0.999
	0.90	35	0.10	270	0.999

Table 4.30. Coefficients (β_1, β_2) and time constants (τ_1, τ_2) in equations (4.22) and (4.23) describing transient temperature response of a 100mm thickness silica gel wheel determined by the thermocouple measurement ($\Delta RH \neq 0$, $\Delta T \neq 0$ and V_{air}=1.6m/s,).

Silica gel wheel	Inlet conditions: hot, dry side:$T_{i,h}\approx 53^oC$, $\Phi_{i,d}\approx 6\%$ cool, wet side:$T_{i,c}\approx 23^oC$, $\Phi_{i,w}\approx 40\%$				
	β_1	τ_1(s)	β_2	τ_2(s)	r^2
Temperature Increase	0.55	21	0.45	50	0.999
	0.74	29	0.26	29	0.989
	0.66	25	0.34	60	0.999
Temperature Decrease	0.82	25	0.18	210	0.999
	0.73	26	0.27	170	0.999
	0.82	27	0.18	210	0.996

Table 4.31. Average coefficients describing the transient temperature response of energy wheels measured by the thermocouple.

Test Conditions	Wheel	Molecular Sieve Wheel		Silica Gel Wheel	
		Increase	Decrease	Increase	Decrease
$\Delta RH \neq 0$ $\Delta T \neq 0$ V_{air}=1.6m/s	$\overline{\beta_1}$	0.92	0.88	0.65	0.79
	$\overline{\tau_1}(s)$	36	33	23	25
	$\overline{\beta_2}$	0.08	0.12	0.35	0.21
	$\overline{\tau_2}(s)$	90	250	46	200

The equations in Table 4.32 demonstrate two energy wheels response to a step change in relative humidity and temperature for two operating conditions. The transient temperature response characteristics are described using the thermocouple measurement data.

Table 4.32. Transient humidity and temperature response of energy wheels.

Operating Conditions	Transient Response of Energy Wheels
$\Delta RH \neq 0$, $\Delta T = 0$, $V_{air} = 1.6 m/s$	A molecular sieve wheel: $\frac{\Delta \phi_w}{\Delta \phi_{wo}}(t)_{ads} = 0.78(1 - e^{-t/6.6}) + 0.22(1 - e^{-t/130})$ $\frac{\Delta \phi_w}{\Delta \phi_{wo}}(t)_{des} = 0.88(1 - e^{-t/7.6}) + 0.12(1 - e^{-t/140})$ A silica gel wheel: $\frac{\Delta \phi_w}{\Delta \phi_{wo}}(t)_{ads} = 0.93(1 - e^{-t/5.7}) + 0.07(1 - e^{-t/140})$ $\frac{\Delta \phi_w}{\Delta \phi_{wo}}(t)_{des} = 0.95(1 - e^{-t/6.8}) + 0.05(1 - e^{-t/290})$
$\Delta RH \neq 0$, $\Delta T \neq 0$, $V_{air} = 1.6 m/s$	A molecular sieve wheel: $\frac{\Delta \phi_w}{\Delta \phi_{wo}}(t)_{ads} = 0.99(1 - e^{-t/161}) + 0.01(1 - e^{-t/2800})$ $\frac{\Delta \phi_w}{\Delta \phi_{wo}}(t)_{des} = 0.78(1 - e^{-t/41}) + 0.22(1 - e^{-t/280})$ $\frac{\Delta T_w}{\Delta T_{wo}}(t)_{inc} = 0.92(1 - e^{-t/36}) + 0.08(1 - e^{-t/90})$ $\frac{\Delta T_w}{\Delta T_{wo}}(t)_{dec} = 0.88(1 - e^{-t/33}) + 0.12(1 - e^{-t/250})$ A silica gel wheel: $\frac{\Delta \phi_w}{\Delta \phi_{wo}}(t)_{ads} = 0.99(1 - e^{-t/157}) + 0.01(1 - e^{-t/2300})$ $\frac{\Delta \phi_w}{\Delta \phi_{wo}}(t)_{des} = 0.81(1 - e^{-t/43}) + 0.19(1 - e^{-t/200})$ $\frac{\Delta T_w}{\Delta T_{wo}}(t)_{inc} = 0.65(1 - e^{-t/23}) + 0.23(1 - e^{-t/46})$ $\frac{\Delta T_w}{\Delta T_{wo}}(t)_{dec} = 0.79(1 - e^{-t/25}) + 0.21(1 - e^{-t/200})$

4.4. Uncertainty Analysis

In this section, the uncertainty of each coefficient for the wheel plus sensor response and the wheel response are presented. The analysis is the same as that described in Section 3.3 for the uncertainty in the sensor alone, the bias uncertainty of the starting time is determined as ±0.2s and the repeatability of coefficients is also calculated. The same approach is applied to analyze the uncertainty of the transient response of the wheel plus sensor and the wheel alone in the following sections.

4.4.1. Uncertainty of Energy Wheel plus Sensor Response

To determine the uncertainty in transient coefficients for the wheel plus the sensor and the wheel plus the thermocouple, the information in Tables 4.1 to 4.4, 4.7 to 4.10, 4.14 and 4.15 are used to calculate the repeatability errors using equations (3.13) to (3.20), and the start time error, ±0.2s, is included to determine total uncertainty of the time constants. The total uncertainties of each parameter are listed in Tables 4.33 to 4.35. The uncertainty of humidity response for the wheel plus the humidity/temperature transmitter is presented in Table 4.33. For $\Delta T=0$, the relative uncertainty of the first time constant and the second time constant is less than ±11% and ±30% in both adsorption and desorption; for $\Delta T\neq 0$, the relative uncertainty of the first time constant is from ±6% to ±18% in adsorption and desorption, the uncertainty of the second time constant is very large, but the second time constant does not play an important role because the fraction factor, X_2, is very small, so the uncertainty is not a significant consideration. The information in Tables 4.34 and 4.35 presents the uncertainty of the temperature response of the energy wheel plus the RTD temperature sensor and plus the thermocouple respectively. In Table 4.34, the uncertainty of the first time constant is less than ±8%, the uncertainty of the second time constant is greater, from ±15% to ±67% for adsorption and desorption. In Table 4.35, the relative uncertainty of first time constant is from ±8% to ±49% and the relative uncertainty of the second time constant is from ±26% to ±35% for both the temperature increase and decrease cases.

Table 4.33. Uncertainty of each coefficient describing transient humidity response for the energy wheels plus the humidity/temperature transmitter.

Test Conditions	Coefficient	Molecular Sieve Wheel		Silica Gel Wheel	
		Adsorption	Desorption	Adsorption	Desorption
ΔRH≠0 ΔT=0 V_{air}=1.6m/s	$\overline{X_1} \pm U(\overline{X_1})$	0.70±0.03	0.85±0.02	0.85±0.03	0.95±0.01
	$\overline{T_1} \pm U(\overline{T_1})(s)$	6.8±0.5	7.7±0.6	6.4±0.7	6.9±0.8
	$\overline{X_2} \pm U(\overline{X_2})$	0.30±0.03	0.15±0.02	0.15±0.03	0.05±0.01
	$\overline{T_2} \pm U(\overline{T_2})(s)$	120±8	110±20	120±10	230±70
ΔRH≠0 ΔT≠0 V_{air}=1.6m/s	$\overline{X_1} \pm U(\overline{X_1})$	0.99±0.02	0.87±0.11	0.98±0.02	0.86±0.07
	$\overline{T_1} \pm U(\overline{T_1})(s)$	163±10	41±6	156±16	44±8
	$\overline{X_2} \pm U(\overline{X_2})$	0.01±0.02	0.13±0.11	0.02±0.02	0.14±0.07
	$\overline{T_2} \pm U(\overline{T_2})(s)$	1100±1800	240±170	1300±470	230±90

Table 4.34. Uncertainty of each coefficient describing transient temperature response for the energy wheel plus humidity/temperature transmitter.

Test Conditions	Coefficient	Molecular Sieve Wheel		Silica Gel Wheel	
		Increase	Decrease	Increase	Decrease
ΔRH≠0 ΔT≠0 V_{air}=1.6m/s	$\overline{Y_1} \pm U(\overline{Y_1})$	0.94±0.002	0.96±0.05	0.95±0.04	0.95±0.003
	$\overline{T_1} \pm U(\overline{T_1})(s)$	104±8	103±30	96±8	95±3
	$\overline{Y_2} \pm U(\overline{Y_2})$	0.06±0.002	0.04±0.05	0.05±0.04	0.05±0.003
	$\overline{T_2} \pm U(\overline{T_2})(s)$	640±130	580±390	530±180	540±80

Table 4.35. Uncertainty of each coefficient describing transient temperature response for the energy wheel plus the thermocouple.

Test Conditions	Coefficient	Molecular Sieve Wheel		Silica Gel Wheel	
		Increase	Decrease	Increase	Decrease
ΔRH≠0 ΔT≠0 V_{air}=1.6m/s	$\overline{Y_1} \pm U(\overline{Y_1})$	0.85±0.06	0.84±0.07	0.76±0.11	0.79±0.12
	$\overline{T_1} \pm U(\overline{T_1})(s)$	37±18	32±6	28±4	25±2
	$\overline{Y_2} \pm U(\overline{Y_2})$	0.15±0.06	0.16±0.07	0.24±0.11	0.21±0.12
	$\overline{T_2} \pm U(\overline{T_2})(s)$	300±100	230±60	190±50	200±70

4.4.2. Uncertainty of Energy Wheel Response

The uncertainty of each coefficient (α_1, α_2, β_1, β_2, τ_1, and τ_2) is presented in Tables 4.36 to 4.37 for a molecular sieve wheel and a silica gel wheel respectively which are tested with and without a temperature change. The uncertainty of time constants includes the bias error, 0.2s, and the precision error calculated using the data in Tables 4.17 to 4.20, 4.23 to 4.26, and 4.29 to 4.30. This uncertainty analysis will be used for future work of studying the effectiveness of energy wheels. The information summarized in Tables 4.36 to 4.38 presents the statistical average value of each coefficient and its uncertainty for the transient humidity and temperature response of the energy wheel alone. For the transient humidity response of the energy wheel (Table 4.36), the relative uncertainty of the first time constant and the second time constant is less than ±11% and ±24% for $\Delta T=0$, respectively; for $\Delta T\neq 0$, the relative uncertainty of the first time constant and the second time constant is less than ±10% and ±76% for the adsorption and desorption, respectively. It is found that the uncertainty of the second time constant is also large but it is not very important. The coefficients and their uncertainty describing the transient temperature response of an energy wheel obtained from humidity/temperature transmitter measurement are shown in Table 4.37 and their relative uncertainty is smaller than ±35% for both temperature increase and decrease. The information in Table 4.38 shows that the relative uncertainty is smaller than ±50% for the first time constant of transient temperature response of the energy wheel obtained from the thermocouple measurement for the temperature increase and decrease cases.

Table 4.36. Uncertainty of each coefficient describing the transient humidity response of energy wheels.

Test Conditions	Coefficient	Molecular Sieve Wheel		Silica Gel Wheel	
		Adsorption	Desorption	Adsorption	Desorption
$\Delta RH\neq 0$ $\Delta T=0$ V_{air}=1.6m/s	$\overline{\alpha_1}\pm U(\overline{\alpha_1})$	0.78±0.04	0.88±0.02	0.93±0.03	0.95±0.02
	$\overline{\tau_1}\pm U(\overline{\tau_1})(s)$	6.6±0.5	7.6±0.6	5.7±0.6	6.8±0.5
	$\overline{\alpha_2}\pm U(\overline{\alpha_2})$	0.22±0.04	0.12±0.02	0.07±0.03	0.05±0.02
	$\overline{\tau_2}\pm U(\overline{\tau_2})(s)$	130±8	140±20	140±30	290±70
$\Delta RH\neq 0$ $\Delta T\neq 0$ V_{air}=1.6m/s	$\overline{\alpha_1}\pm U(\overline{\alpha_1})$	0.99±0	0.78±0.06	0.99±0	0.81±0.05
	$\overline{\tau_1}\pm U(\overline{\tau_1})(s)$	161±9	41±6	157±16	43±10
	$\overline{\alpha_2}\pm U(\overline{\alpha_2})$	0.01±0	0.22±0.06	0.01±0	0.19±0.05
	$\overline{\tau_2}\pm U(\overline{\tau_2})(s)$	2800±1200	280±170	2300±1750	200±70

Table 4.37. Uncertainty of each coefficient describing the transient temperature response of energy wheels measured by the humidity/temperature transmitter.

Test Conditions	Coefficient	Molecular Sieve Wheel		Silica Gel Wheel	
		Increase	Decrease	Increase	Decrease
ΔRH≠0 ΔT≠0 ΔW≠0 V_{air}=1.6m/s	$\overline{\beta_1} \pm U(\overline{\beta_1})$	0.91±0.05	0.82±0.05	0.98±0.02	0.96±0
	$\overline{\tau_1} \pm U(\overline{\tau_1})(s)$	102±7	108±31	91±3	95±4
	$\overline{\beta_2} \pm U(\overline{\beta_2})$	0.09±0.05	0.18±0.05	0.02±0.02	0.04±0
	$\overline{\tau_2} \pm U(\overline{\tau_2})(s)$	111±39	250±90	91±2	450±120

Table 4.38. Uncertainty of each coefficient describing the transient temperature response of energy wheels measured by the thermocouple.

Test Conditions	Coefficient	Molecular Sieve Wheel		Silica Gel Wheel	
		Increase	Decrease	Increase	Decrease
ΔRH≠0 ΔT≠0 ΔW≠0 V_{air}=1.6m/s	$\overline{\beta_1} \pm U(\overline{\beta_1})$	0.92±0.08	0.88±0.05	0.65±0.2	0.79±0.1
	$\overline{\tau_1} \pm U(\overline{\tau_1})(s)$	36±19	33±5	23±10	25±2
	$\overline{\beta_2} \pm U(\overline{\beta_2})$	0.08±0.08	0.12±0.05	0.35±0.2	0.21±0.1
	$\overline{\tau_2} \pm U(\overline{\tau_2})(s)$	90±40	250±65	46±39	200±60

Based on the discussion in Section 4.3, the transient temperature response should be described using data in Table 4.38. Tables 4.36 and 4.38 summarize the coefficients and their uncertainty of the transient humidity and temperature response of a molecular sieve wheel and a silica gel wheel respectively for ΔT=0 and ΔT≠0. This information will be used in the future work to determine the effectiveness of energy wheels based on transient operating conditions.

5. RESEARCH SUMMARY AND CONCLUSIONS

5.1. Research Summary

The general purpose of this research is to develop a new transient test procedure for an energy wheel where humidity and temperature sensors downstream of an energy wheel would detect the response characteristics of the wheel when a step change in the inlet humidity or temperature conditions entering the wheel occurs. The specific purpose of this research is to first determine the transient step change response characteristics of the humidity and temperature sensors and then determine the transient response characteristics of the wheel alone.

The first challenge undertaken in this research is the development of a test facility that maintains the high measurement accuracy needed for prediction of the transient characteristics of a stationary energy wheel. Two small air streams flow parallel to each other flow through the energy wheel prior to each test. Step-like changes in inlet air conditions are facilitied by switching two inlet air tubes 180 degrees as quickly as practical to start each transient test. This same test facility is used to obtain the transient response of each sensor when the energy wheel is excluded from the test. Another challenge is the determination of correlation equations required to describe the transient response of the humidity and temperature sensors. The experimental data show that these responses could be fitted by a double-exponential time decay equation. It is found that the energy wheel transient relative humidity response follows similar correlation equations, albeit with much larger time constants.

Humidity measurement is the most important property measurement to determine the performance of air-to-air energy recovery wheels that transfer heat and moisture. Humidity is often a difficult property to measure accurately. Accurate steady-state calibration of humidity sensors is crucial. By calibrating against a calibrated chilled mirror hygrometer, it is found that the uncertainty of 1% to 2% RH could be obtained for the sensors tested.

Duhamel's equation is used to theoretically determine the response of the measurement system where sensors with known time responses are used downstream of the energy wheel. The transient characteristics of each energy wheel are found as a solution to this equation using the best fitting analytical correlations of the measured data.

The uncertainty analysis used in an experiment is as important as the testing because the uncertainty analysis shows the confidence bounds of the final result.

5.2. Conclusions

This research is intended to design a new test method and facility to investigate the performance of energy wheels under non-steady-state or transient operating conditions. The long-term goal of the facility is to determine the effectiveness of energy wheels using measured data, and incorporate the latest developments in air-to-air energy recovery technology and the instrumentation to test these devices. The following conclusions may be deduced, based on this new method using the newly designed test facility.

1. This research work suggests the new test facility and method can be used to investigate the transient response of humidity and temperature sensors, and the transient response characteristics of an energy wheel can be predicted using these same sensors.
2. The first time constant is about 3s for transient humidity response of the capacitive humidity sensor with $\Delta T=0$ for the range of airflow rates studied in this thesis (50L/min to 200L/min). The relative uncertainty is about ±10%. For the energy wheel alone, the first time constant is about 6 to 8 seconds and the relative uncertainty is less than ±11%.
3. This humidity measurement device, which includes both a temperature and humidity sensor, responds very slowly to a step-like humidity and temperature change under operating conditions with $\Delta T\neq0$ because the transmitter has a large time constant. The first time constant of the humidity sensor is about 40 to 130s under these conditions and the first time constant for the temperature sensor is about 70s.
4. The T-type thermocouple responds quickly to a step change in temperature. The first time constant is about 3 to 5s. The predicted temperature response of an energy wheel is derived from the data measured with a thermocouple and its first time constant is about 30s.
5. The condition of $\Delta RH\neq0$ and $\Delta T=0$ is recommended to determine the latent effectiveness of an energy wheel because both the sensor and energy wheel respond very fast under this operating condition. Other conditions with $\Delta T\neq0$ are not recommended to investigate latent effectiveness of energy wheels because heat conduction inside the energy wheel causes very slowly response of the energy wheel.

6. A new data acquisition system is preferred so that the start time of inlet conditions changing will be determined more accurately and the uncertainty of the start time will be reduced, and the total uncertainty of time constants will decrease as well.

5.3. Future Work

In this thesis, the transient characteristics (time constants) of energy wheels are determined. The effectiveness such as sensible effectiveness, latent effectiveness and total effectiveness of an energy wheel will be studied in the future using the transient properties.

REFERENCES

ARI Standard 1060-2001, *Rating Air-to-Air Energy Recovery Ventilation Equipment*, ARI, Arlington.

ASHRAE, 2001. *Fundamentals Handbook*, ASHRAE, Atlanta.

ASHRAE, 1992. *HVAC Systems and Equipment Handbook*, ASHRAE, Atlanta.

ASHRAE Standard 84-1991. *Method of Testing Air-to-Air Heat Exchangers*, ASHRAE, Atlanta.

ASME PTC 19.1-1998. *Test Uncertainty*, *The American Society of Mechanical Engineers*, ASME, New York

Besant, R.W. and Simonson, C.J., 2000. Air –to-Air Energy Recovery, *ASHRAE Journal*, **42**(5):31-42.

Besant, R.W. and Simonson C.J., 2003. Air-to-Air Exchangers, *ASHRAE Journal*, **45**:42-52.

Brion, K.Carr, 1986. *Moisture Sensors in Process Control*, Elsevier Applied Science Publishers, London and New York.

Ciepliski, D.L., 1997. *Testing an Air-to-Air Rotary Energy Recovery Device Using Performance Test Standard*, M.Sc. thesis in mechanical engineering, University of Saskatchewan, Canada.

Ciepliski, D.L., Besant, R.W. and Simonson, C.J., 1998. Some Recommendations for Improvements to ASHRAE Standard 84-1991, *ASHRAE Transactions*, **104**(1B), 1651-1665.

Delpha, C., Siadat, M. and Lumbreras, M., 2000. Discrimination of A Refrigerant Gas in A Humidity Controlled Atmosphere by Using Modelling Parameters, *Sensors and Actuators B*, **62**, 226-232.

Incropera, F.P. and Dewitt, D.P., 1996. *Fundamentals of Heat and Mass Transfer*, John Wiley & Sons, New York.

Ingleby, P., Gardner, J.W. and Bartlett, P.N., 1999. Effect of Micro-electrode Geometry on Response of Thin-film Poly(pyrrole) and Poly(aniline) Chemoresistive Sensors, *Sensors and Actuators B*, **57**, 17-*27*.

Kuse, Takashi and Takahashi, Sachio, 2000. Transitional Behavior of Tin Oxide Semiconductor under a Step-like Humidity Change. *Sensors and Actuators B*, **67**, 34-42.

Lafarie, J.P., 1985. Relative Humidity Measurement: A Review of Two State-of –The-Art Sensors. *Moisture and Humidity: Measurement and Control in Science and Industry*, **1**, 875-883.

Marchgraber, R.M. and Grote, H.H., 1963. The Dynamic Behavior of The Carbon Humidity Element ML-476. *Moisture and Humidity: Measurement and Control in Science and Industry*, **1**, 331-345.

Minkina, W., 1999. Theoretical and Experimental Identification of the Temperature Sensor Unit Step Response Non-Linearity during Air Temperature Measurement. *Sensors and Actuators*, **78**, 81-87.

Shammas, N.Y.A., Rodriguez, M.P. and Masana, F., 2002. A Simple Method for Evaluating the Transient Thermal Response of Semiconductor Devices. *Microelectronics Reliability*, **42**, 109-117.

Shang, W., 2002. *Evaluation of Energy Wheel Performance*, M.Sc. thesis in mechanical engineering, University of Saskatchewan, Canada.

Simonson, C.J., Ciepliski, D.L. and Besant, R.W., 1999. Determining the Performance of Energy Wheels: Part I- Experimental and Numerical Methods, *ASHRAE Transactions*, **105**(1), 174-187.

Simonson, C.J., Ciepliski, D.L. and Besant, R.W., 1999. Determining the Performance of Energy Wheels: Part II- Experimental Data and Numerical Validation, *ASHRAE Transactions*, **105**(1), 188-205.

Stoecker, W.F., 1989. *Design of Thermal Systems*, McGraw-Hill Book Company, New York,

Taylor, John R., 1982. *An Introduction to Error Analysis: The Study of Uncertainty in Physical Measurements*, University Science Books, Mill Valley.

Tetelin, A., Pellet, C., Laville, C. and N'Kaoua, G., 2003. Fast Response Humidity Sensors for A Medical Microsystem. *Sensors and Actuators B*, **91**, 211-218.

Wylie, C. Ray, 1975. *Advanced Engineering Mathematics*, McGraw-Hill Book Company, New York.

APPENDIX A: DESIGN DRAWINGS

The design drawings for the test facility are presented in this appendix. The first drawing is the layout and dimensions of the test facility with the components set apart but aligned (Figure A.1), the second is the assembling of the inlet and outlet sections (Figure A.2), and the third drawing shows the dimensions of the positioning holes (Figure A.3). The drawings are dimensioned in inches.

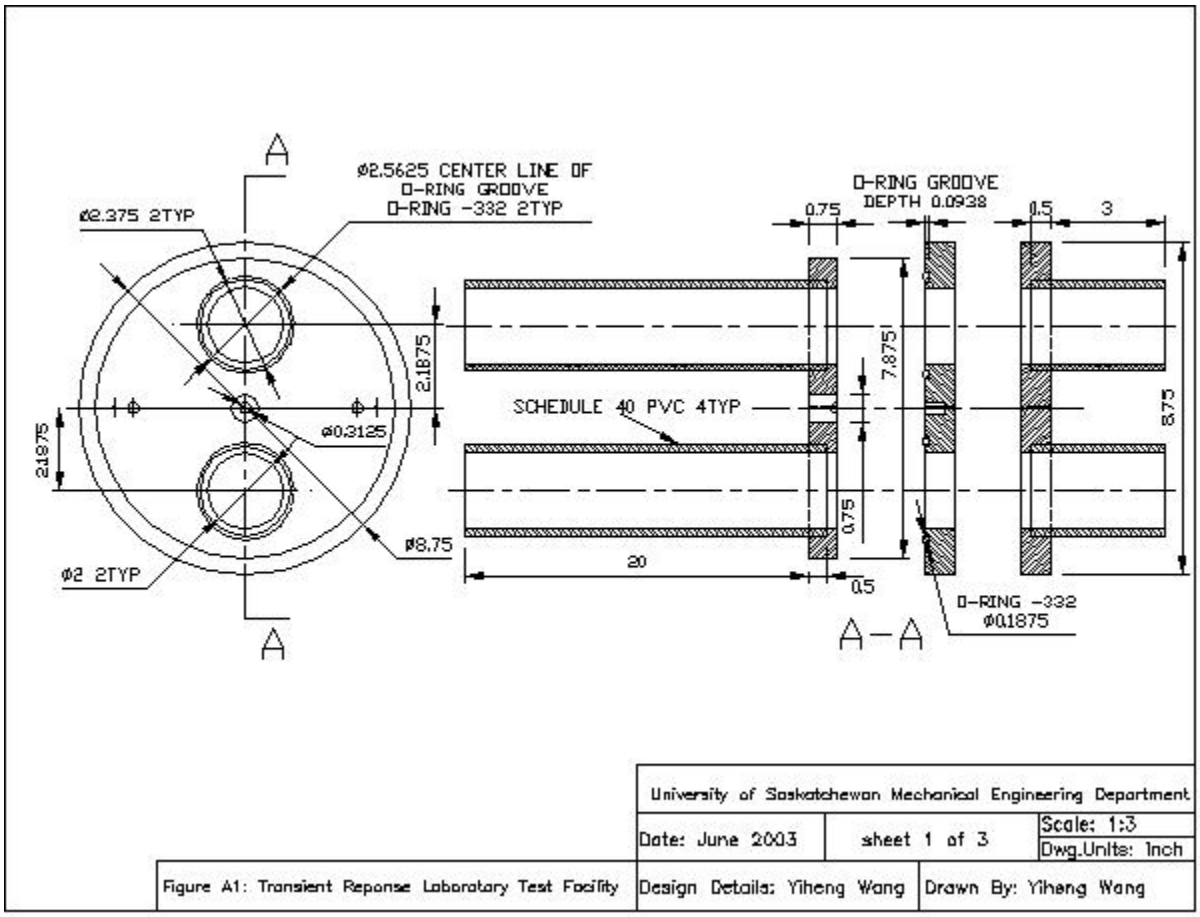

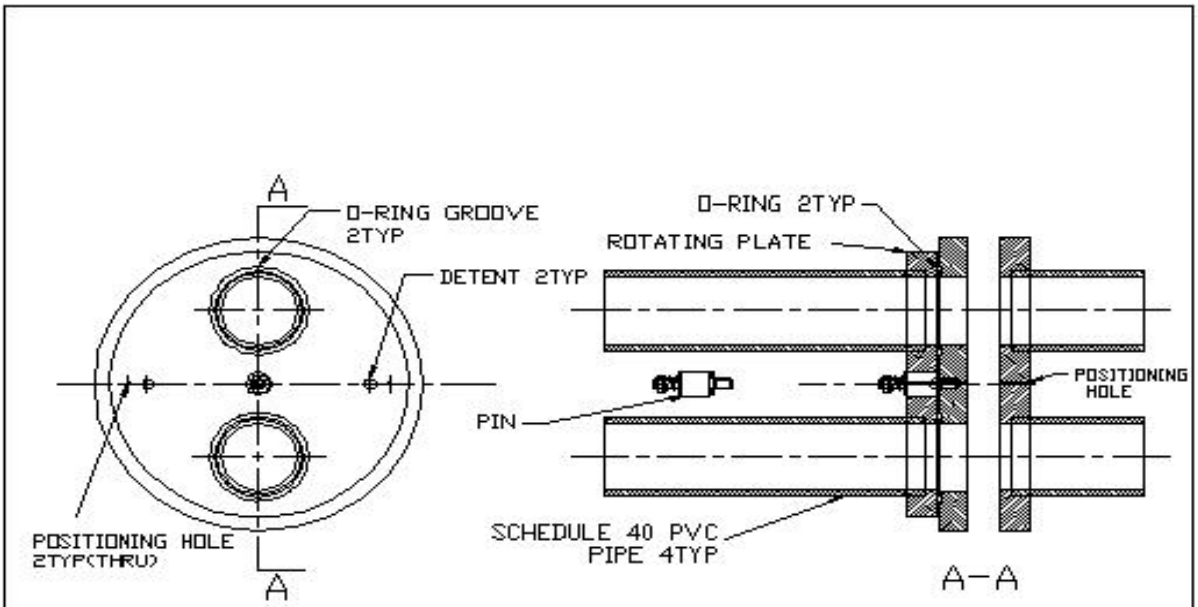

University of Saskatchewan Mechanical Engineering Department		
Date: June 2003	Sheet 2 of 3	Scale: 1:3 Dwg. units: inch
Figure A2: Assembling of Inlet and Outlet Sections	Design Details: Yiheng Wang	Drawn By: Yiheng Wang

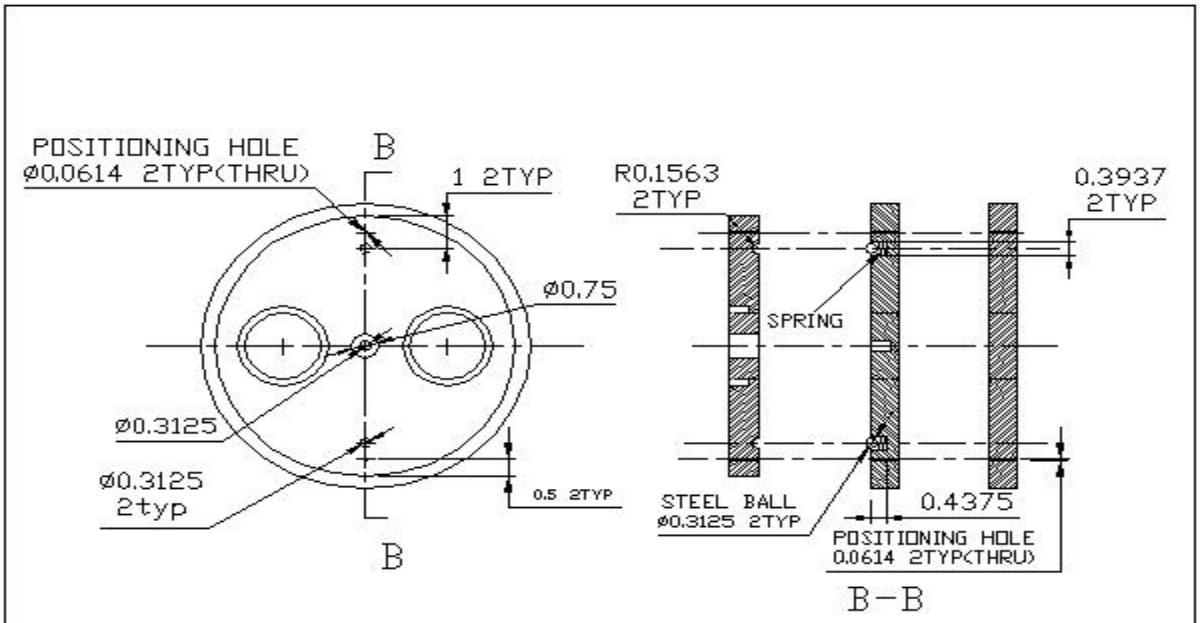

University of Saskatchewan Mechanical Engineering Department		
Date: June 2003	Sheet 3 of 3	Scale: 1:3 Dwg.Units: inch
Figure A3: Positioning Holes	Design Details: Yiheng Wang	Drawn By: Yiheng Wang

APPENDIX B: HEAT CONDUCTION INSIDE THE ENERGY WHEEL

When a temperature difference exists between two air streams flowing through an energy wheel, heat will be conducted between the two air streams through the wheel matrix and also to the other parts of the matrix. The heat transferred between two air cylinders inside the energy wheel is calculated approximately in order to estimate how an energy wheel has an impact on the sensors downstream and also to estimate the temperature difference between inlet and outlet section. Figure B.1 shows the heat conduction physically inside the energy wheel.

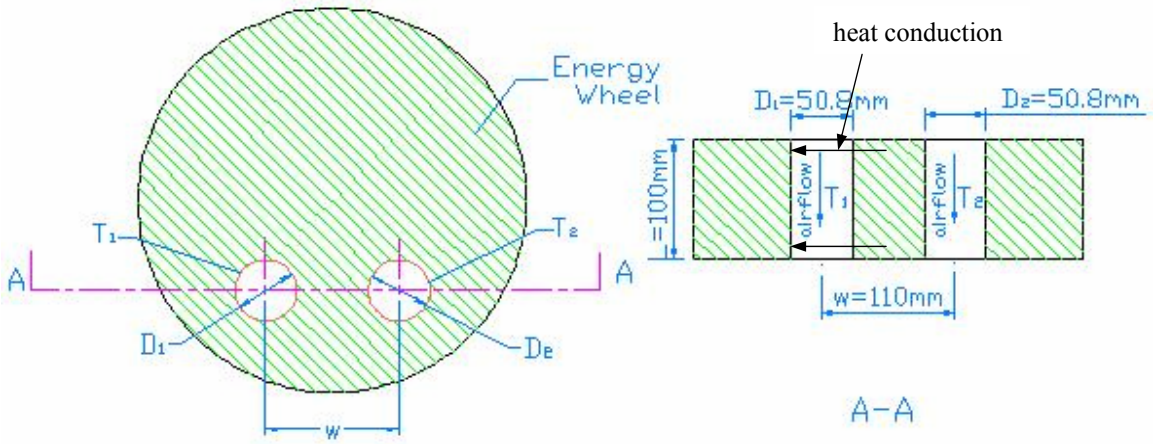

Figure B.1 Hot and cold airstreams flow through an energy wheel and heat conduction inside the energy wheel.

The heat conduction between two cylinders in the matrix, assuming a uniform effective conductivity, k_e, in the wheel matrix and steady-state operating conditions can be calculated with

$$q = Sk_e(T_h - T_c), \tag{B.1}$$

where q is the heat transfer from the tubes, S is the shape factor, and T_h and T_c refer to the hot air stream temperature and cold air stream temperature, respectively.

For this geometry, the shape factor, S, is given by (Incropera and Dewitt, 1996)

$$S = \frac{2\pi L}{\cosh^{-1}\left(\frac{4w^2 - D_1^2 - D_2^2}{2D_1D_2}\right)}, \tag{B.2}$$

The effective thermal conductivity, k_e, is expressed as

$$k_e = \varepsilon k_{air} + (1-\varepsilon)k_{al}, \quad \text{(B.3)}$$

where ε is porosity of the energy wheel, which is approximately 0.85, k_{air}=0.026 W/m·K and k_{al}=237 W/m·K. With these relations, equation (B.1) can be solved for any set of T_h and T_c.

For the experiments in this thesis, the shape factor, S, is 0.23 and k_e=35.6 W/m·K, therefore the heat rate is given by,

$q = Sk_e(T_h - T_c)$=22W,

when the temperature of hot and cold air is at about 53°C and 23°C. This heat transfer will decrease the temperature of the hot air (53°C) and increase the temperature of the room temperature air (23°C), by ΔT that can be calculated as follows

$$\Delta T = \frac{q}{\dot{m}C_p}, \quad \text{(B.4)}$$

where $\dot{m}$ is mass flow rate of air, about 3.9×10^{-3} kg/s, and C_p is specific heat of air (1.007 kJ/kg·K) at room temperature. For these conditions, the temperature difference between the inlet and outlet (ΔT) is 5.7°C.

The discussion above confirmed that the outlet temperature reading does not reach the inlet temperature condition (see Figure 4.4) and also affect the outlet relative humidity reading either (see Figure 4.3).

APPENDIX C: CALCULATION OF WHEEL RESPONSE

C.1. Adsorption Case

The correlation equations for the wheel plus sensor response and the sensor response are:

$$\frac{\Delta\phi_{w+s}}{\Delta\phi_{(w+s)o}}(t)_{ads} = X_1(1-e^{-t/T_1}) + X_2(1-e^{-t/T_2}), \tag{C.1}$$

for the wheel plus sensor and

$$\frac{\Delta\phi_{s}}{\Delta\phi_{so}}(t)_{ads} = \bar{x}_1(1-e^{-t/\bar{t}_1}) + \bar{x}_2(1-e^{-t/\bar{t}_2}), \tag{C.2}$$

for the sensor alone.

Applying Duhamel's equation, $y(t) = \frac{\Delta\phi_{w+s}}{\Delta\phi_{(w+s)o}} = \int_0^t A'(t-t')F(t')dt'$, and the convolution method to solve for the transient response of the wheel alone (F(t)), gives equation (4.14) in the main body of the thesis. The mathematics computer software, Maple, is used to compute the Laplace transform of these equations. The Laplace transform of equation (4.9), $A'(t-t') = \frac{\partial}{\partial t}[\frac{\Delta\phi_s}{\Delta\phi_{so}}(t-t')]$, in the main body is

$$\mathcal{L}[A'(t)] = \frac{\bar{x}_1}{\bar{t}_1(s+\frac{1}{\bar{t}_1})} + \frac{\bar{x}_2}{\bar{t}_2(s+\frac{1}{\bar{t}_2})}, \tag{C.3}$$

where

$$A'(t) = \frac{\partial[\frac{\Delta\phi_s}{\Delta\phi_{so}}(t)_{ads}]}{\partial t} = \frac{\bar{x}_1}{\bar{t}_1}e^{-t/\bar{t}_1} + \frac{\bar{x}_2}{\bar{t}_2}e^{-t/\bar{t}_2}, \tag{C.4}$$

and, likewise, the Laplace transform of equation (4.8), $y(t) = \frac{\Delta\phi_{w+s}}{\Delta\phi_{(w+s)o}}(t)$, is

$$\mathcal{L}[\frac{\Delta\phi_{w+s}}{\Delta\phi_{(w+s)o}}(t)_{ads}] = \frac{X_1}{s} + \frac{X_2}{s} - \frac{X_1}{s+\frac{1}{T_1}} - \frac{X_2}{s+\frac{1}{T_2}}. \tag{C.5}$$

Substituting equations (C.3) and (C.5) into equation (4.13),
$F(t)=\mathcal{L}^{-1}\{\mathcal{L}[y(t)]/\mathcal{L}[A'(t)]\}$, gives

$$F(t)_{ads}=\mathcal{L}^{-1}\left\{\frac{\frac{X_1}{s}+\frac{X_2}{s}-\frac{X_1}{s+\frac{1}{T_1}}-\frac{X_2}{s+\frac{1}{T_2}}}{\frac{\bar{x}_1}{\bar{t}_1(s+\frac{1}{\bar{t}_1})}+\frac{\bar{x}_2}{\bar{t}_2(s+\frac{1}{\bar{t}_2})}}\right\}. \quad \text{(C.6)}$$

The inverse Laplace transform of equation (C.6) is quite difficult so it is carried out using the commercial math package, Maple. The final result in the time domain for the wheel response during adsorption is:

$$F(t)_{ads}=X_1(1-\frac{T_1-k_1+\frac{k_2}{T_1}}{T_1-k_3}e^{-t/T_1})+X_2(1-\frac{k_1-T_2-\frac{k_2}{T_2}}{k_3-T_2}e^{-t/T_2})+ \quad \text{(C.7)}$$
$$[\frac{k_1}{k_3}-\frac{k_2}{k_3^2}-X_1(1+\frac{\frac{T_1k_1}{k_3}-\frac{T_1k_2}{k_3^2}-T_1}{T_1-k_3})-X_2(1+\frac{T_2-\frac{T_2k_1}{k_3}+\frac{T_2k_2}{k_3^2}}{k_3-T_2})]e^{-t/k_3},$$

where

$$k_1=\bar{t}_1+\bar{t}_2, \quad \text{(C.8)}$$

$$k_2=\bar{t}_1\bar{t}_2, \text{ and} \quad \text{(C.9)}$$

$$k_3=\bar{x}_1\bar{t}_2+\bar{x}_2\bar{t}_1, \quad \text{(C.10)}$$

which are some of characteristic constants of the sensor; the others are X_1, X_2, T_1 and T_2.

C.2. Desorption Case

The expressions of the wheel plus sensor response and the sensor response are slightly different than for adsorption. They are:

$$\frac{\Delta\phi_{w+s}}{\Delta\phi_{(w+s)o}}(t)_{des}=X_1e^{-t/T_1}+X_2e^{-t/T_2}, \quad \text{(C.11)}$$

for the wheel plus sensor and

$$\frac{\Delta\phi_s}{\Delta\phi_{so}}(t)_{des}=\bar{x}_1e^{-t/\bar{t}_1}+\bar{x}_2e^{-t/\bar{t}_2}, \quad \text{(C.12)}$$

for the sensor alone.

Using Maple to compute the Laplace transform of equation (4.9), $A'(t-t') = \frac{\partial}{\partial t}[\frac{\Delta\phi_s}{\Delta\phi_{so}}(t-t')]$, then

$$\mathcal{L}[A'(t)] = -\frac{\bar{x}_1}{\bar{t}_1(s+\frac{1}{\bar{t}_1})} - \frac{\bar{x}_2}{\bar{t}_2(s+\frac{1}{\bar{t}_2})}, \tag{C.13}$$

where

$$A'(t) = \frac{\partial[\frac{\Delta\phi_s}{\Delta\phi_{so}}(t)_{des}]}{\partial t} = -\frac{\bar{x}_1}{\bar{t}_1}e^{-t/\bar{t}_1} - \frac{\bar{x}_2}{\bar{t}_2}e^{-t/\bar{t}_2}, \tag{C.14}$$

and to compute the Laplace transform of equation (4.8), $y(t) = \frac{\Delta\phi_{w+s}}{\Delta\phi_{(w+s)o}}(t)$, gives

$$\mathcal{L}[\frac{\Delta\phi_{w+s}}{\Delta\phi_{(w+s)o}}(t)_{des}] = \frac{X_1}{s+\frac{1}{T_1}} + \frac{X_2}{s+\frac{1}{T_2}}. \tag{C.15}$$

Inserting equations (C.13) and (C.15) into equation (4.13) gives the wheel response for desorption,

$$F(t)_{des} = \mathcal{L}^{-1}\left\{\frac{\frac{X_1}{s+\frac{1}{T_1}} + \frac{X_2}{s+\frac{1}{T_2}}}{-\frac{\bar{x}_1}{\bar{t}_1(s+\frac{1}{\bar{t}_1})} - \frac{\bar{x}_2}{\bar{t}_2(s+\frac{1}{\bar{t}_2})}}\right\}$$

$$= X_1\frac{(k_1 - T_1 - \frac{k_2}{T_1})}{T_1 - k_3}e^{-t/T_1} + X_2\frac{(k_1 - T_2 - \frac{k_2}{T_2})}{T_2 - k_3}e^{-t/T_2} + (1 - \frac{k_1}{k_3} + \frac{k_2}{k_3^2})(\frac{X_1T_1}{T_1 - k_3} + \frac{X_2T_2}{T_2 - k_3})e^{-t/k_3}, \tag{C.16}$$

where k_1, k_2 and k_3 are as defined previously in equations (C.8), (C.9) and (C.10).

C.3. Verification of The Energy Wheel Response Equation

To verify that the equations for energy wheel response presented in Section C.1 and C.2 are correct, a theoretical method has been used for the case of $\bar{x}_1$=0, $\bar{t}_1$=0. This represents the case where the humidity sensor has only one time constant, which is a special case of the actual

case with two time constants. The solution to this special case is known analytically and it is used to help verify the accuracy of the equations for F(t) developed in Sections C.1 and C.2. Two cases are considered, adsorption and desorption.

C.3.1. Adsorption Case

If $\bar{t}_1$ and $\bar{x}_1$ are neglected, the correlation for the transient response of the sensor becomes:

$$\frac{\Delta\phi_s}{\Delta\phi_{so}}(t)_{ads} = \bar{x}_2(1-e^{-t/\bar{t}_2}), \tag{C.17}$$

and

$$\mathcal{L}[A'(t)] = \frac{\bar{x}_2}{\bar{t}_2(s+\frac{1}{\bar{t}_2})}, \tag{C.18}$$

where

$$A'(t) = \frac{\partial[\frac{\Delta\phi_s}{\Delta\phi_{so}}(t)_{ads}]}{\partial t} = \frac{\bar{x}_2}{\bar{t}_2}e^{-t/\bar{t}_2}, \tag{C.19}$$

and the correlation equation for transient response of wheel plus sensor is

$$\frac{\Delta\phi_{w+s}}{\Delta\phi_{(w+s)o}}(t)_{ads} = X_1(1-e^{-t/T_1}) + X_2(1-e^{-t/T_2}). \tag{C.20}$$

The Laplace transform of equation (C.20) is

$$\mathcal{L}[\frac{\Delta\phi_{w+s}}{\Delta\phi_{(w+s)o}}(t)_{ads}] = \frac{X_1}{s} + \frac{X_2}{s} - \frac{X_1}{s+\frac{1}{T_1}} - \frac{X_2}{s+\frac{1}{T_2}}. \tag{C.21}$$

Submitting equations (C.18) and (C.21) into equation (4.13) gives

$$\mathrm{F}(t, \bar{t}_2)_{\mathrm{ads}} = \mathcal{L}^{-1}\left\{\frac{\frac{X_1}{s} + \frac{X_2}{s} - \frac{X_1}{s+\frac{1}{T_1}} - \frac{X_2}{s+\frac{1}{T_2}}}{\frac{\bar{x}_2}{\bar{t}_2(s+\frac{1}{\bar{t}_2})}}\right\}$$

$$= \frac{1}{\bar{x}_2}\left[X_1(1-e^{-t/T_1}) + X_2(1-e^{-t/T_2}) + \bar{t}_2\left(\frac{X_1}{T_1}e^{-t/T_1} + \frac{X_2}{T_2}e^{-t/T_2}\right)\right]$$

$$= \left[X_1(1-e^{-t/T_1}) + X_2(1-e^{-t/T_2}) + \bar{t}_2\left(\frac{X_1}{T_1}e^{-t/T_1} + \frac{X_2}{T_2}e^{-t/T_2}\right)\right], \qquad \text{(C.22)}$$

where, $\overline{x_2}$ is taken to be 1.

Comparing equation (C.22) with equation (C.7), for the special case of $\overline{x_1}$=0 and $\overline{t_1}$=0 (a single time constant in the sensor response), shows that the two equations would be identical because $k_1=\overline{t_2}$, k_2=0 and k_3=0 in this case.

C.3.2. Desorption Case

If the $\overline{t_1}$ and $\overline{x_1}$ are neglected, the correlation equation for the transient response of the sensor becomes:

$$\frac{\Delta\phi_s}{\Delta\phi_{so}}(t)_{des} = \bar{x}_2 e^{-t/\bar{t}_2}, \qquad \text{(C.23)}$$

and

$$\mathcal{L}[\,A'(t)\,] = -\frac{\bar{x}_2}{\bar{t}_2\left(s+\frac{1}{\bar{t}_2}\right)}, \qquad \text{(C.24)}$$

where

$$A'(t) = \frac{\partial\left[\frac{\Delta\phi_s}{\Delta\phi_{so}}(t)_{des}\right]}{\partial t} = -\frac{\bar{x}_2}{\bar{t}_2}e^{-t/\bar{t}_2}, \qquad \text{(C.25)}$$

and the correlation equation for transient response of wheel plus sensor is

$$\frac{\Delta\phi_{w+s}}{\Delta\phi_{(w+s)o}}(t)_{des} = X_1 e^{-t/T_1} + X_2 e^{-t/T_2}. \qquad \text{(C.26)}$$

Then the Laplace transformation of equation (C.26) is

$$\mathcal{L}\left[\frac{\Delta\phi_{w+s}}{\Delta\phi_{(w+s)o}}(t)_{des}\right] = \frac{X_1}{s+\frac{1}{T_1}} + \frac{X_2}{s+\frac{1}{T_2}}. \qquad \text{(C.27)}$$

Submitting equations (C.24) and (C.27) into equation (4.13) gives

$$F(t, \overline{t_2})_{des} = \mathcal{L}^{-1}\left\{ \frac{\dfrac{X_1}{s+\dfrac{1}{T_1}} + \dfrac{X_2}{s+\dfrac{1}{T_2}}}{-\dfrac{\overline{x}_2}{\bar{t}_2\left(s+\dfrac{1}{\bar{t}_2}\right)}} \right\}$$

$$= -\frac{1}{\overline{x}_2}\left[(X_1 e^{-t/T_1} + X_2 e^{-t/T_2}) - \bar{t}_2 \left(\frac{X_1}{T_1} e^{-t/T_1} + \frac{X_2}{T_2} e^{-t/T_2}\right) \right]$$

$$= -\left[(X_1 e^{-t/T_1} + X_2 e^{-t/T_2}) - \bar{t}_2 \left(\frac{X_1}{T_1} e^{-t/T_1} + \frac{X_2}{T_2} e^{-t/T_2}\right) \right], \qquad \text{(C.28)}$$

where, $\overline{x_2}$ is assumed as 1.

Comparing equation (C.28) with equation (C.16) for the case of $\overline{x_1}$=0 and $\overline{t_1}$=0 ($\overline{t_1}$=k_1, k_2=0 and k_3=0) gives the identical expression. In addition, for the special case of no energy wheel ($\overline{x_1}$=X_1, $\overline{x_2}$=X_2, $\overline{t_1}$=T_1 and $\overline{t_2}$=T_2), the wheel response, F(t), calculated from equation (C.7) for adsorption and from equation (C.16) for desorption is equal to the unit step for all times greater than zero.